



Measurement of light-by-light scattering and search for axion-like particles with 2.2 nb^{-1} of Pb+Pb data with the ATLAS detector

The ATLAS Collaboration

This paper describes a measurement of light-by-light scattering based on Pb+Pb collision data recorded by the ATLAS experiment during Run 2 of the LHC. The study uses 2.2 nb^{-1} of integrated luminosity collected in 2015 and 2018 at $\sqrt{s_{\text{NN}}} = 5.02 \text{ TeV}$. Light-by-light scattering candidates are selected in events with two photons produced exclusively, each with transverse energy $E_{\text{T}}^{\gamma} > 2.5 \text{ GeV}$, pseudorapidity $|\eta_{\gamma}| < 2.37$, diphoton invariant mass $m_{\gamma\gamma} > 5 \text{ GeV}$, and with small diphoton transverse momentum and diphoton acoplanarity. The integrated and differential fiducial cross sections are measured and compared with theoretical predictions. The diphoton invariant mass distribution is used to set limits on the production of axion-like particles. This result provides the most stringent limits to date on axion-like particle production for masses in the range 6–100 GeV. Cross sections above 2 to 70 nb are excluded at the 95% CL in that mass interval.

Contents

1	Introduction	2
2	ATLAS detector	4
3	Data and Monte Carlo simulation samples	5
4	Event selection	6
5	Detector calibration	8
5.1	Trigger efficiency	8
5.2	Photon reconstruction and identification	9
5.3	Photon energy calibration	10
5.4	Control distributions for exclusive $\gamma\gamma \rightarrow e^+e^-$ production	11
6	Background estimation	11
6.1	Dielectron final states	11
6.2	Central exclusive diphoton production	13
6.3	Other background sources with prompt photons	13
6.4	Other fake-photon background	14
7	Systematic uncertainties	15
8	Results	15
8.1	Kinematic distributions	15
8.2	Integrated fiducial cross section	16
8.3	Differential fiducial cross sections	18
8.4	Search for ALP production	19
9	Conclusions	22

1 Introduction

Light-by-light (LbyL) scattering, $\gamma\gamma \rightarrow \gamma\gamma$, is a process in the Standard Model (SM) that proceeds at lowest order in quantum electrodynamics (QED) via virtual one-loop box diagrams involving charged fermions (leptons and quarks) and W^\pm bosons (Figure 1). LbyL interactions can occur in relativistic heavy-ion collisions at any impact parameters. However, the large impact parameters i.e. larger than twice the radius of the ions, are experimentally preferred as the strong interaction does not play a role in these ultra-peripheral collision (UPC) events. In general, UPC events allow studies of processes involving nuclear photoexcitation, photoproduction of hadrons, and two-photon interactions. Comprehensive reviews of UPC physics can be found in Refs. [1, 2]. The electromagnetic (EM) fields produced by the colliding Pb nuclei can be treated as a beam of quasi-real photons with a small virtuality of $Q^2 < 1/R^2$, where R is the radius of the nuclear charge distribution and so $Q^2 < 10^{-3} \text{ GeV}^2$ [3–5]. The cross section for the reaction $\text{Pb}+\text{Pb}(\gamma\gamma) \rightarrow \text{Pb}^{(*)}+\text{Pb}^{(*)}\gamma\gamma$ can then be calculated by convolving the respective photon flux with the elementary cross section for the process $\gamma\gamma \rightarrow \gamma\gamma$, with a possible EM excitation [6], denoted

by (*). Since the photon flux associated with each nucleus scales as Z^2 , the LbyL cross section is strongly enhanced relative to proton–proton (pp) collisions.

In this measurement, the final-state signature of interest is the exclusive production of two photons, where the diphoton final state is measured in the detector surrounding the Pb+Pb interaction region, and the incoming Pb ions survive the EM interaction. Hence, one expects that two low-energy photons will be detected with no further activity in the central detector. In particular, no reconstructed charged-particle tracks originating from the Pb+Pb interaction point are expected.

The LbyL process has been proposed as a sensitive channel to study physics beyond the SM. Modifications of the $\gamma\gamma \rightarrow \gamma\gamma$ scattering rates can be induced by new exotic charged particles [7] and by the presence of extra spatial dimensions [8]. The LbyL cross sections are also sensitive to Born–Infeld extensions of QED [9], Lorentz-violating operators in electrodynamics [10], and the presence of space-time non-commutativity in QED [11]. Additionally, new neutral particles, such as axion-like particles (ALP), can also contribute in the form of narrow diphoton resonances [12], as shown in Figure 1. ALPs are relatively light, gauge-singlet (pseudo-)scalar particles that appear in many theories with a spontaneously broken global symmetry. Their masses and couplings to SM particles may range over many orders of magnitude. The previous ATLAS searches involving ALP decays to photons are based on pp collision data [13, 14].

LbyL scattering via an electron loop has been precisely, albeit indirectly, tested in measurements of the anomalous magnetic moment of the electron and muon [15, 16]. The $\gamma\gamma \rightarrow \gamma\gamma$ reaction has been measured in photon scattering in the Coulomb field of a nucleus (Delbrück scattering) [17–20] and in the photon splitting process [21]. A related process, in which initial photons fuse to form a pseudoscalar meson which subsequently decays into a pair of photons, has been studied at electron–positron colliders [22–24].

The authors of Ref. [25] proposed to measure LbyL scattering by exploiting the large photon fluxes available in heavy-ion collisions at the LHC. The first direct evidence of the LbyL process in Pb+Pb UPC at the LHC was established by the ATLAS [26] and CMS [27] Collaborations. The evidence was obtained from Pb+Pb data recorded in 2015 at a centre-of-mass energy of $\sqrt{s_{NN}} = 5.02$ TeV with integrated luminosities of 0.48 nb^{-1} (ATLAS) and 0.39 nb^{-1} (CMS). The CMS Collaboration also set upper limits on the cross section for ALP production, $\gamma\gamma \rightarrow a \rightarrow \gamma\gamma$, over a mass range of 5–90 GeV. Exploiting a data sample of Pb+Pb collisions collected in 2018 at the same centre-of-mass energy with an integrated luminosity of 1.73 nb^{-1} , the ATLAS Collaboration observed LbyL scattering with a significance of 8.2σ [28]. These two

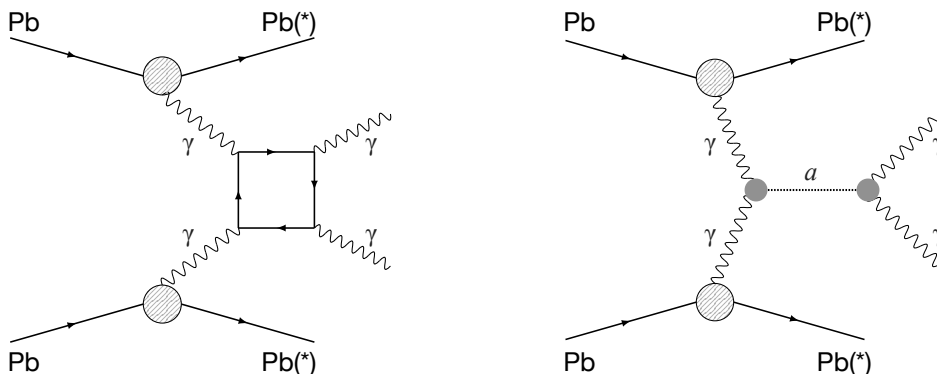


Figure 1: Schematic diagrams of (left) SM LbyL scattering and (right) axion-like particle production in Pb+Pb UPC. A potential electromagnetic excitation of the outgoing Pb ions is denoted by (*).

ATLAS measurements used tight requirements on the diphoton invariant mass (> 6 GeV) and single-photon transverse energy (> 3 GeV).

This paper presents a measurement of the cross sections for Pb+Pb $(\gamma\gamma) \rightarrow \text{Pb}^{(*)} + \text{Pb}^{(*)} \gamma\gamma$ production at $\sqrt{s_{\text{NN}}} = 5.02$ TeV using a combination of Pb+Pb collision data recorded in 2015 and 2018 by the ATLAS experiment, corresponding to an integrated luminosity of 2.2 nb^{-1} . This analysis follows the approach proposed in Ref. [25] and the methodology used in the previous measurements [26, 28]. However, as a result of improvements in the trigger efficiency and purity of the photon identification, a broader kinematic range in diphoton invariant mass (> 5 GeV) and single-photon transverse energy (> 2.5 GeV) is covered. This extension results in an increase of about 50% in expected signal yield in comparison with the previous tighter requirements.

The integrated fiducial cross section and four differential distributions involving kinematic variables of the final-state photons are measured. Two of the distributions characterise the energy of the process: the invariant mass of the diphoton system, $m_{\gamma\gamma}$, and the average transverse momentum of two photons, $(p_{\text{T}}^{\gamma 1} + p_{\text{T}}^{\gamma 2})/2$. The remaining ones probe angular correlations of the $\gamma\gamma$ system. These are the rapidity¹ of the diphoton system, $y_{\gamma\gamma}$, and $|\cos(\theta^*)|$, defined as:

$$|\cos(\theta^*)| = \left| \tanh\left(\frac{\Delta y_{\gamma 1, \gamma 2}}{2}\right) \right|,$$

where θ^* is the $\gamma\gamma$ scattering angle in the $\gamma\gamma$ centre-of-mass frame, and $\Delta y_{\gamma 1, \gamma 2}$ is the difference between the rapidities of the photons.

The measured diphoton invariant mass distribution is used to set limits on ALP production via the process $\gamma\gamma \rightarrow a \rightarrow \gamma\gamma$.

2 ATLAS detector

The ATLAS detector [29] at the LHC covers nearly the entire solid angle around the collision point. It consists of an inner tracking detector surrounded by a thin superconducting solenoid, EM and hadronic calorimeters, and a muon spectrometer incorporating three large superconducting toroid magnets. The inner-detector system (ID) is immersed in a 2 T axial magnetic field and provides charged-particle tracking in the pseudorapidity² range $|\eta| < 2.5$.

The high-granularity silicon pixel detector (Pixel) covers the collision region. Typically, it provides four measurements per track, with the first hit being in the insertable B-layer (IBL) [30, 31], which was installed at a mean distance of 3.3 cm from the beam pipe before the start of Run 2. It is followed by the silicon microstrip tracker (SCT), which usually provides four two-dimensional measurement points per track. These silicon detectors are complemented by the transition radiation tracker, which enables radially extended track reconstruction up to $|\eta| = 2.0$.

¹ Rapidity is defined as $y = \frac{1}{2} \ln \frac{E+p_z}{E-p_z}$, where E and p_z are particle's energy and the component of momentum along the beam axis, respectively.

² ATLAS uses a right-handed coordinate system with origin at the nominal interaction point in the centre of the detector and the z -axis along the beam pipe. The x -axis points from the IP to the centre of the LHC ring, and the y -axis points upwards. Cylindrical coordinates (r, ϕ) are used in the transverse plane, ϕ being the azimuthal angle around the z -axis. The pseudorapidity is defined in terms of the polar angle θ as $\eta = -\ln(\theta/2)$. Angular distance is measured in units of $\Delta R \equiv \sqrt{(\Delta\eta)^2 + (\Delta\phi)^2}$. The transverse energy of a photon or electron is $E_{\text{T}} = E/\cosh(\eta)$, where E is its energy.

The calorimeter system covers the pseudorapidity range $|\eta| < 4.9$. Within the region $|\eta| < 3.2$, EM calorimetry is provided by barrel and endcap lead/liquid-argon (LAr) EM calorimeters (high-granularity for $|\eta| < 2.5$), with an additional thin LAr presampler covering $|\eta| < 1.8$ to correct for energy loss in material upstream of the calorimeters. Hadronic calorimetry is provided by the steel/scintillator-tile calorimeter, segmented into three barrel structures within $|\eta| < 1.7$, and two copper/LAr hadronic endcap calorimeters. The solid angle coverage is completed with forward copper/LAr and tungsten/LAr calorimeter modules (FCal) optimised for EM and hadronic measurements respectively.

The muon spectrometer (MS) comprises high-precision tracking chambers measuring the deflection of muons in a magnetic field generated by the superconducting air-core toroids. The precision chamber system covers the region $|\eta| < 2.7$ with three layers of monitored drift tubes, complemented by cathode strip chambers in the forward region, where the background is highest.

The ATLAS minimum-bias trigger scintillators (MBTS) consist of scintillator slats positioned between the ID and the endcap calorimeters, with each side having an outer ring of four slats segmented in azimuthal angle, covering $2.07 < |\eta| < 2.76$, and an inner ring of eight slats, covering $2.76 < |\eta| < 3.86$.

The ATLAS zero-degree calorimeters (ZDC) consist of four longitudinal compartments on each side of the interaction point (IP), each with one nuclear interaction length of tungsten absorber, with the Cerenkov light read out by 1.5 mm quartz rods. The detectors are located 140 m from the nominal IP in both directions, covering $|\eta| > 8.3$.

The ATLAS LUCID-2 detector [32] consists of 32 photomultiplier tubes for luminosity measurements and luminosity monitoring. Its two modules are placed symmetrically at about ± 17 m from the nominal IP.

The ATLAS trigger system [33] consists of a Level-1 trigger implemented using a combination of dedicated electronics and programmable logic, and a software-based high-level trigger (HLT).

3 Data and Monte Carlo simulation samples

The data used in this measurement is from Pb+Pb collisions with a centre-of-mass energy of $\sqrt{s_{\text{NN}}} = 5.02$ TeV, recorded in 2015 and 2018 with the ATLAS detector at the LHC. The full data set corresponds to an integrated luminosity of 2.2 nb^{-1} . Only high-quality data with all detectors operating normally are analysed.

Monte Carlo (MC) simulated events for the LbyL signal process were generated at leading order (LO) using SuperChic v3.0 [34]. They take into account box diagrams with leptons and quarks (such as the diagram in Figure 1), and W^\pm bosons, including interference effects. The W^\pm contribution is only important for diphoton masses $m_{\gamma\gamma} > 2m_W$. Next-to-leading-order QCD and QED corrections are not included. They increase the $\gamma\gamma \rightarrow \gamma\gamma$ cross section by a few percent [35, 36]. An alternative LbyL signal sample was generated using calculations from Ref. [37]. The difference between the nominal and alternative signal prediction is mainly in the implementation of the non-hadronic overlap condition of the Pb ions. In SuperChic v3.0 the probability for exclusive $\gamma\gamma$ interactions turns on smoothly for Pb+Pb impact parameters in the range of 15–20 fm and it is unity for larger values, while the alternative prediction fully suppresses these interactions for impact parameters below 14 fm when two nuclei overlap during the collision. This difference leads to a fiducial cross section for LbyL scattering that is by about 3% larger in the alternative calculation than in the prediction from SuperChic v3.0.

The exclusive diphoton final state can also be produced via the strong interaction through a quark loop in the exchange of two gluons in a colour-singlet state. This central exclusive production (CEP) background contribution, $gg \rightarrow \gamma\gamma$, was modelled using SuperChic v3.0. Background from two-photon production of quark–antiquark pairs was estimated using HERWIG++ 2.7.1 [38] where the Equivalent Photon Approximation (EPA) formalism in pp collisions is implemented. The sample was then normalised to cover the differences in equivalent photon fluxes between the Pb+Pb and pp cases.

Exclusive dielectron pairs from the reaction $\text{Pb+Pb} (\gamma\gamma) \rightarrow \text{Pb}^{(*)} + \text{Pb}^{(*)} e^+ e^-$ are used for various aspects of the analysis, in particular to validate the EM calorimeter energy scale and resolution. This $\gamma\gamma \rightarrow e^+ e^-$ process was modelled with the STARlight v2.0 MC generator [39], in which the cross section is computed by combining the Pb+Pb photon flux with the LO formula for $\gamma\gamma \rightarrow e^+ e^-$. The background contribution from a related process, $\gamma\gamma \rightarrow \tau^+ \tau^-$, was modelled using STARlight v2.0 interfaced with Pythia 8.212 [40] for the simulation of τ -lepton decays.

Events for the ALP signal were generated using STARlight v2.0 for ALP masses (m_a) ranging between 5 and 100 GeV. A mass spacing of 1 GeV was used for $5 < m_a < 30$ GeV, while for $m_a > 30$ GeV a 10 GeV mass spacing was used. The width of the simulated ALP resonance is well below the detector resolution in all simulated samples.

All generated events were passed through a detector simulation [41] based on GEANT4 [42] and are reconstructed with the standard ATLAS reconstruction software.

4 Event selection

Candidate diphoton events were recorded using a dedicated trigger for events with moderate activity in the calorimeter but little additional activity in the entire detector. The trigger strategies for the 2015 and 2018 data sets were different. In particular, the latter aimed at improving the trigger efficiency at low photon transverse energy, E_T , values. At Level-1 in 2015, the total E_T registered in the calorimeter after noise suppression was required to be between 5 and 200 GeV. In 2018, a logical OR of two Level-1 conditions was required: (1) at least one EM cluster with $E_T > 1$ GeV in coincidence with total E_T registered in the calorimeter between 4–200 GeV, or (2) at least two EM clusters with $E_T > 1$ GeV with total E_T registered in the calorimeter below 50 GeV. At the HLT, events in 2015 were rejected if more than one hit was found in the inner ring of the MBTS (MBTS veto). In 2018, a requirement of total E_T on each side of the FCal detector to be below 3 GeV was imposed. Additionally, in both data sets a veto condition on activity in the Pixel detector, hereafter referred to as Pixel-veto, had to be satisfied. The number of hits was required to be at most 10 in 2015, and at most 15 in 2018.

Photons are reconstructed from EM clusters in the calorimeter and tracking information provided by the ID, which allows the identification of photon conversions [43]. Selection requirements are applied to remove EM clusters with a large amount of energy from poorly functioning calorimeter cells, and a timing requirement is made to reject out-of-time candidates. An energy calibration specifically optimised for photons [44] is applied to the candidates to account for upstream energy loss and both lateral and longitudinal shower leakage. The calibration is derived for nominal pp collisions with dedicated factors applied to account for a negligible contribution from multiple Pb+Pb collisions at the same bunch crossing. A correction [44] is applied to photons in MC samples to account for potential mismodelling of quantities which describe shower shapes of the associated EM showers.

The photon particle identification (photon PID) in this analysis is based on a selection of the shower-shape variables, optimised for the signal events. Only photons with $E_T > 2.5$ GeV and $|\eta| < 2.37$, excluding the

calorimeter transition region $1.37 < |\eta| < 1.52$, are considered. The pseudorapidity requirement ensures that the photon candidates pass through regions of the EM calorimeter where the first layer is segmented into narrow strips, providing good separation between genuine prompt photons and photons coming from the decay of neutral hadrons. The identification is based on a neural network trained on background photons extracted from data and photons from the signal MC simulation, as already used in the previous ATLAS measurement [28]. The PID requirements are optimised for low- E_T photons ($E_T < 20$ GeV) to maintain a constant photon PID efficiency of 95% as a function of η and E_T with respect to reconstructed photon candidates. They also select a purer sample of photons than obtained with the cut-based photon PID utilised in pp collisions [43].

Preselected events are required to have exactly two photons satisfying the above selection criteria, with a diphoton invariant mass greater than 5 GeV. In order to suppress the $\gamma\gamma \rightarrow e^+e^-$ background, a veto on charged-particle tracks (with $p_T > 100$ MeV, $|\eta| < 2.5$, at least one hit in the Pixel detector and at least six hits in the Pixel and SCT detectors in total) is imposed. In order to reduce the background from electrons with poorly reconstructed tracks, candidate events are required to have no ‘pixel tracks’ in the vicinity of the photon candidate. Pixel tracks are reconstructed using only the information from the Pixel detector, and are required to have $p_T > 50$ MeV, $|\eta| < 2.5$, and at least three hits in the Pixel detector. In order to suppress fake pixel tracks due to noise in the Pixel detector, only pixel tracks with $\Delta\eta < 0.5$ from the photons are considered. These requirements reduce the fake-photon background from the dielectron final state by a factor of about 10^4 , according to simulation. They have minor impact on $\gamma\gamma \rightarrow \gamma\gamma$ signal events (93% efficiency for the track veto and 99% for the pixel-track veto), since the probability of photon conversion in the Pixel detector is relatively small and the converted photons have a low probability of being reconstructed at very low E_T due to the presence of low-momentum electron tracks.

Due to the absence of tracks in the LbyL signal events, no primary vertex is reconstructed. The photon direction is estimated using the barycentre of the cluster with respect to the origin of the ATLAS coordinate system.

To reduce other sources of fake-photon background (involving mainly calorimeter noise and cosmic-ray muons), the transverse momentum of the diphoton system ($p_T^{\gamma\gamma}$) is required to be below 1 GeV for $m_{\gamma\gamma} < 12$ GeV and below 2 GeV for $m_{\gamma\gamma} > 12$ GeV. To reduce real-photon background from CEP $gg \rightarrow \gamma\gamma$ reactions, an additional requirement on the diphoton acoplanarity, $A_\phi = (1 - |\Delta\phi_{\gamma\gamma}|/\pi) < 0.01$, is used. The CEP process exhibits a significantly broader acoplanarity distribution than the $\gamma\gamma \rightarrow \gamma\gamma$ process because gluons recoil against the Pb nucleus, which then dissociates.

To select $\gamma\gamma \rightarrow e^+e^-$ candidates, events are required to pass the same trigger as in the diphoton selection. Each electron is reconstructed from an EM energy cluster in the calorimeter matched to a track in the ID [45]. The electrons are required to have a transverse energy $E_T > 2.5$ GeV and pseudorapidity $|\eta| < 2.47$ with the calorimeter transition region $1.37 < |\eta| < 1.52$ excluded. They are also required to meet loose identification criteria based on shower-shape and track-quality variables [45]. The $\gamma\gamma \rightarrow e^+e^-$ events are selected by requiring exactly two oppositely charged electrons, no further charged-particle tracks coming from the interaction region (with the selection requirements as described above), and dielectron acoplanarity below 0.01.

5 Detector calibration

5.1 Trigger efficiency

The trigger sequence used in the analysis consists of three independent requirements: Level-1, MBTS/FCal veto, and the requirement on low activity in the ID.

The Level-1 trigger efficiency was estimated with $\gamma\gamma \rightarrow e^+e^-$ events passing one of the independent supporting triggers. These triggers are designed to select events with single or double dissociation of Pb nuclei and small activity in the ID. They are based on a coincidence of signals in one or both ZDC sides with a requirement on the total E_T in the calorimeter to be below 50 GeV. Dielectron event candidates are required to have exactly two reconstructed tracks and two geometrically matched EM clusters, each with a minimum E_T of 1 GeV and $|\eta| < 1.47$, excluding the calorimeter transition region $1.37 < |\eta| < 1.52$. The electron identification requirements are removed in order to accept more events in this very low E_T region, where the efficiencies to reconstruct and identify electrons are low. Furthermore, dielectron acoplanarity evaluated using electron charged-particle tracks is required to be below 0.01. The extracted Level-1 trigger efficiency is provided as a function of the sum of E_T of the two EM clusters reconstructed offline ($\sum E_T^{\text{clusters}} = E_T^{\text{cluster1}} + E_T^{\text{cluster2}}$). For $\sum E_T^{\text{clusters}} = 5$ GeV this efficiency, shown in Figure 2, reaches 60% for 2018 trigger settings, while it is consistent with 0% for 2015 trigger settings due to higher trigger thresholds. The Level-1 trigger efficiency grows to about 25% (95%) for $\sum E_T^{\text{clusters}} = 7.5$ GeV for 2015 (2018) data. The efficiency plateau is reached around $\sum E_T^{\text{clusters}} = 10$ GeV for the 2015 data-taking period and around $\sum E_T^{\text{clusters}} = 9$ GeV for the 2018 one. The error bars associated with the data points represent statistical uncertainties. The efficiency is parameterised using an error function fit that is used to reweight the MC simulation. The statistical uncertainty is estimated by varying the fit parameters by their uncertainty values. The systematic uncertainty is estimated using modified $\gamma\gamma \rightarrow e^+e^-$ selection criteria.

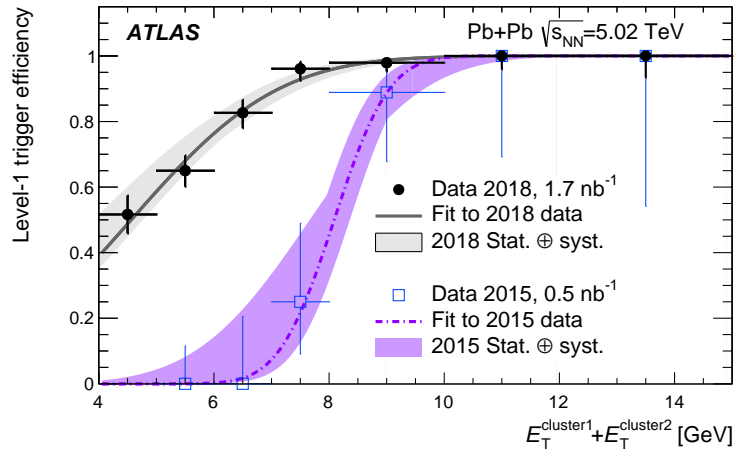


Figure 2: The Level-1 trigger efficiency extracted from $\gamma\gamma \rightarrow e^+e^-$ events that pass the supporting triggers as a function of the sum of E_T of the two EM clusters. Data are shown as points with error bars representing statistical uncertainties, separately for two data-taking periods: 2015 (open squares) and 2018 (full circles). The efficiency is parameterised using the error function fit, shown as a dashed (2015) or solid (2018) line. Shaded bands denote total (statistical and systematic) uncertainty.

The MBTS and FCal veto efficiencies are estimated using $\gamma\gamma \rightarrow e^+e^-$ events recorded by supporting triggers. The MBTS veto efficiency is estimated to be $(98 \pm 2)\%$ [26] and the FCal veto efficiency is found to be $(99.1 \pm 0.6)\%$. Both efficiencies are independent of kinematics.

Due to low conversion probability of signal photons in the Pixel detector, inefficiency of the Pixel-veto requirement at the trigger level is found to be negligible for diphoton event candidates.

The efficiency for selected $\gamma\gamma \rightarrow e^+e^-$ events to satisfy the Pixel-veto requirement is evaluated using a dedicated supporting trigger accepting events with at most 15 tracks at the HLT, out of which at least two had $p_T > 1$ GeV. At Level-1, the same trigger condition was applied as in the diphoton trigger. The FCal veto requirement was also imposed at the HLT. The Pixel-veto efficiency is parameterised using a second-order polynomial as a function of dielectron rapidity, y_{ee} . The efficiency reaches 80–85% for dielectron rapidity $|y_{ee}| < 1$ and drops to 45–50% at $|y_{ee}| \approx 2.5$. This efficiency correction is applied to the $\gamma\gamma \rightarrow e^+e^-$ MC simulation.

5.2 Photon reconstruction and identification

The photon reconstruction efficiency is extracted from data using $\gamma\gamma \rightarrow e^+e^-$ events, where one of the electrons emits a hard-bremsstrahlung photon when interacting with the material of the detector. A tag-and-probe method is performed for events collected by the diphoton trigger with exactly one identified electron and exactly two reconstructed charged-particle tracks. The electron is considered a tag if it can be matched to one of the tracks with a $\Delta R < 1.0$ requirement. The electron is required to have $E_T^e > 4$ GeV and the track that is unmatched with the electron (trk2) must have $p_T < 1.5$ GeV. The electron–trk2 transverse momentum difference is treated as the transverse energy of the probe, since the additional hard-bremsstrahlung photon is expected to have $E_T^\gamma \approx (E_T^e - p_T^{\text{trk2}})$. The $p_T^{\text{trk2}} < 1.5$ GeV requirement ensures a sufficient ΔR separation between the expected photon and the second electron. A hard-bremsstrahlung photon is expected to be within a distance of $\Delta R = 1.0$ around trk2 direction. Any additional background contribution to the exclusive $\gamma\gamma \rightarrow e^+e^-$ reaction is found to be very small in Pb+Pb UPC [46], and therefore it is considered negligible.

The data sample contains 2905 $\gamma\gamma \rightarrow e^+e^- (\gamma)$ bremsstrahlung photons and is used to extract the photon reconstruction efficiency, which is presented in Figure 3. The efficiency in data is approximately 60% for $E_T^\gamma = 2.5$ GeV and reaches 90% at $E_T^\gamma = 6$ GeV. Reasonable agreement between data and simulation is found. The distribution from Figure 3 is used to obtain the data-to-simulation scale factors that are used to correct the MC simulation.

High- p_T exclusive dilepton production ($\gamma\gamma \rightarrow \ell^+\ell^-$ with $\ell^\pm = e^\pm, \mu^\pm$) with final-state radiation (FSR) is used for data-driven measurements of the photon PID efficiency, defined as the probability for a reconstructed photon to satisfy the identification criteria. Events with exactly two oppositely charged tracks with $p_T > 0.5$ GeV are selected in UPC events recorded by the diphoton or dimuon³ triggers. In addition a requirement to reconstruct a photon candidate with $E_T^\gamma > 2.5$ GeV and $|\eta| < 2.37$, excluding the calorimeter transition region $1.37 < |\eta| < 1.52$, is imposed. A photon candidate is required to be separated from each track with the requirement $\Delta R > 0.3$. This condition avoids the leakage of the photon cluster energy to an electron cluster from the $\gamma\gamma \rightarrow e^+e^-$ process. The mass of the dilepton system is required to be above 1.5 GeV. The FSR event candidates are identified using a $p_T^{\text{tt}\gamma} < 1$ GeV requirement, where

³ The dimuon trigger required a muon candidate with $p_T > 4$ GeV reconstructed at Level-1 and at least two tracks with p_T above 1 GeV among up to 15 tracks found at the HLT.

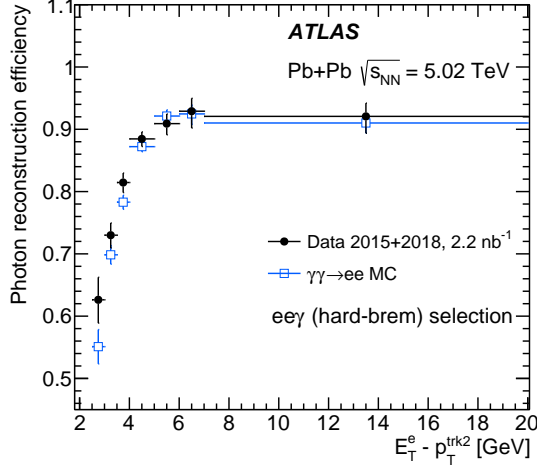


Figure 3: Photon reconstruction efficiency as a function of photon E_T^γ (approximated with $E_T^e - p_T^{\text{trk}2}$) extracted from $\gamma\gamma \rightarrow e^+e^-$ events with a hard-bremstrahlung photon. Data (full symbols) are compared with $\gamma\gamma \rightarrow e^+e^-$ MC simulation (open symbols). The error bars denote statistical uncertainties.

$p_T^{\text{trk}2}$ is the transverse momentum of the three body system consisting of two oppositely charged tracks and a photon. The FSR sample consists of 1333 (212) photon candidates in the 2018 (2015) data set and is statistically independent from the hard-bremstrahlung photon sample used in the photon reconstruction efficiency measurement.

Figure 4 shows the photon PID efficiency as a function of the reconstructed photon E_T for 2015 and 2018 data. The efficiency in data is compared with the efficiency extracted from the signal MC sample. Photon PID efficiencies in MC simulation with 2015 and 2018 data-taking conditions are in good agreement. In the data for photons with $E_T < 5$ GeV, the photon PID efficiency is in the range of 91-93% in the 2018 set, while it is found to be 97-100% in the 2015 set. This difference is due to slightly different detector conditions between the 2015 and 2018 data-taking periods, causing the photon shower-shape distributions to be narrower in the 2015 data. Based on these studies, MC simulated events are corrected using photon E_T -dependent data-to-simulation scale factors separately for the 2015 and 2018 data sets.

5.3 Photon energy calibration

The EM energy scale and energy resolution are validated in data using $\gamma\gamma \rightarrow e^+e^-$ events. The two electrons from the $\gamma\gamma \rightarrow e^+e^-$ reaction exhibit balanced transverse momenta with $|p_T^{e^+} - p_T^{e^-}|$, expected to be below 30 MeV, which is much smaller than the EM calorimeter energy resolution. Therefore, the energy resolution, $\sigma_{E_T^{\text{cluster}}}$, can be determined from the measurement of $E_T^{\text{cluster}1} - E_T^{\text{cluster}2}$ distributions in $\gamma\gamma \rightarrow e^+e^-$ events from the formula:

$$\sigma_{E_T^{\text{cluster}}} \approx \frac{\sigma_{(E_T^{\text{cluster}1} - E_T^{\text{cluster}2})}}{\sqrt{2}},$$

where $E_T^{\text{cluster}1}$ and $E_T^{\text{cluster}2}$ are the transverse energies of the two clusters. At low electron- E_T (below 10 GeV) the value of $\sigma_{E_T^{\text{cluster}}}/E_T^{\text{cluster}}$ is observed to be 8–10% in data, which agrees well with the resolution obtained from simulation.

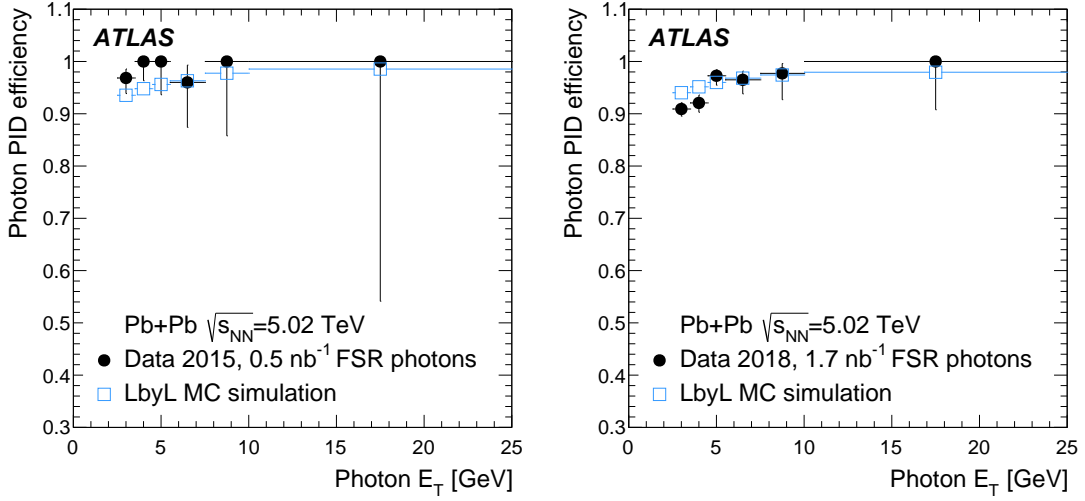


Figure 4: Photon PID efficiency as a function of photon E_T extracted from FSR event candidates in 2015 (left) and 2018 (right) data (full symbols) and signal MC sample (open symbols). The error bars denote statistical uncertainties.

The EM energy scale is cross-checked using the ratio of electron cluster E_T to electron track p_T . It is observed that the simulation provides a good description of the E_T^e/p_T^{trk} distribution.

5.4 Control distributions for exclusive $\gamma\gamma \rightarrow e^+e^-$ production

Figure 5 presents detector-level distributions for events passing the $\gamma\gamma \rightarrow e^+e^-$ selection (outlined in Section 4) in the 2018 Pb+Pb data. In total, 28 045 $\gamma\gamma \rightarrow e^+e^-$ event candidates are observed. The shaded bands reflect systematic uncertainties due to electron energy scale and resolution, electron reconstruction and identification, and trigger efficiency. In general, the STARlight prediction describes the normalisation and shapes of distributions well. Small systematic differences between the central values of the exclusive dielectron data and the MC prediction are seen in the tail of the dielectron p_T distribution, likely due to a missing contribution from the QED final-state radiation which is not simulated by the MC generator.

The low number of $\gamma\gamma \rightarrow e^+e^-$ events collected by a control trigger in the 2015 Pb+Pb data precludes precision comparisons between data and MC simulation in that sample. In particular, the tighter Pixel-veto requirement imposed at the HLT necessitates a dedicated pseudorapidity-dependent trigger efficiency correction which, due to the limited number of $\gamma\gamma \rightarrow e^+e^-$ events, could only be extracted with 20% precision. Nevertheless, overall reasonable agreement was found within large uncertainties as demonstrated in the previous ATLAS publication [26].

6 Background estimation

6.1 Dielectron final states

The $\gamma\gamma \rightarrow e^+e^-$ process has a relatively high cross section and can be a source of fake diphoton events. The electron-to-photon misidentification can occur when the electron track is not reconstructed or the

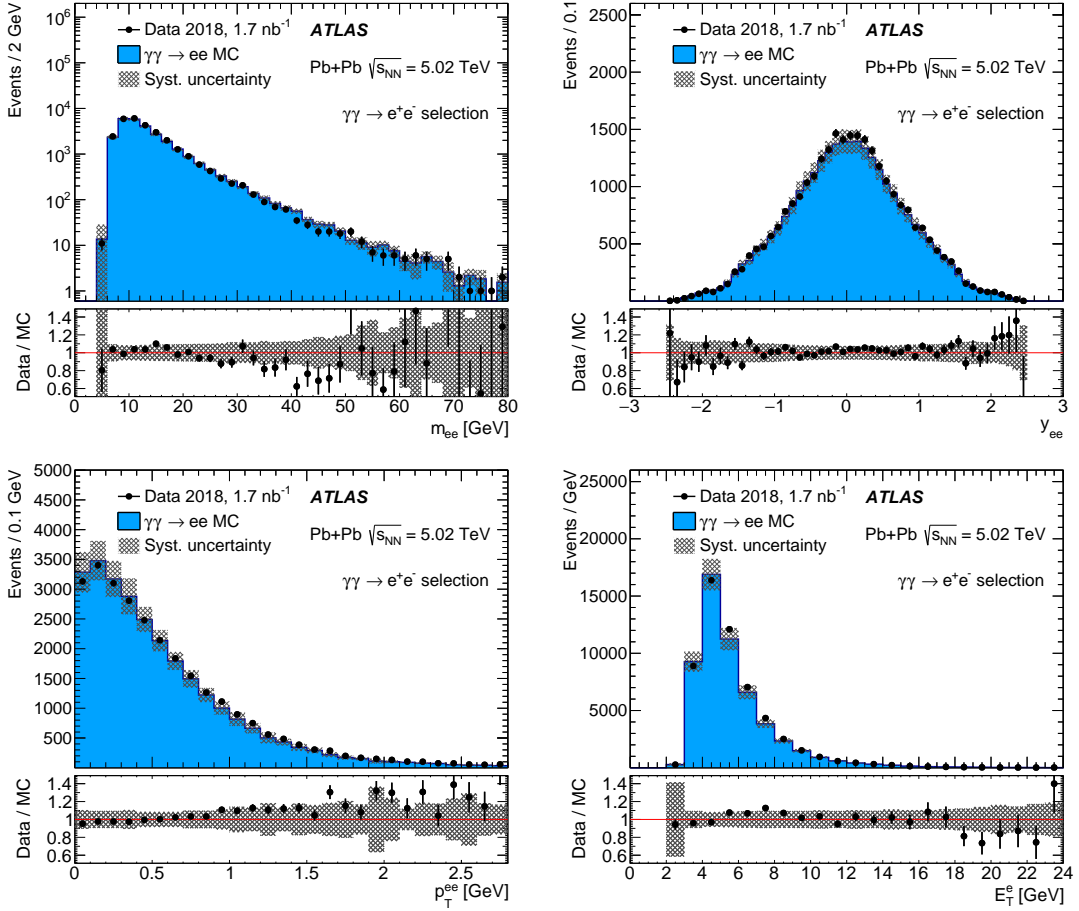


Figure 5: Kinematic distributions for Pb+Pb $(\gamma\gamma) \rightarrow \text{Pb}^{(*)}+\text{Pb}^{(*)} e^+e^-$ event candidates in the 2018 data set: dielectron mass (top-left), dielectron rapidity (top-right), dielectron p_T (bottom-left) and electron transverse energy (bottom-right). Data (points) are compared with MC expectations (histograms). The simulation prediction is normalised to the same integrated luminosity as the data. Systematic uncertainties due to electron energy scale and resolution, electron reconstruction and identification, and trigger efficiency, are shown as shaded bands. The lower panels display the ratio of data to MC predictions. Some values are outside the plotting range.

electron emits a hard bremsstrahlung photon.

The $\gamma\gamma \rightarrow e^+e^-$ yield in the signal region defined in Section 4 is estimated using a fully data-driven method. A control region is defined requiring exactly two photon candidates passing the signal selection, and one or two pixel tracks. This control region is denoted by $\text{CR}_{\text{PixTrk}}^{N=1,2}$. The event yield observed in $\text{CR}_{\text{PixTrk}}^{N=1,2}$ is extrapolated to the signal region using the probability of missing the electron pixel track if the standard track is not reconstructed (p_{mistag}^e).

The p_{mistag}^e value is measured in data using events with exactly one standard track and two photon candidates having $A_\phi < 0.01$. It is measured to be $p_{\text{mistag}}^e = (47 \pm 9)\%$, where the uncertainty is estimated by relaxing the A_ϕ requirement. It is also found that p_{mistag}^e does not depend on the probed photon E_T and η .

The number of $\gamma\gamma \rightarrow e^+e^-$ events in the signal region is estimated to be $N_{\gamma\gamma \rightarrow e^+e^-} = 15 \pm 7$, where the uncertainty accounts for the p_{mistag}^e uncertainty and limited event yield in $\text{CR}_{\text{PixTrk}}^{N=1,2}$. This uncertainty

also covers the differences if the $\gamma\gamma \rightarrow e^+e^-$ yield is instead extrapolated from event yields for individual pixel-track multiplicities ($N = 1$ or $N = 2$).

The distribution shapes of various kinematic variables of $\gamma\gamma \rightarrow e^+e^-$ background in the signal region are taken from data in $\text{CR}_{\text{PixTrk}}^{N=1}$. The shape uncertainty is constructed by comparing kinematic distributions from data in $\text{CR}_{\text{PixTrk}}^{N=1}$ with the distributions from data in $\text{CR}_{\text{PixTrk}}^{N=2}$.

6.2 Central exclusive diphoton production

The CEP $gg \rightarrow \gamma\gamma$ background is estimated from MC simulation with the overall rate of this process evaluated in the A_ϕ control region in the data. The normalisation is constrained using the condition:

$$N_{\text{data}}(A_\phi > 0.01) = N_{gg \rightarrow \gamma\gamma}(A_\phi > 0.01) + N_{\text{sig}}(A_\phi > 0.01) + N_{\gamma\gamma \rightarrow ee}(A_\phi > 0.01) ,$$

where N_{data} denotes the number of observed events, $N_{gg \rightarrow \gamma\gamma}$ is the expected CEP $gg \rightarrow \gamma\gamma$ event yield, N_{sig} is the expected number of signal events (from MC simulation) and $N_{\gamma\gamma \rightarrow ee}$ is the e^+e^- background yield. The $N_{\gamma\gamma \rightarrow ee}$ is estimated using the same data-driven method as described in Section 6.1. The diphoton acoplanarity distribution for events satisfying the signal region selection, but before applying the $A_\phi < 0.01$ requirement is shown in Figure 6. The predictions provide a fair description of the shape of the data distribution.

The uncertainty in the CEP $gg \rightarrow \gamma\gamma$ background process takes into account the limited number of events in the $A_\phi > 0.01$ control region (11%), as well as experimental and modelling uncertainties. It is found that all experimental uncertainties have a negligible impact on the CEP $gg \rightarrow \gamma\gamma$ background estimate. The impact of the MC modelling uncertainty on the shape of the acoplanarity distribution is estimated using an alternative SuperChic v2.0 MC sample with extra gluon interactions (no absorptive effects). This leads to a 21% change in the CEP background yield in the signal region, which is taken as a systematic uncertainty. An additional check is performed by varying the parton distribution function (PDF) of the gluon. The differences between leading-order MMHT 2014 [47], CT14 [48] and NNPDF3.1 [49] PDF sets have negligible impact on the shape of the diphoton acoplanarity distribution.

In addition, the energy deposition in the ZDC, which is sensitive to the dissociation of Pb nuclei, is studied for events before the $A_\phi < 0.01$ requirement is imposed. Good agreement is observed in the $A_\phi > 0.01$ control region between the data-driven CEP estimate and the observed events with a signal corresponding to at least one neutron in the ZDC. In the signal region ($A_\phi < 0.01$), approximately 70% of observed events have a signal corresponding to no neutrons in the ZDC, which is consistent with the signal-plus-background hypothesis.

The background due to CEP in the signal region is estimated to be 12 ± 3 events. In the differential cross-section measurements, the shape uncertainty is evaluated using the alternative SuperChic v2.0 MC sample.

6.3 Other background sources with prompt photons

The contribution from the $\gamma\gamma \rightarrow e^+e^-\gamma\gamma$ process is evaluated using the MADGRAPH5_aMC@NLO v2.4.3 MC generator [50] and the Pb+Pb photon flux from STARlight. This contribution is estimated to be below 1% of the expected signal and is consequently ignored in the analysis.

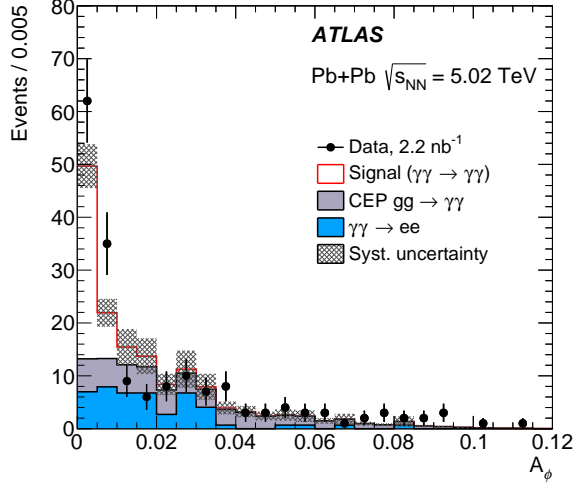


Figure 6: The diphoton acoplanarity distribution for events satisfying the signal region selection, but before applying the $A_\phi < 0.01$ requirement. Data are shown as points with statistical error bars, while the histograms represent the expected signal and background levels. The CEP $gg \rightarrow \gamma\gamma$ background is normalised in the $A_\phi > 0.01$ control region. The signal prediction is normalised to the same integrated luminosity as the data. The shaded band represents the uncertainties in signal and background predictions, excluding the uncertainty in the luminosity.

The contribution from bottomonia production (for example, $\gamma\gamma \rightarrow \eta_b \rightarrow \gamma\gamma$ or $\gamma\text{Pb} \rightarrow \Upsilon \rightarrow \gamma\eta_b \rightarrow 3\gamma$) is calculated using relevant branching fractions from Refs. [51, 52] and found to be negligible.

The contribution from UPC events where both nuclei emit a bremsstrahlung photon is estimated using calculations from Ref. [53]. The cross section for single-bremsstrahlung photon production from a Pb ion in the fiducial region of the measurement is calculated to be below 10^{-4} pb, so the coincidence of two such occurrences is negligible.

6.4 Other fake-photon background

The background contribution from $\gamma\gamma \rightarrow q\bar{q}$ production is estimated using MC simulation based on HERWIG++ and it contributes less than 1 event to the total number of events in the signal region. The expected yield for the background from $\gamma\gamma \rightarrow \tau^+\tau^-$ process is estimated using MC simulation based on STARlight + Pythia 8 and is found to be less than 0.5 events. Both of these background sources are considered negligible.

Exclusive two-meson production can be a potential source of background for LbyL scattering events, mainly due to their similar back-to-back topology. Mesons can fake photons either by their decay into photons (π^0, η, η') or by mis-reconstructed charged-particle tracks (for example π^+, π^- states). Estimates for such contributions are reported in Refs. [25, 54–57] and these contributions are considered to be negligible in the signal region.

The background from fake diphoton events induced by cosmic-ray muons is estimated using a control region with at least one track reconstructed in the muon spectrometer and further studied using the reconstructed photon-cluster time distribution. The latter method is also used to estimate the background originating from calorimeter noise. After imposing the $p_T^{\gamma\gamma}$ requirements, these background contributions are below 1 event and are considered negligible.

7 Systematic uncertainties

Systematic uncertainties in the $\gamma\gamma \rightarrow \gamma\gamma$ cross-section measurements arise from the reconstruction of photons, the background determination, and integrated luminosity uncertainty, as well as the procedures used to correct for detector effects.

The precision of the Level-1 trigger efficiency estimation is limited by the number of events recorded by the supporting trigger. As a systematic check, the e^+e^- event selection is varied. In total, the impact of the Level-1 trigger efficiency uncertainty on the expected signal yield is 5%. The uncertainty in the MBTS/FCal veto efficiency has negligible impact on the results.

The uncertainty in the photon reconstruction and PID efficiencies is estimated by parameterising the scale factors as a function of the photon pseudorapidity, instead of the photon transverse momentum. This affects the expected signal yield by 4% (photon reconstruction efficiency) and 2% (photon PID efficiency). The variation of the selection criteria used in data-driven efficiency measurements has negligible impact on the results. The statistical uncertainty of the photon reconstruction and PID efficiency corrections is propagated using the pseudo-experiment method in which the correction factors are randomly shifted in an ensemble of pseudo-experiments according to the mean and standard deviation of the correction factor. This has negligible impact on the expected signal.

The uncertainties related to the photon energy scale and resolution affect the expected signal yield by 1% and 2%, respectively. The uncertainty due to imperfect knowledge of the photon angular resolution is estimated using electron clusters from the $\gamma\gamma \rightarrow e^+e^-$ process. The data–MC difference in the electron cluster ϕ resolution is applied as an extra smearing to photons from the signal MC sample. This results in a 2% shift of the signal yield, which is taken as a systematic uncertainty.

The uncertainty due to the choice of signal MC generator is estimated by using an alternative signal MC sample, as detailed in Section 3. This affects the signal yield by 1% which is taken as a systematic uncertainty. The uncertainty due to the limited signal MC sample size is 1%.

The uncertainties in the background estimation are evaluated as described in Section 6.

The uncertainty in the integrated luminosity of the data sample is 3.2%. It is derived from the calibration of the luminosity scale using x – y beam-separation scans, following a methodology similar to that detailed in Ref. [58], and using the LUCID-2 detector for the baseline luminosity measurements.

Systematic uncertainties associated with the background estimate, the photon PID and reconstruction efficiency, photon energy scale, and photon angular and energy resolution are fully correlated between the 2015 and 2018 data-taking periods. Systematic uncertainties in the trigger efficiency are computed separately for each data-taking period. They are dominated by the statistical uncertainty of each data set and are thus uncorrelated.

8 Results

8.1 Kinematic distributions

Photon kinematic distributions comparing the selected data with the sum of expected event yields from simulated signal and background processes in the signal region are shown in Figure 7. In total, 97 events are

Source of uncertainty	Detector correction (C)
	0.263 ± 0.021
Trigger efficiency	5%
Photon reco. efficiency	4%
Photon PID efficiency	2%
Photon energy scale	1%
Photon energy resolution	2%
Photon angular resolution	2%
Alternative signal MC	1%
Signal MC statistics	1%
Total	8%

Table 1: The detector correction factor, C , and its uncertainties for the integrated fiducial cross-section measurement. The second row lists the numerical value of C together with the total uncertainty. The total uncertainty on C is a quadratic sum of systematic and statistical components.

observed in data where 45 signal events and 27 background events are expected. This excess of observed events is visible in all distributions shown in Figure 7.

8.2 Integrated fiducial cross section

The inclusive cross section for the $\gamma\gamma \rightarrow \gamma\gamma$ process is measured in a fiducial phase space, defined by the following requirements on the diphoton final state, reflecting the selection at reconstruction level: both photons have to be within $|\eta| < 2.4$ with a transverse momentum of $p_T > 2.5$ GeV. The invariant mass of the diphoton system has to be $m_{\gamma\gamma} > 5$ GeV with transverse momentum of $p_T^{\gamma\gamma} < 1$ GeV. In addition, the photons must fulfil an acoplanarity requirement of $A_\phi < 0.01$.

The integrated fiducial cross section is obtained as follows:

$$\sigma_{\text{fid}} = \frac{N_{\text{data}} - N_{\text{bkg}}}{C \times \int L dt}, \quad (1)$$

where $N_{\text{data}} = 97$ is the number of selected events in data, $N_{\text{bkg}} = 27 \pm 5$ is the number of background events, $\int L dt = 2.22 \pm 0.07 \text{ nb}^{-1}$ is the integrated luminosity of the data sample and $C = 0.263 \pm 0.021$ is the overall correction factor that accounts for detector efficiencies and resolution effects, and for signal events passing the event selection but originating from outside the fiducial phase space (fiducial corrections). The C factor is defined as the ratio of the number of reconstructed MC signal events passing the selection to the number of generated MC signal events satisfying the fiducial requirements.

The uncertainty in C is estimated by varying the data/MC correction factors within their uncertainties as described in Section 7, in particular for the photon reconstruction and PID efficiencies, photon energy scale and resolution and trigger efficiency. An overview of the various uncertainties in C is given in Table 1.

The uncertainty in N_{bkg} is dominated by the uncertainty in the $\gamma\gamma \rightarrow e^+e^-$ background. This has a 6% impact on the estimated integrated fiducial cross section.

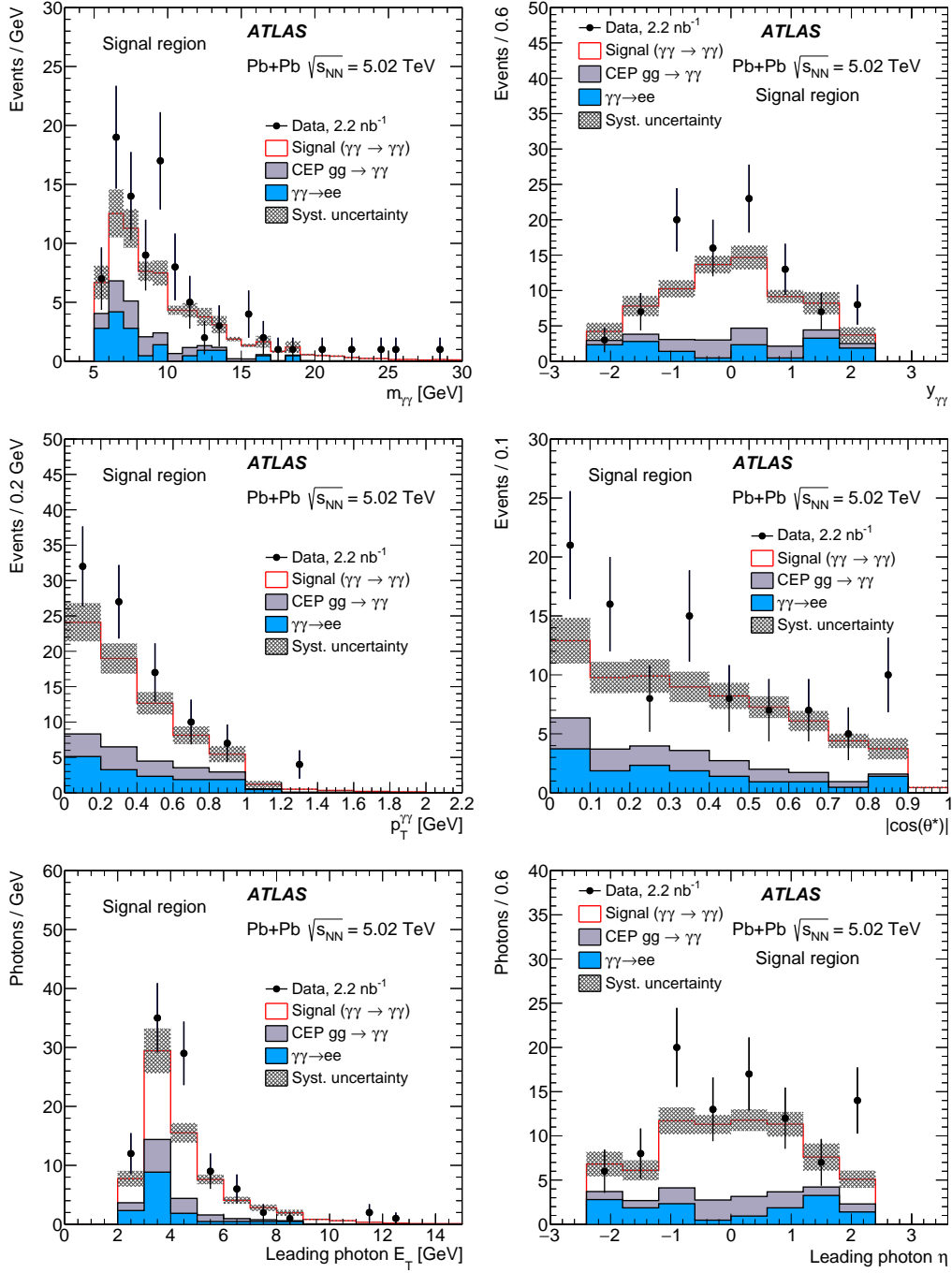


Figure 7: Kinematic distributions for $\gamma\gamma \rightarrow \gamma\gamma$ event candidates: diphoton invariant mass (top-left), diphoton rapidity (top-right), diphoton transverse momentum (mid-left), diphoton $|\cos(\theta^*)|$ (mid-right), leading photon transverse energy (bottom-left) and leading photon pseudorapidity (bottom-right). Data (points) are compared with the sum of signal and background expectations (histograms). The signal prediction is normalised to the same integrated luminosity as the data. Systematic uncertainties in the signal and background processes, excluding that in the luminosity, are shown as shaded bands.

The measured integrated fiducial cross section is $\sigma_{\text{fid}} = 120 \pm 17$ (stat.) ± 13 (syst.) ± 4 (lumi.) nb, which can be compared with the predicted values of 80 ± 8 nb from Ref. [37] and 78 ± 8 nb from the SuperChic v3.0 MC generator [34]. The data-to-theory ratios are 1.50 ± 0.32 and 1.54 ± 0.32 , respectively.

The theoretical uncertainty in the cross section is primarily due to limited knowledge of the nuclear (EM) form-factors and the related initial photon fluxes. This is extensively studied in Ref. [59] and the relevant uncertainty is estimated to be 10% within the fiducial phase space of the measurement. For masses below 100 GeV, this uncertainty does not exhibit a dependence on the diphoton mass. Higher-order corrections (not included in the calculations) are also part of the theoretical uncertainty and are of the order of 1–3% in the corresponding invariant mass range [35, 36].

8.3 Differential fiducial cross sections

Differential fiducial cross sections as a function of diphoton invariant mass, diphoton absolute rapidity, average photon transverse momentum and diphoton $|\cos \theta^*|$ are unfolded to particle level in the fiducial phase space described in the previous section.

The differential fiducial cross sections are determined using an iterative Bayesian unfolding method [60] with one iteration for all distributions. The unfolding procedure corrects for bin migrations between particle- and detector-level distributions due to detector resolution effects, and applies reconstruction efficiency as well as fiducial corrections. The reconstruction efficiency corrects for events inside the fiducial region that are not reconstructed in the signal region due to detector inefficiencies; the fiducial corrections take into account events that are reconstructed in the signal region, but originate from outside the fiducial region. The background contributions are subtracted from data prior to unfolding.

The statistical uncertainty of the data is estimated using 1000 Poisson-distributed pseudo-data sets, constructed by smearing the observed number of events in each bin of the detector-level distribution. The root mean square of the differences between the resulting unfolded distributions and the unfolded data is taken as the statistical uncertainty in each bin.

In the measurement of differential fiducial cross sections, the full set of experimental systematic uncertainties described in Section 7 is considered. In addition, uncertainties due to the unfolding procedure and the modelling of the signal process are considered by repeating the cross-section extraction with modified inputs [61]. The distributions are reweighted at generator level to obtain better agreement between data and simulation after event reconstruction. The obtained prediction at detector level, which is then similar to data, is unfolded with the input of the default unfolding and the difference from the reweighted prediction at generator level is considered as an uncertainty. The size of this uncertainty is typically below 1%. The impact of statistical uncertainties in the signal simulation is estimated using pseudo-data and is found to be 1–3%.

The unfolded differential fiducial cross sections are shown in Figure 8. They are compared with the predictions from SuperChic v3.0, which provide a fair description of the data, except for the overall normalisation differences. For nearly all variables and bins the total uncertainties in the cross-section measurements are dominated by statistical uncertainties, ranging from 25% to 75%. The background systematic uncertainties are large and comparable to statistical uncertainties in some bins (up to 40%, mainly at high $|y_{\gamma\gamma}|$) due to the limited number of events in the data control regions. Global χ^2 comparisons are carried out for the shapes of differential distributions. They do not display any significant differences between predictions and data, with the largest χ^2 per degree of freedom being 4.3/3 when comparing the

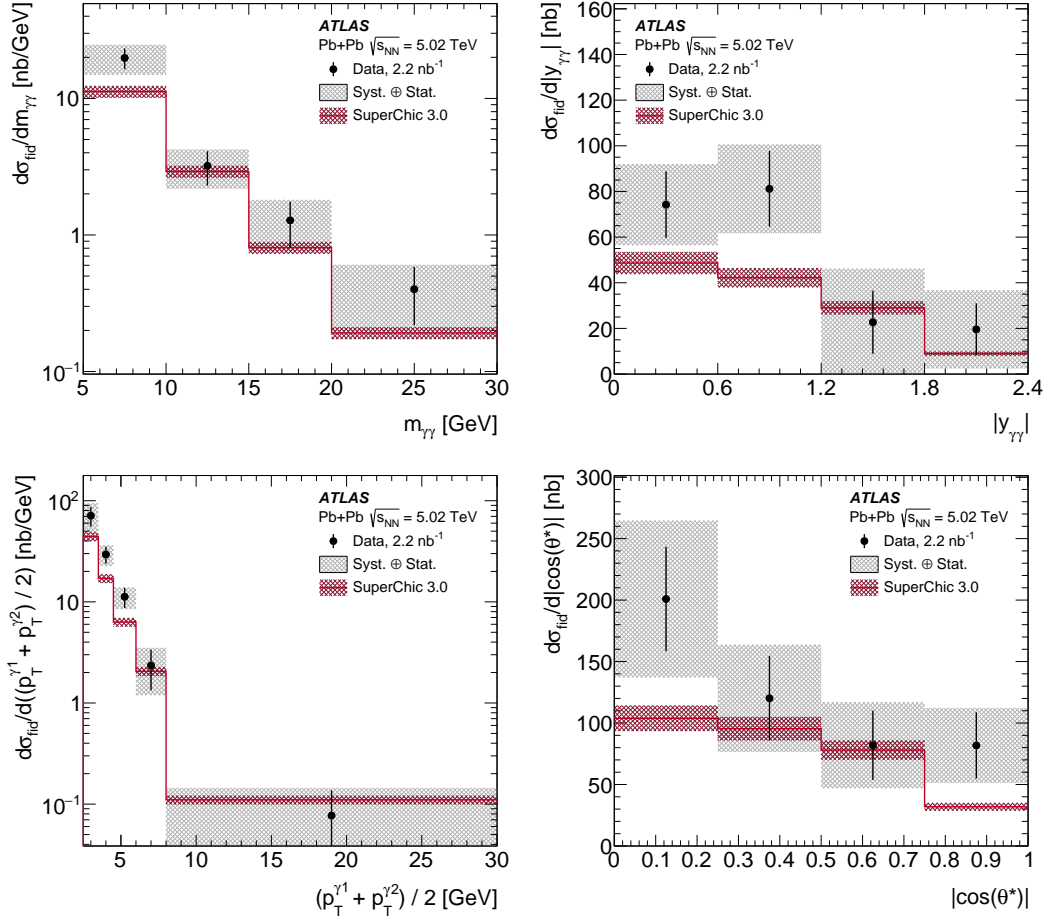


Figure 8: Measured differential fiducial cross sections of $\gamma\gamma \rightarrow \gamma\gamma$ production in Pb+Pb collisions at $\sqrt{s_{\text{NN}}} = 5.02$ TeV for four observables (from left to right and top to bottom): diphoton invariant mass, diphoton absolute rapidity, average photon transverse momentum and diphoton $|\cos(\theta^*)|$. The measured cross-section values are shown as points with error bars giving the statistical uncertainty and grey bands indicating the size of the total uncertainty. The results are compared with the prediction from the SuperChic v3.0 MC generator (solid line) with bands denoting the theoretical uncertainty.

shape of $|\cos(\theta^*)|$ distribution. The $m_{\gamma\gamma}$ differential fiducial distribution is measured up to $m_{\gamma\gamma} = 30$ GeV. For $m_{\gamma\gamma} > 30$ GeV, no events are observed in data versus a total expectation of 0.8 events.

The cross sections for all distributions shown in this paper, including normalised differential fiducial cross sections, are available in HepData [62].

8.4 Search for ALP production

Any particle coupling directly to photons could be produced in an s -channel process in photon–photon collisions, leading to a resonance peak in the invariant mass spectrum. One popular candidate for producing a narrow diphoton resonance is an axion-like particle (ALP) [12]. The measured diphoton invariant mass spectrum, as shown in Figure 7, is used to search for $\gamma\gamma \rightarrow a \rightarrow \gamma\gamma$ process, where a denotes the ALP.

The LbyL, $\gamma\gamma \rightarrow e^+e^-$ and CEP $gg \rightarrow \gamma\gamma$ processes are considered as background. The contribution from $\gamma\gamma \rightarrow e^+e^-$ and CEP $gg \rightarrow \gamma\gamma$ processes is estimated using data-driven techniques as described in Section 6. The LbyL background is estimated using simulated events generated with SuperChic v3.0. These events are normalised to the data yield, after subtracting $\gamma\gamma \rightarrow e^+e^-$ and CEP $gg \rightarrow \gamma\gamma$ contributions and excluding the mass search region. To smooth statistical fluctuations in the background shape at high mass, a Crystal Ball function is fitted to the sum of all background contributions, while assigning the fit residuals as additional systematic uncertainty.

Events simulated with STARlight v2.0 [39], which implements the ALP couplings as described in Ref. [12], for various ALP masses between 5 GeV and 100 GeV are used to build an analytical model of the ALP signal, interpolating between the simulated mass points. The efficiency of ALP events to satisfy the selection criteria (outlined in Section 4) is about 20% for $m_a = 6$ GeV and increases up to 45% for $m_a = 12$ GeV. An efficiency plateau of about 80% is reached for an ALP mass around 40 GeV. The diphoton invariant mass resolution for simulated ALP signal ranges from 0.5 GeV at $m_a = 6$ GeV to 1.5 GeV at $m_a = 100$ GeV and is dominated by the photon energy resolution. The impact of the uncertainty on the primary-vertex position has a subdominant effect on the diphoton invariant mass resolution over the full mass range.

In every analysis bin a cut-and-count analysis is performed to estimate the expected numbers of background and signal events. The bin-width is chosen to include at least 80% of a reconstructed ALP signal peak within a given bin and ranges from 2 GeV to 20 GeV. To cover the entire mass range, the analysis bins overlap and have an equidistant distance of 1 GeV between the bin centres. The signal contribution is fitted individually for every bin using a maximum-likelihood fit implemented in the HistFitter software [63–65] which is based on HistFactory [66], RooFit [67] and RooStats [68].

Since no significant deviation from the background-only hypothesis is observed, the result is then used to estimate the upper limit on the ALP signal strength (μ_{CLs}) at 95% confidence level (CL). The corresponding test-statistic distributions are evaluated using pseudo-experiments.

Experimental systematic uncertainties affecting the ALP signal model originate from the trigger, photon PID and reconstruction efficiencies, and photon energy scale and resolution. The systematic uncertainties are evaluated identically to the treatment in the cross-section measurements, described in Section 7. The theoretical uncertainty in the calculated ALP signal cross section is 10% in the full mass range, due to the limited knowledge of the initial photon fluxes [59]. This uncertainty is considered uncorrelated with other sources of uncertainty.

The limits set on the signal strength μ_{CLs} are transformed into limits on the cross section $\sigma_{\gamma\gamma \rightarrow a \rightarrow \gamma\gamma}^{\text{CLs}} = \mu_{\text{CLs}} \cdot \sigma_{a,\text{gen}}^{\text{MC}}$. Additionally, limits on the ALP coupling to photons ($1/\Lambda_a^{\text{CLs}}$) are calculated from $1/\Lambda_a^{\text{CLs}} = \sqrt{\mu_{\text{CLs}}} \cdot 1/\Lambda_a^{\text{gen}}$. $\sigma_{a,\text{gen}}^{\text{MC}}$ and Λ_a^{gen} are the cross section and coupling used in the MC generator. The observed and expected 95% CL limits on the ALP production cross section and ALP coupling to photons are presented in Figure 9. The limits set on the cross section $\sigma_{\gamma\gamma \rightarrow a \rightarrow \gamma\gamma}$ for an ALP with a mass of 6–100 GeV range from 70 nb to 2 nb. The derived constraints on $1/\Lambda_a$ range from 0.3 TeV⁻¹ to 0.06 TeV⁻¹. The widths of the one- and two-standard-deviation bands of the expected limit distribution decrease for ALP masses above 30 GeV. This behaviour is driven by the change in the background rate, which has a low Poisson mean for high ALP masses. For low ALP masses the background rate is sufficiently high to populate the $N > 0$ expected background outcomes and raise the +1 and +2-standard-deviation boundaries. The discontinuity at $m_a = 70$ GeV is caused by the increase of the mass-bin width which brings an increase in signal acceptance.

Assuming a 100% ALP decay branching fraction into photons, the derived constraints on the ALP mass and its coupling to photons are compared in Figure 10 with those obtained from various experiments [27, 69–72]. The exclusion limits from this analysis are the strongest so far for the mass range of $6 < m_a < 100$ GeV.

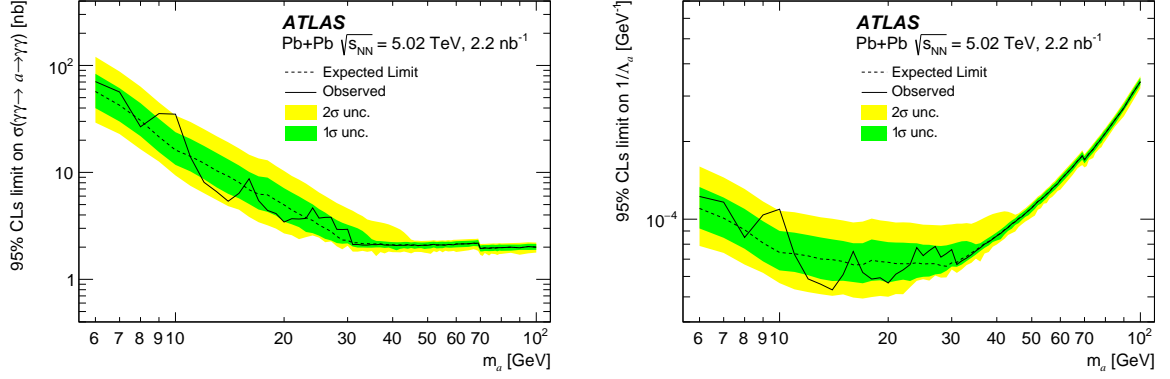


Figure 9: The 95% CL upper limit on the ALP cross section $\sigma_{\gamma\gamma \rightarrow a \rightarrow \gamma\gamma}$ (left) and ALP coupling $1/\Lambda_a$ (right) for the $\gamma\gamma \rightarrow a \rightarrow \gamma\gamma$ process as a function of ALP mass m_a . The observed upper limit is shown as a solid black line and the expected upper limit is shown by the dashed black line with its ± 1 and ± 2 standard deviation bands. The discontinuity at $m_a = 70$ GeV is caused by the increase of the mass-bin width which brings an increase in signal acceptance.

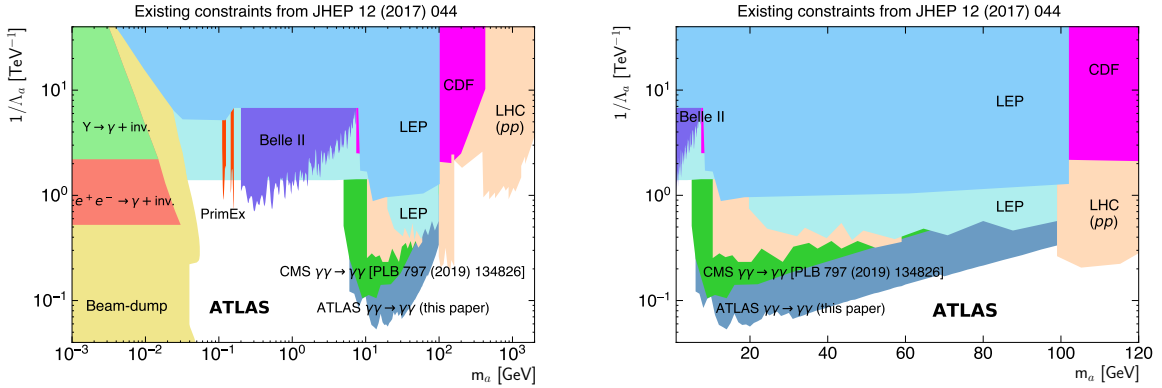


Figure 10: Compilation of exclusion limits at 95% CL in the ALP–photon coupling ($1/\Lambda_a$) versus ALP mass (m_a) plane obtained by different experiments. The existing limits, derived from Refs. [27, 69–72] are compared with the limits extracted from this measurement. The exclusion limits labelled “LHC (pp)” are based on pp collision data from ATLAS and CMS. All measurements assume a 100% ALP decay branching fraction into photons. The plot on the right is a zoomed-in version covering the range $1 < m_a < 120$ GeV.

9 Conclusions

This paper presents a measurement of the light-by-light scattering process in quasi-real photon interactions from ultra-peripheral Pb+Pb collisions at $\sqrt{s_{\text{NN}}} = 5.02$ TeV by the ATLAS experiment at the LHC. The measurement is based on the full Run 2 data set corresponding to an integrated luminosity of 2.2 nb^{-1} . After the selection criteria, 97 events are selected in the data while 27 ± 5 background events are expected. The dominant background processes are estimated using data-driven methods.

After background subtraction and corrections for detector effects are applied, the integrated fiducial cross section of the $\gamma\gamma \rightarrow \gamma\gamma$ process is measured to be $\sigma_{\text{fid}} = 120 \pm 17$ (stat.) ± 13 (syst.) ± 4 (lumi.) nb. The data-to-theory ratios are 1.50 ± 0.32 and 1.54 ± 0.32 for predictions from Ref. [37] and from the SuperChic v3.0 MC generator, respectively. Differential fiducial cross sections are measured as a function of several properties of the final-state photons and are compared with Standard Model theory predictions for light-by-light scattering. All measured cross sections are consistent within 2 standard deviations with the predictions. The measurement precision is limited in all kinematic regions by statistical uncertainties.

The measured diphoton invariant mass distribution is used to search for axion-like particles and set new exclusion limits on their production in the $\text{Pb+Pb}(\gamma\gamma) \rightarrow \text{Pb}^{(*)} + \text{Pb}^{(*)} \gamma\gamma$ reaction. Integrated cross sections above 2 to 70 nb are excluded at the 95% CL, depending on the diphoton invariant mass in the range 6–100 GeV. These results provide, to this date and within the aforementioned mass range, the most stringent constraints in the search for ALP signals.

Acknowledgements

We thank CERN for the very successful operation of the LHC, as well as the support staff from our institutions without whom ATLAS could not be operated efficiently.

We acknowledge the support of ANPCyT, Argentina; YerPhI, Armenia; ARC, Australia; BMFWF and FWF, Austria; ANAS, Azerbaijan; SSTC, Belarus; CNPq and FAPESP, Brazil; NSERC, NRC and CFI, Canada; CERN; ANID, Chile; CAS, MOST and NSFC, China; COLCIENCIAS, Colombia; MSMT CR, MPO CR and VSC CR, Czech Republic; DNRF and DNSRC, Denmark; IN2P3-CNRS and CEA-DRF/IRFU, France; SRNSFG, Georgia; BMBF, HGF and MPG, Germany; GSRT, Greece; RGC and Hong Kong SAR, China; ISF and Benozziyo Center, Israel; INFN, Italy; MEXT and JSPS, Japan; CNRST, Morocco; NWO, Netherlands; RCN, Norway; MNiSW and NCN, Poland; FCT, Portugal; MNE/IFA, Romania; JINR; MES of Russia and NRC KI, Russian Federation; MESTD, Serbia; MSSR, Slovakia; ARRS and MIZŠ, Slovenia; DST/NRF, South Africa; MICINN, Spain; SRC and Wallenberg Foundation, Sweden; SERI, SNSF and Cantons of Bern and Geneva, Switzerland; MOST, Taiwan; TAEK, Turkey; STFC, United Kingdom; DOE and NSF, United States of America. In addition, individual groups and members have received support from BCKDF, CANARIE, Compute Canada, CRC and IVADO, Canada; Beijing Municipal Science & Technology Commission, China; COST, ERC, ERDF, Horizon 2020 and Marie Skłodowska-Curie Actions, European Union; Investissements d’Avenir Labex, Investissements d’Avenir Idex and ANR, France; DFG and AvH Foundation, Germany; Herakleitos, Thales and Aristeia programmes co-financed by EU-ESF and the Greek NSRF, Greece; BSF-NSF and GIF, Israel; La Caixa Banking Foundation, CERCA Programme Generalitat de Catalunya and PROMETEO and GenT Programmes Generalitat Valenciana, Spain; Göran Gustafssons Stiftelse, Sweden; The Royal Society and Leverhulme Trust, United Kingdom.

The crucial computing support from all WLCG partners is acknowledged gratefully, in particular from CERN, the ATLAS Tier-1 facilities at TRIUMF (Canada), NDGF (Denmark, Norway, Sweden), CC-IN2P3 (France), KIT/GridKA (Germany), INFN-CNAF (Italy), NL-T1 (Netherlands), PIC (Spain), ASGC (Taiwan), RAL (UK) and BNL (USA), the Tier-2 facilities worldwide and large non-WLCG resource providers. Major contributors of computing resources are listed in Ref. [73].

References

- [1] A. J. Baltz et al., *The physics of ultraperipheral collisions at the LHC*, *Phys. Rept.* **458** (2008) 1, arXiv: [0706.3356 \[nucl-ex\]](#).
- [2] S. R. Klein and P. Steinberg, *Photonuclear and Two-Photon Interactions at High-Energy Nuclear Colliders*, *Annu. Rev. Nucl. Part. Sci.* **70** (2020) 323, arXiv: [2005.01872 \[nucl-ex\]](#).
- [3] E. Fermi, *Sulla teoria dell' urto tra atomi e corpuscoli elettrici*, *Nuovo Cim.* **2** (1925) 143, arXiv: [hep-th/0205086](#).
- [4] C. F. Weizsäcker, *Ausstrahlung bei Stößen sehr schneller Elektronen*, *Z. Phys.* **88** (1934) 612.
- [5] E. J. Williams, *Nature of the High Energy Particles of Penetrating Radiation and Status of Ionization and Radiation Formulae*, *Phys. Rev.* **45** (1934) 729.
- [6] ALICE Collaboration, *Measurement of the Cross Section for Electromagnetic Dissociation with Neutron Emission in Pb-Pb Collisions at $\sqrt{s_{NN}} = 2.76$ TeV*, *Phys. Rev. Lett.* **109** (2012) 252302, arXiv: [1203.2436 \[nucl-ex\]](#).
- [7] S. Fichtel, G. von Gersdorff, B. Lenzi, C. Royon and M. Saimpert, *Light-by-light scattering with intact protons at the LHC: from standard model to new physics*, *JHEP* **02** (2015) 165, arXiv: [1411.6629 \[hep-ph\]](#).
- [8] S. C. Inan and A. V. Kisselev, *Probe of the Randall-Sundrum-like model with the small curvature via light-by-light scattering at the LHC*, *Phys. Rev. D* **100** (2019) 095004, arXiv: [1902.08615 \[hep-ph\]](#).
- [9] J. Ellis, N. E. Mavromatos and T. You, *Light-by-Light Scattering Constraint on Born-Infeld Theory*, *Phys. Rev. Lett.* **118** (2017) 261802, arXiv: [1703.08450 \[hep-ph\]](#).
- [10] V. A. Kostelecky and Z. Li, *Gauge field theories with Lorentz-violating operators of arbitrary dimension*, *Phys. Rev. D* **99** (2019) 056016, arXiv: [1812.11672 \[hep-ph\]](#).
- [11] R. Horvat, D. Latas, J. Trampetić and J. You, *Light-by-light scattering and spacetime noncommutativity*, *Phys. Rev. D* **101** (2020) 095035, arXiv: [2002.01829 \[hep-ph\]](#).
- [12] S. Knapen, T. Lin, H. K. Lou and T. Melia, *Searching for Axionlike Particles with Ultraperipheral Heavy-Ion Collisions*, *Phys. Rev. Lett.* **118** (2017) 171801, arXiv: [1607.06083 \[hep-ph\]](#).
- [13] ATLAS Collaboration, *Search for new phenomena in events with at least three photons collected in pp collisions at $\sqrt{s} = 8$ TeV with the ATLAS detector*, *Eur. Phys. J. C* **76** (2016) 210, arXiv: [1509.05051 \[hep-ex\]](#).

- [14] ATLAS Collaboration, *Search for pairs of highly collimated photon-jets in pp collisions at $\sqrt{s} = 13$ TeV with the ATLAS detector*, *Phys. Rev. D* **99** (2019) 012008, arXiv: [1808.10515 \[hep-ex\]](#).
- [15] D. Hanneke, S. Fogwell and G. Gabrielse, *New Measurement of the Electron Magnetic Moment and the Fine Structure Constant*, *Phys. Rev. Lett.* **100** (2008) 120801, arXiv: [0801.1134 \[physics.atom-ph\]](#).
- [16] Muon $g - 2$ Collaboration, *Final report of the muon E821 anomalous magnetic moment measurement at BNL*, *Phys. Rev. D* **73** (2006) 072003, arXiv: [hep-ex/0602035 \[hep-ex\]](#).
- [17] R. R. Wilson, *Scattering of 1.33 MeV Gamma-Rays by an Electric Field*, *Phys. Rev.* **90** (1953) 720.
- [18] G. Jarlskog et al., *Measurement of Delbrück Scattering and Observation of Photon Splitting at High Energies*, *Phys. Rev. D* **8** (1973) 3813.
- [19] M. Schumacher, I. Borchert, F. Smend and P. Rullhusen, *Delbrück scattering of 2.75 MeV photons by lead*, *Phys. Lett. B* **59** (1975) 134.
- [20] S. Z. Akhmadaliev et al., *Delbrück scattering at energies of 140 – 450 MeV*, *Phys. Rev. C* **58** (1998) 2844.
- [21] S. Z. Akhmadaliev et al., *Experimental Investigation of High-Energy Photon Splitting in Atomic Fields*, *Phys. Rev. Lett.* **89** (2002) 061802, arXiv: [hep-ex/0111084](#).
- [22] JADE Collaboration, *A measurement of the η radiative width $\Gamma_{\eta \rightarrow \gamma\gamma}$* , *Phys. Lett. B* **158** (1985) 511.
- [23] TPC/Two-Gamma Collaboration, *Study of η formation in photon-photon collisions*, *Phys. Rev. D* **33** (1986) 844.
- [24] D. A. Williams et al., *Formation of the pseudoscalars π^0 , η , and η' in the reaction $\gamma\gamma \rightarrow \gamma\gamma$* , *Phys. Rev. D* **38** (1988) 1365.
- [25] D. d’Enterria and G. G. da Silveira, *Observing Light-by-Light Scattering at the Large Hadron Collider*, *Phys. Rev. Lett.* **111** (2013) 080405, [Erratum: *Phys. Rev. Lett.* **116** (2016) 129901], arXiv: [1305.7142 \[hep-ph\]](#).
- [26] ATLAS Collaboration, *Evidence for light-by-light scattering in heavy-ion collisions with the ATLAS detector at the LHC*, *Nature Phys.* **13** (2017) 852, arXiv: [1702.01625 \[hep-ex\]](#).
- [27] CMS Collaboration, *Evidence for light-by-light scattering and searches for axion-like particles in ultraperipheral PbPb collisions at $\sqrt{s_{NN}} = 5.02$ TeV*, *Phys. Lett. B* **797** (2019) 134826, arXiv: [1810.04602 \[hep-ex\]](#).
- [28] ATLAS Collaboration, *Observation of Light-by-Light Scattering in Ultraperipheral Pb+Pb Collisions with the ATLAS Detector*, *Phys. Rev. Lett.* **123** (2019) 052001, arXiv: [1904.03536 \[hep-ex\]](#).
- [29] ATLAS Collaboration, *The ATLAS experiment at the CERN Large Hadron Collider*, *JINST* **3** (2008) S08003.

- [30] ATLAS Collaboration, *ATLAS Insertable B-Layer Technical Design Report*, ATLAS-TDR-19, 2010, URL: <https://cds.cern.ch/record/1291633>,
ATLAS Insertable B-Layer Technical Design Report Addendum, ATLAS-TDR-19-ADD-1, 2012, URL: <https://cds.cern.ch/record/1451888>.
- [31] B. Abbott et al., *Production and Integration of the ATLAS Insertable B-Layer*, *JINST* **13** (2018) T05008, arXiv: [1803.00844](https://arxiv.org/abs/1803.00844) [[physics.ins-det](#)].
- [32] G. Avoni et al., *The new LUCID-2 detector for luminosity measurement and monitoring in ATLAS*, *JINST* **13** (2018) P07017.
- [33] ATLAS Collaboration, *Performance of the ATLAS trigger system in 2015*, *Eur. Phys. J. C* **77** (2017) 317, arXiv: [1611.09661](https://arxiv.org/abs/1611.09661) [[hep-ex](#)].
- [34] L. A. Harland-Lang, V. A. Khoze and M. G. Ryskin, *Exclusive LHC physics with heavy ions: SuperChic 3*, *Eur. Phys. J. C* **79** (2019) 39, arXiv: [1810.06567](https://arxiv.org/abs/1810.06567) [[hep-ph](#)].
- [35] Z. Bern, A. De Freitas, L. J. Dixon, A. Ghinculov and H. L. Wong, *QCD and QED corrections to light-by-light scattering*, *JHEP* **11** (2001) 031, arXiv: [hep-ph/0109079](https://arxiv.org/abs/hep-ph/0109079).
- [36] M. Klusek-Gawenda, W. Schäfer and A. Szczurek, *Two-gluon exchange contribution to elastic $\gamma\gamma \rightarrow \gamma\gamma$ scattering and production of two-photons in ultraperipheral ultrarelativistic heavy ion and proton-proton collisions*, *Phys. Lett. B* **761** (2016) 399, arXiv: [1606.01058](https://arxiv.org/abs/1606.01058).
- [37] M. Klusek-Gawenda, P. Lebiedowicz and A. Szczurek, *Light-by-light scattering in ultraperipheral Pb-Pb collisions at energies available at the CERN Large Hadron Collider*, *Phys. Rev. C* **93** (2016) 044907, arXiv: [1601.07001](https://arxiv.org/abs/1601.07001) [[nucl-th](#)].
- [38] M. Bähr et al., *Herwig++ physics and manual*, *Eur. Phys. J. C* **58** (2008) 639, arXiv: [0803.0883](https://arxiv.org/abs/0803.0883) [[hep-ph](#)].
- [39] S. R. Klein, J. Nystrand, J. Seger, Y. Gorbunov and J. Butterworth, *STARlight: A Monte Carlo simulation program for ultra-peripheral collisions of relativistic ions*, *Comput. Phys. Commun.* **212** (2017) 258, arXiv: [1607.03838](https://arxiv.org/abs/1607.03838) [[hep-ph](#)].
- [40] T. Sjöstrand et al., *An introduction to PYTHIA 8.2*, *Comput. Phys. Commun.* **191** (2015) 159, arXiv: [1410.3012](https://arxiv.org/abs/1410.3012) [[hep-ph](#)].
- [41] ATLAS Collaboration, *The ATLAS Simulation Infrastructure*, *Eur. Phys. J. C* **70** (2010) 823, arXiv: [1005.4568](https://arxiv.org/abs/1005.4568) [[physics.ins-det](#)].
- [42] GEANT4 Collaboration, S. Agostinelli et al., *GEANT4 – a simulation toolkit*, *Nucl. Instrum. Meth. A* **506** (2003) 250.
- [43] ATLAS Collaboration, *Measurement of the photon identification efficiencies with the ATLAS detector using LHC Run 2 data collected in 2015 and 2016*, *Eur. Phys. J. C* **79** (2019) 205, arXiv: [1810.05087](https://arxiv.org/abs/1810.05087) [[hep-ex](#)].
- [44] ATLAS Collaboration, *Electron and photon performance measurements with the ATLAS detector using the 2015–2017 LHC proton-proton collision data*, *JINST* **14** (2019) P12006, arXiv: [1908.00005](https://arxiv.org/abs/1908.00005) [[hep-ex](#)].
- [45] ATLAS Collaboration, *Electron reconstruction and identification in the ATLAS experiment using the 2015 and 2016 LHC proton-proton collision data at $\sqrt{s} = 13$ TeV*, *Eur. Phys. J. C* **79** (2019) 639, arXiv: [1902.04655](https://arxiv.org/abs/1902.04655) [[physics.ins-det](#)].

- [46] ALICE Collaboration, *Charmonium and e^+e^- pair photoproduction at mid-rapidity in ultra-peripheral Pb-Pb collisions at $\sqrt{s_{NN}}=2.76$ TeV*, *Eur. Phys. J. C* **73** (2013) 2617, arXiv: [1305.1467 \[nucl-ex\]](#).
- [47] L. A. Harland-Lang, A. D. Martin, P. Motylinski and R. S. Thorne, *Parton distributions in the LHC era: MMHT 2014 PDFs*, *Eur. Phys. J. C* **75** (2015) 204, arXiv: [1412.3989 \[hep-ph\]](#).
- [48] S. Dulat et al., *New parton distribution functions from a global analysis of quantum chromodynamics*, *Phys. Rev. D* **93** (2016) 033006, arXiv: [1506.07443 \[hep-ph\]](#).
- [49] NNPDF Collaboration, *Parton distributions from high-precision collider data*, *Eur. Phys. J. C* **77** (2017) 663, arXiv: [1706.00428 \[hep-ph\]](#).
- [50] J. Alwall et al., *The automated computation of tree-level and next-to-leading order differential cross sections, and their matching to parton shower simulations*, *JHEP* **07** (2014) 079, arXiv: [1405.0301 \[hep-ph\]](#).
- [51] D. Ebert, R. N. Faustov and V. O. Galkin, *Properties of heavy quarkonia and B_c mesons in the relativistic quark model*, *Phys. Rev. D* **67** (2003) 014027, arXiv: [hep-ph/0210381](#).
- [52] J. Segovia, P. G. Ortega, D. R. Entem and F. Fernandez, *Bottomonium spectrum revisited*, *Phys. Rev. D* **93** (2016) 074027, arXiv: [1601.05093 \[hep-ph\]](#).
- [53] C. A. Bertulani and G. Baur, *Electromagnetic processes in relativistic heavy ion collisions*, *Phys. Rept.* **163** (1988) 299.
- [54] M. Klusek-Gawenda and A. Szczurek, *Exclusive production of large invariant mass pion pairs in ultraperipheral ultrarelativistic heavy ion collisions*, *Phys. Lett. B* **700** (2011) 322, arXiv: [1104.0571 \[nucl-th\]](#).
- [55] M. Klusek-Gawenda, R. McNulty, R. Schicker and A. Szczurek, *Light-by-light scattering in ultraperipheral heavy-ion collisions at low diphoton masses*, *Phys. Rev. D* **99** (2019) 093013, arXiv: [1904.01243 \[hep-ph\]](#).
- [56] L.A. Harland-Lang, V.A. Khoze, M.G. Ryskin, W.J. Stirling, *Central exclusive meson pair production in the perturbative regime at hadron colliders*, *Eur. Phys. J. C* **71** (2011) 1714, arXiv: [1105.1626 \[hep-ph\]](#).
- [57] L.A. Harland-Lang, V.A. Khoze, M.G. Ryskin, W.J. Stirling, *Central exclusive production as a probe of the gluonic component of the η' and η mesons*, *Eur. Phys. J. C* **73** (2013) 2429, arXiv: [1302.2004 \[hep-ph\]](#).
- [58] ATLAS Collaboration, *Luminosity determination in pp collisions at $\sqrt{s} = 13$ TeV using the ATLAS detector at the LHC*, ATLAS-CONF-2019-021, 2019, URL: <https://cds.cern.ch/record/2677054>.
- [59] C. Azevedo, V. P. Goncalves and B. D. Moreira, *Exclusive dilepton production in ultraperipheral PbPb collisions at the LHC*, *Eur. Phys. J. C* **79** (2019) 432, arXiv: [1902.00268 \[hep-ph\]](#).
- [60] G. D'Agostini, *A Multidimensional unfolding method based on Bayes' theorem*, *Nucl. Instrum. Meth. A* **362** (1995) 487.

- [61] B. Malaescu, *An Iterative, dynamically stabilized method of data unfolding*, (2009), arXiv: [0907.3791](https://arxiv.org/abs/0907.3791) [[physics.data-an](#)].
- [62] *High Energy Physics Data Repository*, URL: <https://hepdata.net>.
- [63] A. L. Read, *Presentation of search results: The CL(s) technique*, *J. Phys. G* **28** (2002) 2693, ed. by M. Whalley and L. Lyons.
- [64] M. Baak et al., *HistFitter software framework for statistical data analysis*, *Eur. Phys. J. C* **75** (2015) 153, arXiv: [1410.1280](https://arxiv.org/abs/1410.1280) [[hep-ex](#)].
- [65] G. Cowan, K. Cranmer, E. Gross and O. Vitells, *Asymptotic formulae for likelihood-based tests of new physics*, *Eur. Phys. J. C* **71** (2011) 1554, [Erratum: *Eur. Phys. J. C* **73** (2013) 2501], arXiv: [1007.1727](https://arxiv.org/abs/1007.1727) [[physics.data-an](#)].
- [66] K. Cranmer, G. Lewis, L. Moneta, A. Shibata and W. Verkerke, *HistFactory: A tool for creating statistical models for use with RooFit and RooStats*, CERN-OPEN-2012-016, 2012, URL: <http://cdsweb.cern.ch/record/1456844>.
- [67] W. Verkerke and D. Kirkby, *The RooFit toolkit for data modeling*, 2003, arXiv: [physics/0306116](https://arxiv.org/abs/physics/0306116) [[physics.data-an](#)].
- [68] L. Moneta et al., *The RooStats Project*, *PoS ACAT* (2010) 057, arXiv: [1009.1003](https://arxiv.org/abs/1009.1003) [[physics.data-an](#)].
- [69] M. Bauer, M. Neubert and A. Thamm, *Collider probes of axion-like particles*, *JHEP* **12** (2017) 044, arXiv: [1708.00443](https://arxiv.org/abs/1708.00443) [[hep-ph](#)].
- [70] D. Aloni, C. Fanelli, Y. Soreq and M. Williams, *Photoproduction of Axionlike Particles*, *Phys. Rev. Lett.* **123** (2019) 071801, arXiv: [1903.03586](https://arxiv.org/abs/1903.03586) [[hep-ph](#)].
- [71] NA64 Collaboration, *Search for Axionlike and Scalar Particles with the NA64 Experiment*, *Phys. Rev. Lett.* **125** (2020) 081801, arXiv: [2005.02710](https://arxiv.org/abs/2005.02710) [[hep-ex](#)].
- [72] Belle II Collaboration, *Search for Axionlike Particles Produced in e^+e^- Collisions at Belle II*, *Phys. Rev. Lett.* **125** (2020) 161806, arXiv: [2007.13071](https://arxiv.org/abs/2007.13071) [[hep-ex](#)].
- [73] ATLAS Collaboration, *ATLAS Computing Acknowledgements*, ATL-SOFT-PUB-2020-001, URL: <https://cds.cern.ch/record/2717821>.

The ATLAS Collaboration

G. Aad¹⁰², B. Abbott¹²⁸, D.C. Abbott¹⁰³, A. Abed Abud³⁶, K. Abeling⁵³, D.K. Abhayasinghe⁹⁴, S.H. Abidi¹⁶⁷, O.S. AbouZeid⁴⁰, N.L. Abraham¹⁵⁶, H. Abramowicz¹⁶¹, H. Abreu¹⁶⁰, Y. Abulaiti⁶, B.S. Acharya^{67a,67b,n}, B. Achkar⁵³, L. Adam¹⁰⁰, C. Adam Bourdarios⁵, L. Adamczyk^{84a}, L. Adamek¹⁶⁷, J. Adelman¹²¹, M. Adersberger¹¹⁴, A. Adiguzel^{12c,ae}, S. Adorni⁵⁴, T. Adye¹⁴³, A.A. Affolder¹⁴⁵, Y. Afik¹⁶⁰, C. Agapopoulou⁶⁵, M.N. Agaras³⁸, A. Aggarwal¹¹⁹, C. Agheorghiesei^{27c}, J.A. Aguilar-Saavedra^{139f,139a,ad}, A. Ahmad³⁶, F. Ahmadov⁸⁰, W.S. Ahmed¹⁰⁴, X. Ai¹⁸, G. Aielli^{74a,74b}, S. Akatsuka⁸⁶, M. Akbiyik¹⁰⁰, T.P.A. Åkesson⁹⁷, E. Akilli⁵⁴, A.V. Akimov¹¹¹, K. Al Houry⁶⁵, G.L. Alberghi^{23b,23a}, J. Albert¹⁷⁶, M.J. Alconada Verzini¹⁶¹, S. Alderweireldt³⁶, M. Aleksa³⁶, I.N. Aleksandrov⁸⁰, C. Alexa^{27b}, T. Alexopoulos¹⁰, A. Alfonsi¹²⁰, F. Alfonsi^{23b,23a}, M. Alhroob¹²⁸, B. Ali¹⁴¹, S. Ali¹⁵⁸, M. Aliev¹⁶⁶, G. Alimonti^{69a}, C. Allaire³⁶, B.M.M. Allbrooke¹⁵⁶, B.W. Allen¹³¹, P.P. Allport²¹, A. Aloisio^{70a,70b}, F. Alonso⁸⁹, C. Alpigiani¹⁴⁸, E. Alunno Camelia^{74a,74b}, M. Alvarez Estevez⁹⁹, M.G. Alviggi^{70a,70b}, Y. Amaral Coutinho^{81b}, A. Ambler¹⁰⁴, L. Ambroz¹³⁴, C. Amelung²⁶, D. Amidei¹⁰⁶, S.P. Amor Dos Santos^{139a}, S. Amoroso⁴⁶, C.S. Amrouche⁵⁴, F. An⁷⁹, C. Anastopoulos¹⁴⁹, N. Andari¹⁴⁴, T. Andeen¹¹, J.K. Anders²⁰, S.Y. Andrean^{45a,45b}, A. Andreazza^{69a,69b}, V. Andrei^{61a}, C.R. Anelli¹⁷⁶, S. Angelidakis⁹, A. Angerami³⁹, A.V. Anisenkov^{122b,122a}, A. Annovi^{72a}, C. Antel⁵⁴, M.T. Anthony¹⁴⁹, E. Antipov¹²⁹, M. Antonelli⁵¹, D.J.A. Antrim¹⁷¹, F. Anulli^{73a}, M. Aoki⁸², J.A. Aparisi Pozo¹⁷⁴, M.A. Aparo¹⁵⁶, L. Aperio Bella⁴⁶, N. Aranzabal³⁶, V. Araujo Ferraz^{81a}, R. Araujo Pereira^{81b}, C. Arcangeletti⁵¹, A.T.H. Arce⁴⁹, F.A. Arduh⁸⁹, J-F. Arguin¹¹⁰, S. Argyropoulos⁵², J.-H. Arling⁴⁶, A.J. Armbruster³⁶, A. Armstrong¹⁷¹, O. Arnaez¹⁶⁷, H. Arnold¹²⁰, Z.P. Arrubarrena Tame¹¹⁴, G. Artoni¹³⁴, H. Asada¹¹⁷, K. Asai¹²⁶, S. Asai¹⁶³, T. Asawatavonvanich¹⁶⁵, N. Asbah⁵⁹, E.M. Asimakopoulou¹⁷², L. Asquith¹⁵⁶, J. Assahsah^{35d}, K. Assamagan²⁹, R. Astalos^{28a}, R.J. Atkin^{33a}, M. Atkinson¹⁷³, N.B. Atlay¹⁹, H. Atmani⁶⁵, K. Augsten¹⁴¹, V.A. Austrup¹⁸², G. Avolio³⁶, M.K. Ayoub^{15a}, G. Azeulos^{110,am}, H. Bachacou¹⁴⁴, K. Bachas¹⁶², F. Backman^{45a,45b}, P. Bagnaia^{73a,73b}, M. Bahmani⁸⁵, H. Bahrasemani¹⁵², A.J. Bailey¹⁷⁴, V.R. Bailey¹⁷³, J.T. Baines¹⁴³, C. Bakalis¹⁰, O.K. Baker¹⁸³, P.J. Bakker¹²⁰, E. Bakos¹⁶, D. Bakshi Gupta⁸, S. Balaji¹⁵⁷, R. Balasubramanian¹²⁰, E.M. Baldin^{122b,122a}, P. Balek¹⁸⁰, F. Balli¹⁴⁴, W.K. Balunas¹³⁴, J. Balz¹⁰⁰, E. Banas⁸⁵, M. Bandieramonte¹³⁸, A. Bandyopadhyay²⁴, Sw. Banerjee^{181,i}, L. Barak¹⁶¹, W.M. Barbe³⁸, E.L. Barberio¹⁰⁵, D. Barberis^{55b,55a}, M. Barbero¹⁰², G. Barbour⁹⁵, T. Barillari¹¹⁵, M-S. Barisits³⁶, J. Barkeloo¹³¹, T. Barklow¹⁵³, R. Barnea¹⁶⁰, B.M. Barnett¹⁴³, R.M. Barnett¹⁸, Z. Barnovska-Blenessy^{60a}, A. Baroncelli^{60a}, G. Barone²⁹, A.J. Barr¹³⁴, L. Barranco Navarro^{45a,45b}, F. Barreiro⁹⁹, J. Barreiro Guimarães da Costa^{15a}, U. Barron¹⁶¹, S. Barsov¹³⁷, F. Bartels^{61a}, R. Bartoldus¹⁵³, G. Bartolini¹⁰², A.E. Barton⁹⁰, P. Bartos^{28a}, A. Basalae⁴⁶, A. Basan¹⁰⁰, A. Bassalat^{65,aj}, M.J. Basso¹⁶⁷, R.L. Bates⁵⁷, S. Batlamous^{35e}, J.R. Batley³², B. Batool¹⁵¹, M. Battaglia¹⁴⁵, M. Baue^{73a,73b}, F. Bauer¹⁴⁴, P. Bauer²⁴, H.S. Bawa³¹, A. Bayirli^{12c}, J.B. Beacham⁴⁹, T. Beau¹³⁵, P.H. Beauchemin¹⁷⁰, F. Becherer⁵², P. Bechtel²⁴, H.C. Beck⁵³, H.P. Beck^{20,p}, K. Becker¹⁷⁸, C. Becot⁴⁶, A. Beddall^{12d}, A.J. Beddall^{12a}, V.A. Bednyakov⁸⁰, M. Bedognetti¹²⁰, C.P. Bee¹⁵⁵, T.A. Beermann¹⁸², M. Begalli^{81b}, M. Begel²⁹, A. Behera¹⁵⁵, J.K. Behr⁴⁶, F. Beisiegel²⁴, M. Belfkir⁵, A.S. Bell⁹⁵, G. Bella¹⁶¹, L. Bellagamba^{23b}, A. Bellerive³⁴, P. Bellos⁹, K. Beloborodov^{122b,122a}, K. Belotskiy¹¹², N.L. Belyaev¹¹², D. Bencheikroun^{35a}, N. Benekos¹⁰, Y. Benhammou¹⁶¹, D.P. Benjamin⁶, M. Benoit²⁹, J.R. Bensinger²⁶, S. Bentvelsen¹²⁰, L. Beresford¹³⁴, M. Beretta⁵¹, D. Berge¹⁹, E. Bergeaas Kuutmann¹⁷², N. Berger⁵, B. Bergmann¹⁴¹, L.J. Bergsten²⁶, J. Beringer¹⁸, S. Berlendis⁷, G. Bernardi¹³⁵, C. Bernius¹⁵³, F.U. Bernlochner²⁴, T. Berry⁹⁴, P. Berta¹⁰⁰, A. Berthold⁴⁸, I.A. Bertram⁹⁰, O. Bessidskaia Bylund¹⁸², N. Besson¹⁴⁴, A. Bethani¹⁰¹, S. Bethke¹¹⁵, A. Betti⁴², A.J. Bevan⁹³, J. Beyer¹¹⁵, D.S. Bhattacharya¹⁷⁷, P. Bhattarai²⁶, V.S. Bhopatkar⁶, R. Bi¹³⁸, R.M. Bianchi¹³⁸, O. Biebel¹¹⁴, D. Biedermann¹⁹, R. Bielski³⁶, K. Bierwagen¹⁰⁰, N.V. Biesuz^{72a,72b}, M. Biglietti^{75a}, T.R.V. Billoud¹⁴¹, M. Bindi⁵³, A. Bingul^{12d},

C. Bini^{73a,73b}, S. Biondi^{23b,23a}, C.J. Birch-sykes¹⁰¹, M. Birman¹⁸⁰, T. Bisanz³⁶, J.P. Biswal³, D. Biswas^{181,i}, A. Bitadze¹⁰¹, C. Bittrich⁴⁸, K. Bjørke¹³³, T. Blazek^{28a}, I. Bloch⁴⁶, C. Blocker²⁶, A. Blue⁵⁷, U. Blumenschein⁹³, G.J. Bobbink¹²⁰, V.S. Bobrovnikov^{122b,122a}, S.S. Bocchetta⁹⁷, D. Bogavac¹⁴, A.G. Bogdanchikov^{122b,122a}, C. Bohm^{45a}, V. Boisvert⁹⁴, P. Bokan^{172,53}, T. Bold^{84a}, A.E. Bolz^{61b}, M. Bomben¹³⁵, M. Bona⁹³, J.S. Bonilla¹³¹, M. Boonekamp¹⁴⁴, C.D. Booth⁹⁴, A.G. Borbély⁵⁷, H.M. Borecka-Bielska⁹¹, L.S. Borgna⁹⁵, A. Borisov¹²³, G. Borissov⁹⁰, D. Bortoletto¹³⁴, D. Boscherini^{23b}, M. Bosman¹⁴, J.D. Bossio Sola¹⁰⁴, K. Bouaouda^{35a}, J. Boudreau¹³⁸, E.V. Bouhova-Thacker⁹⁰, D. Boumediene³⁸, A. Boveia¹²⁷, J. Boyd³⁶, D. Boye^{33c}, I.R. Boyko⁸⁰, A.J. Bozson⁹⁴, J. Bracinik²¹, N. Brahim^{60d}, G. Brandt¹⁸², O. Brandt³², F. Braren⁴⁶, B. Brau¹⁰³, J.E. Brau¹³¹, W.D. Breaden Madden⁵⁷, K. Brendlinger⁴⁶, R. Brenner¹⁶⁰, L. Brenner³⁶, R. Brenner¹⁷², S. Bressler¹⁸⁰, B. Brickwedde¹⁰⁰, D.L. Briglin²¹, D. Britton⁵⁷, D. Britzger¹¹⁵, I. Brock²⁴, R. Brock¹⁰⁷, G. Brooijmans³⁹, W.K. Brooks^{146d}, E. Brost²⁹, P.A. Bruckman de Renstrom⁸⁵, B. Brüers⁴⁶, D. Bruncko^{28b}, A. Bruni^{23b}, G. Bruni^{23b}, M. Bruschi^{23b}, N. Brusino^{73a,73b}, L. Bryngemark¹⁵³, T. Buanes¹⁷, Q. Buat¹⁵⁵, P. Buchholz¹⁵¹, A.G. Buckley⁵⁷, I.A. Budagov⁸⁰, M.K. Bugge¹³³, F. Bühner⁵², O. Bulekov¹¹², B.A. Bullard⁵⁹, T.J. Burch¹²¹, S. Burdin⁹¹, C.D. Burgard¹²⁰, A.M. Burger¹²⁹, B. Burghgrave⁸, J.T.P. Burr⁴⁶, C.D. Burton¹¹, J.C. Burzynski¹⁰³, V. Büscher¹⁰⁰, E. Buschmann⁵³, P.J. Bussey⁵⁷, J.M. Butler²⁵, C.M. Buttar⁵⁷, J.M. Butterworth⁹⁵, P. Butti³⁶, W. Buttinger³⁶, C.J. Buxo Vazquez¹⁰⁷, A. Buzatu¹⁵⁸, A.R. Buzykaev^{122b,122a}, G. Cabras^{23b,23a}, S. Cabrera Urbán¹⁷⁴, D. Caforio⁵⁶, H. Cai¹³⁸, V.M.M. Cairo¹⁵³, O. Cakir^{4a}, N. Calace³⁶, P. Calafiura¹⁸, G. Calderini¹³⁵, P. Calfayan⁶⁶, G. Callea⁵⁷, L.P. Caloba^{81b}, A. Caltabiano^{74a,74b}, S. Calvente Lopez⁹⁹, D. Calvet³⁸, S. Calvet³⁸, T.P. Calvet¹⁰², M. Calvetti^{72a,72b}, R. Camacho Toro¹³⁵, S. Camarda³⁶, D. Camarero Munoz⁹⁹, P. Camarri^{74a,74b}, M.T. Camerlingo^{75a,75b}, D. Cameron¹³³, C. Camincher³⁶, S. Campana³⁶, M. Campanelli⁹⁵, A. Camplani⁴⁰, V. Canale^{70a,70b}, A. Canesse¹⁰⁴, M. Cano Bret⁷⁸, J. Cantero¹²⁹, T. Cao¹⁶¹, Y. Cao¹⁷³, M.D.M. Capeans Garrido³⁶, M. Capua^{41b,41a}, R. Cardarelli^{74a}, F. Cardillo¹⁷⁴, G. Carducci^{41b,41a}, I. Carli¹⁴², T. Carli³⁶, G. Carlino^{70a}, B.T. Carlson¹³⁸, E.M. Carlson^{176,168a}, L. Carminati^{69a,69b}, R.M.D. Carney¹⁵³, S. Caron¹¹⁹, E. Carquin^{146d}, S. Carrá⁴⁶, G. Carratta^{23b,23a}, J.W.S. Carter¹⁶⁷, T.M. Carter⁵⁰, M.P. Casado^{14,f}, A.F. Casha¹⁶⁷, E.G. Castiglia¹⁸³, F.L. Castillo¹⁷⁴, L. Castillo Garcia¹⁴, V. Castillo Gimenez¹⁷⁴, N.F. Castro^{139a,139e}, A. Catinaccio³⁶, J.R. Catmore¹³³, A. Cattai³⁶, V. Cavaliere²⁹, V. Cavasinni^{72a,72b}, E. Celebi^{12b}, F. Celli¹³⁴, K. Cerny¹³⁰, A.S. Cerqueira^{81a}, A. Cerri¹⁵⁶, L. Cerrito^{74a,74b}, F. Cerutti¹⁸, A. Cervelli^{23b,23a}, S.A. Cetin^{12b}, Z. Chadi^{35a}, D. Chakraborty¹²¹, J. Chan¹⁸¹, W.S. Chan¹²⁰, W.Y. Chan⁹¹, J.D. Chapman³², B. Chargeishvili^{159b}, D.G. Charlton²¹, T.P. Charman⁹³, M. Chatterjee²⁰, C.C. Chau³⁴, S. Che¹²⁷, S. Chekanov⁶, S.V. Chekulaev^{168a}, G.A. Chelkov^{80,ah}, B. Chen⁷⁹, C. Chen^{60a}, C.H. Chen⁷⁹, H. Chen^{15c}, H. Chen²⁹, J. Chen^{60a}, J. Chen³⁹, J. Chen²⁶, S. Chen¹³⁶, S.J. Chen^{15c}, X. Chen^{15b}, Y. Chen^{60a}, Y-H. Chen⁴⁶, H.C. Cheng^{63a}, H.J. Cheng^{15a}, A. Cheplakov⁸⁰, E. Cheremushkina¹²³, R. Cherkaoui El Moursli^{35e}, E. Cheu⁷, K. Cheung⁶⁴, T.J.A. Chevalérias¹⁴⁴, L. Chevalier¹⁴⁴, V. Chiarella⁵¹, G. Chiarelli^{72a}, G. Chiodini^{68a}, A.S. Chisholm²¹, A. Chitan^{27b}, I. Chiu¹⁶³, Y.H. Chiu¹⁷⁶, M.V. Chizhov⁸⁰, K. Choi¹¹, A.R. Chomont^{73a,73b}, Y.S. Chow¹²⁰, L.D. Christopher^{33e}, M.C. Chu^{63a}, X. Chu^{15a,15d}, J. Chudoba¹⁴⁰, J.J. Chwastowski⁸⁵, L. Chytka¹³⁰, D. Cieri¹¹⁵, K.M. Ciesla⁸⁵, V. Cindro⁹², I.A. Cioară^{27b}, A. Ciocio¹⁸, F. Ciroto^{70a,70b}, Z.H. Citron^{180j}, M. Citterio^{69a}, D.A. Ciubotaru^{27b}, B.M. Ciungu¹⁶⁷, A. Clark⁵⁴, M.R. Clark³⁹, P.J. Clark⁵⁰, S.E. Clawson¹⁰¹, C. Clement^{45a,45b}, Y. Coadou¹⁰², M. Cokal^{67a,67c}, A. Coccaro^{55b}, J. Cochran⁷⁹, R. Coelho Lopes De Sa¹⁰³, H. Cohen¹⁶¹, A.E.C. Coimbra³⁶, B. Cole³⁹, A.P. Colijn¹²⁰, J. Collot⁵⁸, P. Conde Muiño^{139a,139h}, S.H. Connell^{33c}, I.A. Connelly⁵⁷, S. Constantinescu^{27b}, F. Conventi^{70a,an}, A.M. Cooper-Sarkar¹³⁴, F. Cormier¹⁷⁵, K.J.R. Cormier¹⁶⁷, L.D. Corpe⁹⁵, M. Corradi^{73a,73b}, E.E. Corrigan⁹⁷, F. Corriveau^{104,ab}, M.J. Costa¹⁷⁴, F. Costanza⁵, D. Costanzo¹⁴⁹, G. Cowan⁹⁴, J.W. Cowley³², J. Crane¹⁰¹, K. Cranmer¹²⁵, R.A. Creager¹³⁶, S. Crépe-Renaudin⁵⁸, F. Crescioli¹³⁵, M. Cristinziani²⁴, V. Croft¹⁷⁰, G. Crosetti^{41b,41a}, A. Cueto⁵, T. Cuhadar Donszelmann¹⁷¹, H. Cui^{15a,15d}, A.R. Cukierman¹⁵³, W.R. Cunningham⁵⁷, S. Czekaierda⁸⁵, P. Czodrowski³⁶,

M.M. Czurylo^{61b}, M.J. Da Cunha Sargedas De Sousa^{60b}, J.V. Da Fonseca Pinto^{81b}, C. Da Via¹⁰¹,
W. Dabrowski^{84a}, F. Dachs³⁶, T. Dado⁴⁷, S. Dahbi^{33e}, T. Dai¹⁰⁶, C. Dallapiccola¹⁰³, M. Dam⁴⁰,
G. D'amen²⁹, V. D'Amico^{75a,75b}, J. Damp¹⁰⁰, J.R. Dandoy¹³⁶, M.F. Daneri³⁰, M. Danninger¹⁵², V. Dao³⁶,
G. Darbo^{55b}, O. Dartsis⁵, A. Dattagupta¹³¹, T. Daubney⁴⁶, S. D'Auria^{69a,69b}, C. David^{168b}, T. Davidek¹⁴²,
D.R. Davis⁴⁹, I. Dawson¹⁴⁹, K. De⁸, R. De Asmundis^{70a}, M. De Beurs¹²⁰, S. De Castro^{23b,23a},
N. De Groot¹¹⁹, P. de Jong¹²⁰, H. De la Torre¹⁰⁷, A. De Maria^{15c}, D. De Pedis^{73a}, A. De Salvo^{73a},
U. De Sanctis^{74a,74b}, M. De Santis^{74a,74b}, A. De Santo¹⁵⁶, J.B. De Vivie De Regie⁶⁵, D.V. Dedovich⁸⁰,
A.M. Deiana⁴², J. Del Peso⁹⁹, Y. Delabat Diaz⁴⁶, D. Delgove⁶⁵, F. Deliot¹⁴⁴, C.M. Delitzsch⁷,
M. Della Pietra^{70a,70b}, D. Della Volpe⁵⁴, A. Dell'Acqua³⁶, L. Dell'Asta^{74a,74b}, M. Delmastro⁵,
C. Delporte⁶⁵, P.A. Delsart⁵⁸, D.A. DeMarco¹⁶⁷, S. Demers¹⁸³, M. Demichev⁸⁰, G. Demontigny¹¹⁰,
S.P. Denisov¹²³, L. D'Eramo¹²¹, D. Derendarz⁸⁵, J.E. Derkaoui^{35d}, F. Derue¹³⁵, P. Dervan⁹¹, K. Desch²⁴,
K. Dette¹⁶⁷, C. Deutsch²⁴, M.R. Devesa³⁰, P.O. Deviveiros³⁶, F.A. Di Bello^{73a,73b}, A. Di Ciaccio^{74a,74b},
L. Di Ciaccio⁵, W.K. Di Clemente¹³⁶, C. Di Donato^{70a,70b}, A. Di Girolamo³⁶, G. Di Gregorio^{72a,72b},
B. Di Micco^{75a,75b}, R. Di Nardo^{75a,75b}, K.F. Di Petrillo⁵⁹, R. Di Sipio¹⁶⁷, C. Diaconu¹⁰², F.A. Dias¹²⁰,
T. Dias Do Vale^{139a}, M.A. Diaz^{146a}, F.G. Diaz Capriles²⁴, J. Dickinson¹⁸, M. Didenko¹⁶⁶, E.B. Diehl¹⁰⁶,
J. Dietrich¹⁹, S. Díez Cornell⁴⁶, C. Diez Pardos¹⁵¹, A. Dimitrievska¹⁸, W. Ding^{15b}, J. Dingfelder²⁴,
S.J. Dittmeier^{61b}, F. Dittus³⁶, F. Djama¹⁰², T. Djobava^{159b}, J.I. Djuvslund¹⁷, M.A.B. Do Vale¹⁴⁷,
M. Dobre^{27b}, D. Dodsworth²⁶, C. Doglioni⁹⁷, J. Dolejsi¹⁴², Z. Dolezal¹⁴², M. Donadelli^{81c}, B. Dong^{60c},
J. Donini³⁸, A. D'onofrio^{15c}, M. D'Onofrio⁹¹, J. Dopke¹⁴³, A. Doria^{70a}, M.T. Dova⁸⁹, A.T. Doyle⁵⁷,
E. Drechsler¹⁵², E. Dreyer¹⁵², T. Dreyer⁵³, A.S. Drobac¹⁷⁰, D. Du^{60b}, T.A. du Pree¹²⁰, Y. Duan^{60d},
F. Dubinin¹¹¹, M. Dubovsky^{28a}, A. Dubreuil⁵⁴, E. Duchovni¹⁸⁰, G. Duckeck¹¹⁴, O.A. Ducu³⁶, D. Duda¹¹⁵,
A. Dudarev³⁶, A.C. Dudder¹⁰⁰, E.M. Duffield¹⁸, M. D'uffizi¹⁰¹, L. Duflo⁶⁵, M. Dührssen³⁶, C. Dülsen¹⁸²,
M. Dumancic¹⁸⁰, A.E. Dumitriu^{27b}, M. Dunford^{61a}, A. Duperrin¹⁰², H. Duran Yildiz^{4a}, M. Düren⁵⁶,
A. Durglishvili^{159b}, D. Duschinger⁴⁸, B. Dutta⁴⁶, D. Duvnjak¹, G.I. Dyckes¹³⁶, M. Dyndal³⁶, S. Dysch¹⁰¹,
B.S. Dziedzic⁸⁵, M.G. Eggleston⁴⁹, T. Eifert⁸, G. Eigen¹⁷, K. Einsweiler¹⁸, T. Ekelof¹⁷², H. El Jarrari^{35e},
V. Ellajosyula¹⁷², M. Ellert¹⁷², F. Ellinghaus¹⁸², A.A. Elliot⁹³, N. Ellis³⁶, J. Elmsheuser²⁹, M. Elsing³⁶,
D. Emelianov¹⁴³, A. Emerman³⁹, Y. Enari¹⁶³, M.B. Epland⁴⁹, J. Erdmann⁴⁷, A. Ereditato²⁰,
P.A. Erland⁸⁵, M. Errenst¹⁸², M. Escalier⁶⁵, C. Escobar¹⁷⁴, O. Estrada Pastor¹⁷⁴, E. Etzion¹⁶¹,
G.E. Evans^{139a,139b}, H. Evans⁶⁶, M.O. Evans¹⁵⁶, A. Ezhilov¹³⁷, F. Fabbri⁵⁷, L. Fabbri^{23b,23a}, V. Fabiani¹¹⁹,
G. Facini¹⁷⁸, R.M. Fakhruddinov¹²³, S. Falciano^{73a}, P.J. Falke²⁴, S. Falke³⁶, J. Faltova¹⁴², Y. Fang^{15a},
Y. Fang^{15a}, G. Fanourakis⁴⁴, M. Fanti^{69a,69b}, M. Faraj^{67a,67c}, A. Farbin⁸, A. Farilla^{75a}, E.M. Farina^{71a,71b},
T. Farooque¹⁰⁷, S.M. Farrington⁵⁰, P. Farthouat³⁶, F. Fassi^{35e}, P. Fassnacht³⁶, D. Fassouliotis⁹,
M. Faucci Giannelli⁵⁰, W.J. Fawcett³², L. Fayard⁶⁵, O.L. Fedin^{137,o}, W. Fedorko¹⁷⁵, A. Fehr²⁰,
M. Feickert¹⁷³, L. Feligioni¹⁰², A. Fell¹⁴⁹, C. Feng^{60b}, M. Feng⁴⁹, M.J. Fenton¹⁷¹, A.B. Fenyuk¹²³,
S.W. Ferguson⁴³, J. Ferrando⁴⁶, A. Ferrante¹⁷³, A. Ferrari¹⁷², P. Ferrari¹²⁰, R. Ferrari^{71a},
D.E. Ferreira de Lima^{61b}, A. Ferrer¹⁷⁴, D. Ferrere⁵⁴, C. Ferretti¹⁰⁶, F. Fiedler¹⁰⁰, A. Filipčić⁹²,
F. Filthaut¹¹⁹, K.D. Finelli²⁵, M.C.N. Fiolhais^{139a,139c,a}, L. Fiorini¹⁷⁴, F. Fischer¹¹⁴, J. Fischer¹⁰⁰,
W.C. Fisher¹⁰⁷, T. Fitschen²¹, I. Fleck¹⁵¹, P. Fleischmann¹⁰⁶, T. Flick¹⁸², B.M. Flierl¹¹⁴, L. Flores¹³⁶,
L.R. Flores Castillo^{63a}, F.M. Follega^{76a,76b}, N. Fomin¹⁷, J.H. Foo¹⁶⁷, G.T. Forcolin^{76a,76b}, B.C. Forland⁶⁶,
A. Formica¹⁴⁴, F.A. Förster¹⁴, A.C. Forti¹⁰¹, E. Fortin¹⁰², M.G. Foti¹³⁴, D. Fournier⁶⁵, H. Fox⁹⁰,
P. Francavilla^{72a,72b}, S. Francescato^{73a,73b}, M. Franchini^{23b,23a}, S. Franchino^{61a}, D. Francis³⁶, L. Franco⁵,
L. Franconi²⁰, M. Franklin⁵⁹, G. Frattari^{73a,73b}, A.N. Fray⁹³, P.M. Freeman²¹, B. Freund¹¹⁰,
W.S. Freund^{81b}, E.M. Freundlich⁴⁷, D.C. Frizzell¹²⁸, D. Froidevaux³⁶, J.A. Frost¹³⁴, M. Fujimoto¹²⁶,
C. Fukunaga¹⁶⁴, E. Fullana Torregrosa¹⁷⁴, T. Fusayasu¹¹⁶, J. Fuster¹⁷⁴, A. Gabrielli^{23b,23a}, A. Gabrielli³⁶,
S. Gadatsch⁵⁴, P. Gadow¹¹⁵, G. Gagliardi^{55b,55a}, L.G. Gagnon¹¹⁰, G.E. Gallardo¹³⁴, E.J. Gallas¹³⁴,
B.J. Gallop¹⁴³, R. Gamboa Goni⁹³, K.K. Gan¹²⁷, S. Ganguly¹⁸⁰, J. Gao^{60a}, Y. Gao⁵⁰, Y.S. Gao^{31,1},
F.M. Garay Walls^{146a}, C. García¹⁷⁴, J.E. García Navarro¹⁷⁴, J.A. García Pascual^{15a}, C. Garcia-Argos⁵²,

M. Garcia-Sciveres¹⁸, R.W. Gardner³⁷, N. Garelli¹⁵³, S. Gargiulo⁵², C.A. Garner¹⁶⁷, V. Garonne¹³³,
S.J. Gasiorowski¹⁴⁸, P. Gaspar^{81b}, A. Gaudiello^{55b,55a}, G. Gaudio^{71a}, P. Gauzzi^{73a,73b}, I.L. Gavrilenko¹¹¹,
A. Gavriluk¹²⁴, C. Gay¹⁷⁵, G. Gaycken⁴⁶, E.N. Gazis¹⁰, A.A. Geanta^{27b}, C.M. Gee¹⁴⁵, C.N.P. Gee¹⁴³,
J. Geisen⁹⁷, M. Geisen¹⁰⁰, C. Gemme^{55b}, M.H. Genest⁵⁸, C. Geng¹⁰⁶, S. Gentile^{73a,73b}, S. George⁹⁴,
T. Geralis⁴⁴, L.O. Gerlach⁵³, P. Gessinger-Befurt¹⁰⁰, G. Gessner⁴⁷, S. Ghasemi¹⁵¹,
M. Ghasemi Bostanabad¹⁷⁶, M. Ghneimat¹⁵¹, A. Ghosh⁶⁵, A. Ghosh⁷⁸, B. Giacobbe^{23b}, S. Giagu^{73a,73b},
N. Giangiacomi^{23b,23a}, P. Giannetti^{72a}, A. Giannini^{70a,70b}, G. Giannini¹⁴, S.M. Gibson⁹⁴, M. Gignac¹⁴⁵,
D.T. Gil^{84b}, B.J. Gilbert³⁹, D. Gillberg³⁴, G. Gilles¹⁸², N.E.K. Gillwald⁴⁶, D.M. Gingrich^{3,am},
M.P. Giordani^{67a,67c}, P.F. Giraud¹⁴⁴, G. Giugliarelli^{67a,67c}, D. Giugni^{69a}, F. Giuli^{74a,74b}, S. Gkaitatzis¹⁶²,
I. Gkialas^{9,g}, E.L. Gkoukousis¹⁴, P. Gkountoumis¹⁰, L.K. Gladilin¹¹³, C. Glasman⁹⁹, J. Glatzer¹⁴,
P.C.F. Glaysher⁴⁶, A. Glazov⁴⁶, G.R. Gledhill¹³¹, I. Gnesi^{41b,b}, M. Goblirsch-Kolb²⁶, D. Godin¹¹⁰,
S. Goldfarb¹⁰⁵, T. Golling⁵⁴, D. Golubkov¹²³, A. Gomes^{139a,139b}, R. Goncalves Gama⁵³,
R. Gonçalves^{139a,139c}, G. Gonella¹³¹, L. Gonella²¹, A. Gongadze⁸⁰, F. Gonnella²¹, J.L. Gonski³⁹,
S. González de la Hoz¹⁷⁴, S. Gonzalez Fernandez¹⁴, R. Gonzalez Lopez⁹¹, C. Gonzalez Renteria¹⁸,
R. Gonzalez Suarez¹⁷², S. Gonzalez-Sevilla⁵⁴, G.R. Gonzalvo Rodriguez¹⁷⁴, L. Goossens³⁶,
N.A. Gorasia²¹, P.A. Gorbounov¹²⁴, H.A. Gordon²⁹, B. Gorini³⁶, E. Gorini^{68a,68b}, A. Gorišek⁹²,
A.T. Goshaw⁴⁹, M.I. Gostkin⁸⁰, C.A. Gottardo¹¹⁹, M. Gouighri^{35b}, A.G. Goussiou¹⁴⁸, N. Govender^{33c},
C. Goy⁵, I. Grabowska-Bold^{84a}, E.C. Graham⁹¹, J. Gramling¹⁷¹, E. Gramstad¹³³, S. Grancagnolo¹⁹,
M. Grandi¹⁵⁶, V. Gratchev¹³⁷, P.M. Gravila^{27f}, F.G. Gravili^{68a,68b}, C. Gray⁵⁷, H.M. Gray¹⁸, C. Grefe²⁴,
K. Gregersen⁹⁷, I.M. Gregor⁴⁶, P. Grenier¹⁵³, K. Grevtsov⁴⁶, C. Grieco¹⁴, N.A. Grieser¹²⁸, A.A. Grillo¹⁴⁵,
K. Grimm^{31,k}, S. Grinstein^{14,w}, J.-F. Grivaz⁶⁵, S. Groh¹⁰⁰, E. Gross¹⁸⁰, J. Grosse-Knetter⁵³, Z.J. Grout⁹⁵,
C. Grud¹⁰⁶, A. Grummer¹¹⁸, J.C. Grundy¹³⁴, L. Guan¹⁰⁶, W. Guan¹⁸¹, C. Gubbels¹⁷⁵, J. Guenther⁷⁷,
A. Guerguichon⁶⁵, J.G.R. Guerrero Rojas¹⁷⁴, F. Guescini¹¹⁵, D. Guest¹⁷¹, R. Gugel¹⁰⁰, A. Guida⁴⁶,
T. Guillemin⁵, S. Guindon³⁶, J. Guo^{60c}, W. Guo¹⁰⁶, Y. Guo^{60a}, Z. Guo¹⁰², R. Gupta⁴⁶, S. Gurbuz^{12c},
G. Gustavino¹²⁸, M. Guth⁵², P. Gutierrez¹²⁸, C. Gutschow⁹⁵, C. Guyot¹⁴⁴, C. Gwenlan¹³⁴,
C.B. Gwilliam⁹¹, E.S. Haaland¹³³, A. Haas¹²⁵, C. Haber¹⁸, H.K. Hadavand⁸, A. Hadeif^{60a}, M. Haleem¹⁷⁷,
J. Haley¹²⁹, J.J. Hall¹⁴⁹, G. Halladjian¹⁰⁷, G.D. Hallewell¹⁰², K. Hamano¹⁷⁶, H. Hamdaoui^{35e}, M. Hamer²⁴,
G.N. Hamity⁵⁰, K. Han^{60a,v}, L. Han^{15c}, L. Han^{60a}, S. Han¹⁸, Y.F. Han¹⁶⁷, K. Hanagaki^{82,t}, M. Hance¹⁴⁵,
D.M. Handl¹¹⁴, M.D. Hank³⁷, R. Hankache¹³⁵, E. Hansen⁹⁷, J.B. Hansen⁴⁰, J.D. Hansen⁴⁰, M.C. Hansen²⁴,
P.H. Hansen⁴⁰, E.C. Hanson¹⁰¹, K. Hara¹⁶⁹, T. Harenberg¹⁸², S. Harkusha¹⁰⁸, P.F. Harrison¹⁷⁸,
N.M. Hartman¹⁵³, N.M. Hartmann¹¹⁴, Y. Hasegawa¹⁵⁰, A. Hasib⁵⁰, S. Hassani¹⁴⁴, S. Haug²⁰,
R. Hauser¹⁰⁷, L.B. Havener³⁹, M. Havranek¹⁴¹, C.M. Hawkes²¹, R.J. Hawkings³⁶, S. Hayashida¹¹⁷,
D. Hayden¹⁰⁷, C. Hayes¹⁰⁶, R.L. Hayes¹⁷⁵, C.P. Hays¹³⁴, J.M. Hays⁹³, H.S. Hayward⁹¹, S.J. Haywood¹⁴³,
F. He^{60a}, Y. He¹⁶⁵, M.P. Heath⁵⁰, V. Hedberg⁹⁷, A.L. Heggelund¹³³, C. Heidegger⁵², K.K. Heidegger⁵²,
W.D. Heidorn⁷⁹, J. Heilman³⁴, S. Heim⁴⁶, T. Heim¹⁸, B. Heinemann^{46,ak}, J.G. Heinlein¹³⁶, J.J. Heinrich¹³¹,
L. Heinrich³⁶, J. Hejbal¹⁴⁰, L. Helary⁴⁶, A. Held¹²⁵, S. Hellesund¹³³, C.M. Helling¹⁴⁵, S. Hellman^{45a,45b},
C. Helsen³⁶, R.C.W. Henderson⁹⁰, Y. Heng¹⁸¹, L. Henkelmann³², A.M. Henriques Correia³⁶, H. Herde²⁶,
Y. Hernández Jiménez^{33e}, H. Herr¹⁰⁰, M.G. Herrmann¹¹⁴, T. Herrmann⁴⁸, G. Herten⁵², R. Hertenberger¹¹⁴,
L. Hervas³⁶, T.C. Herwig¹³⁶, G.G. Hesketh⁹⁵, N.P. Hesse^{168a}, H. Hibi⁸³, S. Higashino⁸²,
E. Higón-Rodríguez¹⁷⁴, K. Hildebrand³⁷, J.C. Hill³², K.K. Hill²⁹, K.H. Hiller⁴⁶, S.J. Hillier²¹, M. Hils⁴⁸,
I. Hinchliffe¹⁸, F. Hinterkeuser²⁴, M. Hirose¹³², S. Hirose¹⁶⁹, D. Hirschbuehl¹⁸², B. Hiti⁹², O. Hladik¹⁴⁰,
J. Hobbs¹⁵⁵, N. Hod¹⁸⁰, M.C. Hodgkinson¹⁴⁹, A. Hoecker³⁶, D. Hohn⁵², D. Hohov⁶⁵, T. Holm²⁴,
T.R. Holmes³⁷, M. Holzbock¹¹⁵, L.B.A.H. Hommels³², T.M. Hong¹³⁸, J.C. Honig⁵², A. Hönle¹¹⁵,
B.H. Hooberman¹⁷³, W.H. Hopkins⁶, Y. Horii¹¹⁷, P. Horn⁴⁸, L.A. Horyn³⁷, S. Hou¹⁵⁸, A. Houmada^{35a},
J. Howarth⁵⁷, J. Hoya⁸⁹, M. Hrabovsky¹³⁰, J. Hrivnac⁶⁵, A. Hrynevich¹⁰⁹, T. Hryn'ova⁵, P.J. Hsu⁶⁴,
S.-C. Hsu¹⁴⁸, Q. Hu²⁹, S. Hu^{60c}, Y.F. Hu^{15a,15d,ao}, D.P. Huang⁹⁵, X. Huang^{15c}, Y. Huang^{60a}, Y. Huang^{15a},
Z. Hubacek¹⁴¹, F. Hubaut¹⁰², M. Huebner²⁴, F. Huegging²⁴, T.B. Huffman¹³⁴, M. Huhtinen³⁶,

R. Hulsken⁵⁸, R.F.H. Hunter³⁴, N. Huseynov^{80,ac}, J. Huston¹⁰⁷, J. Huth⁵⁹, R. Hyneman¹⁵³, S. Hyrych^{28a}, G. Iacobucci⁵⁴, G. Iakovidis²⁹, I. Ibragimov¹⁵¹, L. Iconomidou-Fayard⁶⁵, P. Iengo³⁶, R. Ignazzi⁴⁰, O. Igonkina^{120,y,*}, R. Iguchi¹⁶³, T. Iizawa⁵⁴, Y. Ikegami⁸², M. Ikeno⁸², N. Ilic^{119,167,ab}, F. Iltzsche⁴⁸, H. Imam^{35a}, G. Introzzi^{71a,71b}, M. Iodice^{75a}, K. Iordanidou^{168a}, V. Ippolito^{73a,73b}, M.F. Isacson¹⁷², M. Ishino¹⁶³, W. Islam¹²⁹, C. Issever^{19,46}, S. Istin¹⁶⁰, J.M. Iturbe Ponce^{63a}, R. Iuppa^{76a,76b}, A. Ivina¹⁸⁰, J.M. Izen⁴³, V. Izzo^{70a}, P. Jacka¹⁴⁰, P. Jackson¹, R.M. Jacobs⁴⁶, B.P. Jaeger¹⁵², V. Jain², G. Jäkel¹⁸², K.B. Jakobi¹⁰⁰, K. Jakobs⁵², T. Jakoubek¹⁸⁰, J. Jamieson⁵⁷, K.W. Janas^{84a}, R. Jansky⁵⁴, M. Janus⁵³, P.A. Janus^{84a}, G. Jarlskog⁹⁷, A.E. Jaspan⁹¹, N. Javadov^{80,ac}, T. Javûrek³⁶, M. Javurkova¹⁰³, F. Jeanneau¹⁴⁴, L. Jeanty¹³¹, J. Jejelava^{159a}, P. Jenni^{52,c}, N. Jeong⁴⁶, S. Jézéquel⁵, H. Ji¹⁸¹, J. Jia¹⁵⁵, Z. Jia^{15c}, H. Jiang⁷⁹, Y. Jiang^{60a}, Z. Jiang¹⁵³, S. Jiggins⁵², F.A. Jimenez Morales³⁸, J. Jimenez Pena¹¹⁵, S. Jin^{15c}, A. Jinaru^{27b}, O. Jinnouchi¹⁶⁵, H. Jivan^{33e}, P. Johansson¹⁴⁹, K.A. Johns⁷, C.A. Johnson⁶⁶, E. Jones¹⁷⁸, R.W.L. Jones⁹⁰, S.D. Jones¹⁵⁶, T.J. Jones⁹¹, J. Jongmanns^{61a}, J. Jovicevic³⁶, X. Ju¹⁸, J.J. Junggeburth¹¹⁵, A. Juste Rozas^{14,w}, A. Kaczmarek⁸⁵, M. Kado^{73a,73b}, H. Kagan¹²⁷, M. Kagan¹⁵³, A. Kahn³⁹, C. Kahra¹⁰⁰, T. Kaji¹⁷⁹, E. Kajomovitz¹⁶⁰, C.W. Kalderon²⁹, A. Kaluza¹⁰⁰, A. Kamenshchikov¹²³, M. Kaneda¹⁶³, N.J. Kang¹⁴⁵, S. Kang⁷⁹, Y. Kano¹¹⁷, J. Kanzaki⁸², L.S. Kaplan¹⁸¹, D. Kar^{33e}, K. Karava¹³⁴, M.J. Kareem^{168b}, I. Karkanias¹⁶², S.N. Karpov⁸⁰, Z.M. Karpova⁸⁰, V. Kartvelishvili⁹⁰, A.N. Karyukhin¹²³, E. Kasimi¹⁶², A. Kastanas^{45a,45b}, C. Kato^{60d}, J. Katzy⁴⁶, K. Kawade¹⁵⁰, K. Kawagoe⁸⁸, T. Kawaguchi¹¹⁷, T. Kawamoto¹⁴⁴, G. Kawamura⁵³, E.F. Kay¹⁷⁶, S. Kazakos¹⁴, V.F. Kazanin^{122b,122a}, J.M. Keaveney^{33a}, R. Keeler¹⁷⁶, J.S. Keller³⁴, E. Kellermann⁹⁷, D. Kelsey¹⁵⁶, J.J. Kempster²¹, J. Kendrick²¹, K.E. Kennedy³⁹, O. Kepka¹⁴⁰, S. Kersten¹⁸², B.P. Kerševan⁹², S. Ketabchi Haghghat¹⁶⁷, M. Khader¹⁷³, F. Khalil-Zada¹³, M. Khandoga¹⁴⁴, A. Khanov¹²⁹, A.G. Kharlamov^{122b,122a}, T. Kharlamova^{122b,122a}, E.E. Khoda¹⁷⁵, A. Khodinov¹⁶⁶, T.J. Khoo⁷⁷, G. Khorauli¹⁷⁷, E. Khramov⁸⁰, J. Khubua^{159b}, S. Kido⁸³, M. Kiehn³⁶, E. Kim¹⁶⁵, Y.K. Kim³⁷, N. Kimura⁹⁵, A. Kirchhoff⁵³, D. Kirchmeier⁴⁸, J. Kirk¹⁴³, A.E. Kiryunin¹¹⁵, T. Kishimoto¹⁶³, D.P. Kisliuk¹⁶⁷, V. Kitali⁴⁶, C. Kitsaki¹⁰, O. Kivernyk²⁴, T. Klapdor-Kleingrothaus⁵², M. Klassen^{61a}, C. Klein³⁴, M.H. Klein¹⁰⁶, M. Klein⁹¹, U. Klein⁹¹, K. Kleinknecht¹⁰⁰, P. Klimek³⁶, A. Klimentov²⁹, T. Klingl²⁴, T. Klioutchnikova³⁶, F.F. Klitzner¹¹⁴, P. Kluit¹²⁰, S. Kluth¹¹⁵, E. Kneringer⁷⁷, E.B.F.G. Knoop¹⁰², A. Knue⁵², D. Kobayashi⁸⁸, M. Kobel⁴⁸, M. Kocian¹⁵³, T. Kodama¹⁶³, P. Kodys¹⁴², D.M. Koeck¹⁵⁶, P.T. Koenig²⁴, T. Koffas³⁴, N.M. Köhler³⁶, M. Kolb¹⁴⁴, I. Koletsou⁵, T. Komarek¹³⁰, T. Kondo⁸², K. Köneke⁵², A.X.Y. Kong¹, A.C. König¹¹⁹, T. Kono¹²⁶, V. Konstantinides⁹⁵, N. Konstantinidis⁹⁵, B. Konya⁹⁷, R. Kopeliansky⁶⁶, S. Koperny^{84a}, K. Korcyl⁸⁵, K. Kordas¹⁶², G. Koren¹⁶¹, A. Korn⁹⁵, I. Korolkov¹⁴, E.V. Korolkova¹⁴⁹, N. Korotkova¹¹³, O. Kortner¹¹⁵, S. Kortner¹¹⁵, V.V. Kostyukhin^{149,166}, A. Kotskechagia⁶⁵, A. Kotwal⁴⁹, A. Koulouris¹⁰, A. Kourkoumeli-Charalampidi^{71a,71b}, C. Kourkoumelis⁹, E. Kourlitis⁶, V. Kouskoura²⁹, R. Kowalewski¹⁷⁶, W. Kozanecki¹⁰¹, A.S. Kozhin¹²³, V.A. Kramarenko¹¹³, G. Kramberger⁹², D. Krasnopevtsev^{60a}, M.W. Krasny¹³⁵, A. Krasznahorkay³⁶, D. Krauss¹¹⁵, J.A. Kremer¹⁰⁰, J. Kretzschmar⁹¹, P. Krieger¹⁶⁷, F. Krieter¹¹⁴, A. Krishnan^{61b}, M. Krivos¹⁴², K. Krizka¹⁸, K. Kroeninger⁴⁷, H. Kroha¹¹⁵, J. Kroll¹⁴⁰, J. Kroll¹³⁶, K.S. Krowpman¹⁰⁷, U. Kruchonak⁸⁰, H. Krüger²⁴, N. Krumnack⁷⁹, M.C. Kruse⁴⁹, J.A. Krzysiak⁸⁵, A. Kubota¹⁶⁵, O. Kuchinskaia¹⁶⁶, S. Kudah^{4b}, D. Kuechler⁴⁶, J.T. Kuechler⁴⁶, S. Kuehn³⁶, T. Kuhl⁴⁶, V. Kukhtin⁸⁰, Y. Kulchitsky^{108,af}, S. Kuleshov^{146b}, Y.P. Kulinich¹⁷³, M. Kuna⁵⁸, A. Kupco¹⁴⁰, T. Kupfer⁴⁷, O. Kuprash⁵², H. Kurashige⁸³, L.L. Kurchaninov^{168a}, Y.A. Kurochkin¹⁰⁸, A. Kurova¹¹², M.G. Kurth^{15a,15d}, E.S. Kuwertz³⁶, M. Kuze¹⁶⁵, A.K. Kvam¹⁴⁸, J. Kvita¹³⁰, T. Kwan¹⁰⁴, F. La Ruffa^{41b,41a}, C. Lacasta¹⁷⁴, F. Lacava^{73a,73b}, D.P.J. Lack¹⁰¹, H. Lacker¹⁹, D. Lacour¹³⁵, E. Ladygin⁸⁰, R. Lafaye⁵, B. Laforge¹³⁵, T. Lagouri^{146c}, S. Lai⁵³, I.K. Lakomic^{84a}, J.E. Lambert¹²⁸, S. Lammers⁶⁶, W. Lampl⁷, C. Lampoudis¹⁶², E. Lançon²⁹, U. Landgraf⁵², M.P.J. Landon⁹³, V.S. Lang⁵², J.C. Lange⁵³, R.J. Langenberg¹⁰³, A.J. Lankford¹⁷¹, F. Lanni²⁹, K. Lantzsck²⁴, A. Lanza^{71a}, A. Lapertosa^{55b,55a}, J.F. Laporte¹⁴⁴, T. Lari^{69a}, F. Lasagni Manghi^{23b,23a}, M. Lassnig³⁶, V. Latonova¹⁴⁰, T.S. Lau^{63a}, A. Laudrain¹⁰⁰, A. Laurier³⁴, M. Lavorgna^{70a,70b}, S.D. Lawlor⁹⁴, M. Lazzaroni^{69a,69b}, B. Le¹⁰¹,

E. Le Guirriec¹⁰², A. Lebedev⁷⁹, M. LeBlanc⁷, T. LeCompte⁶, F. Ledroit-Guillon⁵⁸, A.C.A. Lee⁹⁵,
 C.A. Lee²⁹, G.R. Lee¹⁷, L. Lee⁵⁹, S.C. Lee¹⁵⁸, S. Lee⁷⁹, B. Lefebvre^{168a}, H.P. Lefebvre⁹⁴, M. Lefebvre¹⁷⁶,
 C. Leggett¹⁸, K. Lehmann¹⁵², N. Lehmann²⁰, G. Lehmann Miotto³⁶, W.A. Leight⁴⁶, A. Leisos^{162,u},
 M.A.L. Leite^{81c}, C.E. Leitgeb¹¹⁴, R. Leitner¹⁴², D. Lellouch^{180,*}, K.J.C. Leney⁴², T. Lenz²⁴, S. Leone^{72a},
 C. Leonidopoulos⁵⁰, A. Leopold¹³⁵, C. Leroy¹¹⁰, R. Les¹⁰⁷, C.G. Lester³², M. Levchenko¹³⁷, J. Levêque⁵,
 D. Levin¹⁰⁶, L.J. Levinson¹⁸⁰, D.J. Lewis²¹, B. Li^{15b}, B. Li¹⁰⁶, C-Q. Li^{60c,60d}, F. Li^{60c}, H. Li^{60a}, H. Li^{60b},
 J. Li^{60c}, K. Li¹⁴⁸, L. Li^{60c}, M. Li^{15a,15d}, Q. Li^{15a,15d}, Q.Y. Li^{60a}, S. Li^{60d,60c}, X. Li⁴⁶, Y. Li⁴⁶, Z. Li^{60b},
 Z. Li¹³⁴, Z. Li¹⁰⁴, Z. Liang^{15a}, M. Liberatore⁴⁶, B. Liberti^{74a}, K. Lie^{63c}, S. Lim²⁹, C.Y. Lin³², K. Lin¹⁰⁷,
 R.A. Linck⁶⁶, R.E. Lindley⁷, J.H. Lindon²¹, A. Linss⁴⁶, A.L. Lioni⁵⁴, E. Lipeles¹³⁶, A. Lipniacka¹⁷,
 T.M. Liss^{173,al}, A. Lister¹⁷⁵, J.D. Little⁸, B. Liu⁷⁹, B.X. Liu¹⁵², H.B. Liu²⁹, J.B. Liu^{60a}, J.K.K. Liu³⁷,
 K. Liu^{60d}, M. Liu^{60a}, M.Y. Liu^{60a}, P. Liu^{15a}, X. Liu^{60a}, Y. Liu⁴⁶, Y. Liu^{15a,15d}, Y.L. Liu¹⁰⁶, Y.W. Liu^{60a},
 M. Livan^{71a,71b}, A. Lleres⁵⁸, J. Llorente Merino¹⁵², S.L. Lloyd⁹³, C.Y. Lo^{63b}, E.M. Lobodzinska⁴⁶,
 P. Loch⁷, S. Loffredo^{74a,74b}, T. Lohse¹⁹, K. Lohwasser¹⁴⁹, M. Lokajicek¹⁴⁰, J.D. Long¹⁷³, R.E. Long⁹⁰,
 I. Longarini^{73a,73b}, L. Longo³⁶, K.A. Looper¹²⁷, I. Lopez Paz¹⁰¹, A. Lopez Solis¹⁴⁹, J. Lorenz¹¹⁴,
 N. Lorenzo Martinez⁵, A.M. Lory¹¹⁴, P.J. Lösel¹¹⁴, A. Lösle⁵², X. Lou^{45a,45b}, X. Lou^{15a}, A. Lounis⁶⁵,
 J. Love⁶, P.A. Love⁹⁰, J.J. Lozano Bahilo¹⁷⁴, M. Lu^{60a}, Y.J. Lu⁶⁴, H.J. Lubatti¹⁴⁸, C. Luci^{73a,73b},
 F.L. Lucio Alves^{15c}, A. Lucotte⁵⁸, F. Luehring⁶⁶, I. Luise¹⁵⁵, L. Luminari^{73a}, B. Lund-Jensen¹⁵⁴,
 M.S. Lutz¹⁶¹, D. Lynn²⁹, H. Lyons⁹¹, R. Lysak¹⁴⁰, E. Lytken⁹⁷, F. Lyu^{15a}, V. Lyubushkin⁸⁰,
 T. Lyubushkina⁸⁰, H. Ma²⁹, L.L. Ma^{60b}, Y. Ma⁹⁵, D.M. Mac Donell¹⁷⁶, G. Maccarrone⁵¹,
 A. Macchiolo¹¹⁵, C.M. Macdonald¹⁴⁹, J.C. MacDonald¹⁴⁹, J. Machado Miguens¹³⁶, D. Madaffari¹⁷⁴,
 R. Madar³⁸, W.F. Mader⁴⁸, M. Madugoda Ralalage Don¹²⁹, N. Madysa⁴⁸, J. Maeda⁸³, T. Maeno²⁹,
 M. Maerker⁴⁸, V. Magerl⁵², N. Magini⁷⁹, J. Magro^{67a,67c,q}, D.J. Mahon³⁹, C. Maidantchik^{81b}, T. Maier¹¹⁴,
 A. Maio^{139a,139b,139d}, K. Maj^{84a}, O. Majersky^{28a}, S. Majewski¹³¹, Y. Makida⁸², N. Makovec⁶⁵,
 B. Malaescu¹³⁵, Pa. Malecki⁸⁵, V.P. Maleev¹³⁷, F. Malek⁵⁸, D. Malito^{41b,41a}, U. Mallik⁷⁸, C. Malone³²,
 S. Maltezos¹⁰, S. Malyukov⁸⁰, J. Mamuzic¹⁷⁴, G. Mancini⁵¹, I. Mandić⁹²,
 L. Manhaes de Andrade Filho^{81a}, I.M. Maniatis¹⁶², J. Manjarres Ramos⁴⁸, K.H. Mankinen⁹⁷, A. Mann¹¹⁴,
 A. Manousos⁷⁷, B. Mansoulie¹⁴⁴, I. Manthos¹⁶², S. Manzoni¹²⁰, A. Marantis¹⁶², G. Marceca³⁰,
 L. Marchese¹³⁴, G. Marchiori¹³⁵, M. Marcisovsky¹⁴⁰, L. Maccoccia^{74a,74b}, C. Marcon⁹⁷, M. Marjanovic¹²⁸,
 Z. Marshall¹⁸, M.U.F. Martensson¹⁷², S. Marti-Garcia¹⁷⁴, C.B. Martin¹²⁷, T.A. Martin¹⁷⁸, V.J. Martin⁵⁰,
 B. Martin dit Latour¹⁷, L. Martinelli^{75a,75b}, M. Martinez^{14,w}, P. Martinez Agullo¹⁷⁴,
 V.I. Martinez Outschoorn¹⁰³, S. Martin-Haugh¹⁴³, V.S. Martoiu^{27b}, A.C. Martyniuk⁹⁵, A. Marzin³⁶,
 S.R. Maschek¹¹⁵, L. Masetti¹⁰⁰, T. Mashimo¹⁶³, R. Mashinistov¹¹¹, J. Masik¹⁰¹, A.L. Maslennikov^{122b,122a},
 L. Massa^{23b,23a}, P. Massarotti^{70a,70b}, P. Mastrandrea^{72a,72b}, A. Mastroberardino^{41b,41a}, T. Masubuchi¹⁶³,
 D. Matakias²⁹, A. Matic¹¹⁴, N. Matsuzawa¹⁶³, P. Mättig²⁴, J. Maurer^{27b}, B. Maček⁹²,
 D.A. Maximov^{122b,122a}, R. Mazini¹⁵⁸, I. Maznas¹⁶², S.M. Mazza¹⁴⁵, J.P. Mc Gowan¹⁰⁴, S.P. Mc Kee¹⁰⁶,
 T.G. McCarthy¹¹⁵, W.P. McCormack¹⁸, E.F. McDonald¹⁰⁵, A.E. McDougall¹²⁰, J.A. Mcfayden¹⁸,
 G. Mchedlidze^{159b}, M.A. McKay⁴², K.D. McLean¹⁷⁶, S.J. McMahon¹⁴³, P.C. McNamara¹⁰⁵,
 C.J. McNicol¹⁷⁸, R.A. McPherson^{176,ab}, J.E. Mdhluli^{33e}, Z.A. Meadows¹⁰³, S. Meehan³⁶, T. Megy³⁸,
 S. Mehlhase¹¹⁴, A. Mehta⁹¹, B. Meirose⁴³, D. Melini¹⁶⁰, B.R. Mellado Garcia^{33e}, J.D. Mellenthin⁵³,
 M. Melo^{28a}, F. Meloni⁴⁶, A. Melzer²⁴, E.D. Mendes Gouveia^{139a,139e}, A.M. Mendes Jacques Da Costa²¹,
 L. Meng³⁶, X.T. Meng¹⁰⁶, S. Menke¹¹⁵, E. Meoni^{41b,41a}, S. Mergelmeyer¹⁹, S.A.M. Merkt¹³⁸,
 C. Merlassino¹³⁴, P. Mermod⁵⁴, L. Merola^{70a,70b}, C. Meroni^{69a}, G. Merz¹⁰⁶, O. Meshkov^{113,111},
 J.K.R. Meshreki¹⁵¹, J. Metcalfe⁶, A.S. Mete⁶, C. Meyer⁶⁶, J-P. Meyer¹⁴⁴, M. Michetti¹⁹, R.P. Middleton¹⁴³,
 L. Mijovic⁵⁰, G. Mikenberg¹⁸⁰, M. Mikestikova¹⁴⁰, M. Mikuz⁹², H. Mildner¹⁴⁹, A. Milic¹⁶⁷, C.D. Milke⁴²,
 D.W. Miller³⁷, L.S. Miller³⁴, A. Milov¹⁸⁰, D.A. Milstead^{45a,45b}, R.A. Mina¹⁵³, A.A. Minaenko¹²³,
 I.A. Minashvili^{159b}, A.I. Mincer¹²⁵, B. Mindur^{84a}, M. Mineev⁸⁰, Y. Minegishi¹⁶³, Y. Mino⁸⁶, L.M. Mir¹⁴,
 M. Mironova¹³⁴, K.P. Mistry¹³⁶, T. Mitani¹⁷⁹, J. Mitrevski¹¹⁴, V.A. Mitsou¹⁷⁴, M. Mittal^{60c}, O. Miu¹⁶⁷,

A. Miucci²⁰, P.S. Miyagawa⁹³, A. Mizukami⁸², J.U. Mjörnmark⁹⁷, T. Mkrtychyan^{61a}, M. Mlynarikova¹²¹,
 T. Moa^{45a,45b}, S. Mobius⁵³, K. Mochizuki¹¹⁰, P. Mogg¹¹⁴, S. Mohapatra³⁹, R. Moles-Valls²⁴, K. Mönig⁴⁶,
 E. Monnier¹⁰², A. Montalbano¹⁵², J. Montejo Berlingen³⁶, M. Montella⁹⁵, F. Monticelli⁸⁹, S. Monzani^{69a},
 N. Morange⁶⁵, A.L. Moreira De Carvalho^{139a}, D. Moreno^{22a}, M. Moreno Llácer¹⁷⁴,
 C. Moreno Martinez¹⁴, P. Morettini^{55b}, M. Morgenstern¹⁶⁰, S. Morgenstern⁴⁸, D. Mori¹⁵², M. Morii⁵⁹,
 M. Morinaga¹⁷⁹, V. Morisbak¹³³, A.K. Morley³⁶, G. Mornacchi³⁶, A.P. Morris⁹⁵, L. Morvaj¹⁵⁵,
 P. Moschovakos³⁶, B. Moser¹²⁰, M. Mosidze^{159b}, T. Moskalets¹⁴⁴, P. Moskvitina¹¹⁹, J. Moss^{31,m},
 E.J.W. Moyse¹⁰³, S. Muanza¹⁰², J. Mueller¹³⁸, R.S.P. Mueller¹¹⁴, D. Muenstermann⁹⁰, G.A. Mullier⁹⁷,
 D.P. Mungo^{69a,69b}, J.L. Munoz Martinez¹⁴, F.J. Munoz Sanchez¹⁰¹, P. Murin^{28b}, W.J. Murray^{178,143},
 A. Murrone^{69a,69b}, J.M. Muse¹²⁸, M. Muškinja¹⁸, C. Mwewa^{33a}, A.G. Myagkov^{123,ah}, A.A. Myers¹³⁸,
 G. Myers⁶⁶, J. Myers¹³¹, M. Myska¹⁴¹, B.P. Nachman¹⁸, O. Nackenhorst⁴⁷, A.Nag Nag⁴⁸, K. Nagai¹³⁴,
 K. Nagano⁸², Y. Nagasaka⁶², J.L. Nagle²⁹, E. Nagy¹⁰², A.M. Nairz³⁶, Y. Nakahama¹¹⁷, K. Nakamura⁸²,
 T. Nakamura¹⁶³, H. Nanjo¹³², F. Napolitano^{61a}, R.F. Naranjo Garcia⁴⁶, R. Narayan⁴², I. Naryshkin¹³⁷,
 M. Naseri³⁴, T. Naumann⁴⁶, G. Navarro^{22a}, P.Y. Nechaeva¹¹¹, F. Nechansky⁴⁶, T.J. Neep²¹, A. Negri^{71a,71b},
 M. Negrini^{23b}, C. Nellist¹¹⁹, C. Nelson¹⁰⁴, M.E. Nelson^{45a,45b}, S. Nemecek¹⁴⁰, M. Nessi^{36,e},
 M.S. Neubauer¹⁷³, F. Neuhaus¹⁰⁰, M. Neumann¹⁸², R. Newhouse¹⁷⁵, P.R. Newman²¹, C.W. Ng¹³⁸,
 Y.S. Ng¹⁹, Y.W.Y. Ng¹⁷¹, B. Ngair^{35e}, H.D.N. Nguyen¹⁰², T. Nguyen Manh¹¹⁰, E. Nibigira³⁸,
 R.B. Nickerson¹³⁴, R. Nicolaidou¹⁴⁴, D.S. Nielsen⁴⁰, J. Nielsen¹⁴⁵, M. Niemeyer⁵³, N. Nikiforou¹¹,
 V. Nikolaenko^{123,ah}, I. Nikolic-Audit¹³⁵, K. Nikolopoulos²¹, P. Nilsson²⁹, H.R. Nindhito⁵⁴, A. Nisati^{73a},
 N. Nishu^{60c}, R. Nisius¹¹⁵, I. Nitsche⁴⁷, T. Nitta¹⁷⁹, T. Nobe¹⁶³, D.L. Noel³², Y. Noguchi⁸⁶, I. Nomidis¹³⁵,
 M.A. Nomura²⁹, M. Nordberg³⁶, J. Novak⁹², T. Novak⁹², O. Novgorodova⁴⁸, R. Novotny¹⁴¹, L. Nozka¹³⁰,
 K. Ntekas¹⁷¹, E. Nurse⁹⁵, F.G. Oakham^{34,am}, H. Oberlack¹¹⁵, J. Ocariz¹³⁵, A. Ochi⁸³, I. Ochoa³⁹,
 J.P. Ochoa-Ricoux^{146a}, K. O'Connor²⁶, S. Oda⁸⁸, S. Odaka⁸², S. Oerdek⁵³, A. Ogrodnik^{84a}, A. Oh¹⁰¹,
 C.C. Ohm¹⁵⁴, H. Oide¹⁶⁵, M.L. Ojeda¹⁶⁷, H. Okawa¹⁶⁹, Y. Okazaki⁸⁶, M.W. O'Keefe⁹¹, Y. Okumura¹⁶³,
 A. Olariu^{27b}, L.F. Oleiro Seabra^{139a}, S.A. Olivares Pino^{146a}, D. Oliveira Damazio²⁹, J.L. Oliver¹,
 M.J.R. Olsson¹⁷¹, A. Olszewski⁸⁵, J. Olszowska⁸⁵, Ö.O. Öncel²⁴, D.C. O'Neil¹⁵², A.P. O'Neill¹³⁴,
 A. Onofre^{139a,139e}, P.U.E. Onyisi¹¹, H. Oppen¹³³, R.G. Oreamuno Madriz¹²¹, M.J. Oreglia³⁷,
 G.E. Orellana⁸⁹, D. Orestano^{75a,75b}, N. Orlando¹⁴, R.S. Orr¹⁶⁷, V. O'Shea⁵⁷, R. Ospanov^{60a},
 G. Otero y Garzon³⁰, H. Otono⁸⁸, P.S. Ott^{61a}, G.J. Ottino¹⁸, M. Ouchrif^{35d}, J. Ouellette²⁹,
 F. Ould-Saada¹³³, A. Ouraou^{144,*}, Q. Ouyang^{15a}, M. Owen⁵⁷, R.E. Owen¹⁴³, V.E. Ozcan^{12c}, N. Ozturk⁸,
 J. Pacalt¹³⁰, H.A. Pacey³², K. Pachal⁴⁹, A. Pacheco Pages¹⁴, C. Padilla Aranda¹⁴, S. Pagan Griso¹⁸,
 G. Palacino⁶⁶, S. Palazzo⁵⁰, S. Palestini³⁶, M. Palka^{84b}, P. Palni^{84a}, C.E. Pandini⁵⁴,
 J.G. Panduro Vazquez⁹⁴, P. Pani⁴⁶, G. Panizzo^{67a,67c}, L. Paolozzi⁵⁴, C. Papadatos¹¹⁰, K. Papageorgiou^{9,g},
 S. Parajuli⁴², A. Paramonov⁶, C. Paraskevopoulos¹⁰, D. Paredes Hernandez^{63b}, S.R. Paredes Saenz¹³⁴,
 B. Parida¹⁸⁰, T.H. Park¹⁶⁷, A.J. Parker³¹, M.A. Parker³², F. Parodi^{55b,55a}, E.W. Parrish¹²¹, J.A. Parsons³⁹,
 U. Parzefall⁵², L. Pascual Dominguez¹³⁵, V.R. Pascuzzi¹⁸, J.M.P. Pasner¹⁴⁵, F. Pasquali¹²⁰,
 E. Pasqualucci^{73a}, S. Passaggio^{55b}, F. Pastore⁹⁴, P. Pasuwan^{45a,45b}, S. Patariaia¹⁰⁰, J.R. Pater¹⁰¹,
 A. Pathak^{181,i}, J. Patton⁹¹, T. Pauly³⁶, J. Parkes¹⁵³, B. Pearson¹¹⁵, M. Pedersen¹³³, L. Pedraza Diaz¹¹⁹,
 R. Pedro^{139a}, T. Peiffer⁵³, S.V. Peleganchuk^{122b,122a}, O. Penc¹⁴⁰, C. Peng^{63b}, H. Peng^{60a}, B.S. Peralva^{81a},
 M.M. Perego⁶⁵, A.P. Pereira Peixoto^{139a}, L. Pereira Sanchez^{45a,45b}, D.V. Perepelitsa²⁹, E. Perez Codina^{168a},
 F. Peri¹⁹, L. Perini^{69a,69b}, H. Pernegger³⁶, S. Perrella³⁶, A. Perrevoort¹²⁰, K. Peters⁴⁶, R.F.Y. Peters¹⁰¹,
 B.A. Petersen³⁶, T.C. Petersen⁴⁰, E. Petit¹⁰², V. Petousis¹⁴¹, C. Petridou¹⁶², F. Petrucci^{75a,75b}, M. Pettee¹⁸³,
 N.E. Pettersson¹⁰³, K. Petukhova¹⁴², A. Peyaud¹⁴⁴, R. Pezoa^{146d}, L. Pezzotti^{71a,71b}, T. Pham¹⁰⁵,
 P.W. Phillips¹⁴³, M.W. Phipps¹⁷³, G. Piacquadio¹⁵⁵, E. Pianori¹⁸, A. Picazio¹⁰³, R.H. Pickles¹⁰¹,
 R. Piegai³⁰, D. Pietreanu^{27b}, J.E. Pilcher³⁷, A.D. Pilkington¹⁰¹, M. Pinamonti^{67a,67c}, J.L. Pinfold³,
 C. Pitman Donaldson⁹⁵, M. Pitt¹⁶¹, L. Pizzimento^{74a,74b}, A. Pizzini¹²⁰, M.-A. Pleier²⁹, V. Plesanovs⁵²,
 V. Pleskot¹⁴², E. Plotnikova⁸⁰, P. Podberezko^{122b,122a}, R. Poettgen⁹⁷, R. Poggi⁵⁴, L. Poggioli¹³⁵,

I. Pogrebnyak¹⁰⁷, D. Pohl²⁴, I. Pokharel⁵³, G. Polesello^{71a}, A. Poley^{152,168a}, A. Policicchio^{73a,73b},
 R. Polifka¹⁴², A. Polini^{23b}, C.S. Pollard⁴⁶, V. Polychronakos²⁹, D. Ponomarenko¹¹², L. Pontecorvo³⁶,
 S. Popa^{27a}, G.A. Popeneciu^{27d}, L. Portales⁵, D.M. Portillo Quintero⁵⁸, S. Pospisil¹⁴¹, K. Potamianos⁴⁶,
 I.N. Potrap⁸⁰, C.J. Potter³², H. Potti¹¹, T. Poulsen⁹⁷, J. Poveda¹⁷⁴, T.D. Powell¹⁴⁹, G. Pownall⁴⁶,
 M.E. Pozo Astigarraga³⁶, A. Prades Ibanez¹⁷⁴, P. Pralavorio¹⁰², M.M. Prapa⁴⁴, S. Prell⁷⁹, D. Price¹⁰¹,
 M. Primavera^{68a}, M.L. Proffitt¹⁴⁸, N. Proklova¹¹², K. Prokofiev^{63c}, F. Prokoshin⁸⁰, S. Protopopescu²⁹,
 J. Proudfoot⁶, M. Przybycien^{84a}, D. Pudzha¹³⁷, A. Puri¹⁷³, P. Puzo⁶⁵, D. Pyatiizbyantseva¹¹², J. Qian¹⁰⁶,
 Y. Qin¹⁰¹, A. Quadt⁵³, M. Queitsch-Maitland³⁶, M. Racko^{28a}, F. Ragusa^{69a,69b}, G. Rahal⁹⁸, J.A. Raine⁵⁴,
 S. Rajagopalan²⁹, A. Ramirez Morales⁹³, K. Ran^{15a,15d}, D.M. Rauch⁴⁶, F. Rauscher¹¹⁴, S. Rave¹⁰⁰,
 B. Ravina⁵⁷, I. Ravinovich¹⁸⁰, J.H. Rawling¹⁰¹, M. Raymond³⁶, A.L. Read¹³³, N.P. Readioff¹⁴⁹,
 M. Reale^{68a,68b}, D.M. Rebuffi^{71a,71b}, G. Redlinger²⁹, K. Reeves⁴³, D. Reikher¹⁶¹, A. Reiss¹⁰⁰, A. Rej¹⁵¹,
 C. Rembser³⁶, A. Renardi⁴⁶, M. Renda^{27b}, M.B. Rendel¹¹⁵, A.G. Rennie⁵⁷, S. Resconi^{69a},
 E.D. Resseguie¹⁸, S. Rettie⁹⁵, B. Reynolds¹²⁷, E. Reynolds²¹, O.L. Rezanova^{122b,122a}, P. Reznicek¹⁴²,
 E. Ricci^{76a,76b}, R. Richter¹¹⁵, S. Richter⁴⁶, E. Richter-Was^{84b}, M. Ridel¹³⁵, P. Rieck¹¹⁵, O. Rifki⁴⁶,
 M. Rijssenbeek¹⁵⁵, A. Rimoldi^{71a,71b}, M. Rimoldi⁴⁶, L. Rinaldi^{23b}, T.T. Rinn¹⁷³, G. Ripellino¹⁵⁴, I. Riu¹⁴,
 P. Rivadeneira⁴⁶, J.C. Rivera Vergara¹⁷⁶, F. Rizatdinova¹²⁹, E. Rizvi⁹³, C. Rizzi³⁶, S.H. Robertson^{104,ab},
 M. Robin⁴⁶, D. Robinson³², C.M. Robles Gajardo^{146d}, M. Robles Manzano¹⁰⁰, A. Robson⁵⁷,
 A. Rocchi^{74a,74b}, E. Rocco¹⁰⁰, C. Roda^{72a,72b}, S. Rodriguez Bosca¹⁷⁴, A. Rodriguez Rodriguez⁵²,
 A.M. Rodríguez Vera^{168b}, S. Roe³⁶, J. Roggel¹⁸², O. Røhne¹³³, R. Röhrig¹¹⁵, R.A. Rojas^{146d}, B. Roland⁵²,
 C.P.A. Roland⁶⁶, J. Roloff²⁹, A. Romaniouk¹¹², M. Romano^{23b,23a}, N. Rompotis⁹¹, M. Ronzani¹²⁵,
 L. Roos¹³⁵, S. Rosati^{73a}, G. Rosin¹⁰³, B.J. Rosser¹³⁶, E. Rossi⁴⁶, E. Rossi^{75a,75b}, E. Rossi^{70a,70b},
 L.P. Rossi^{55b}, L. Rossini⁴⁶, R. Rosten¹⁴, M. Rotaru^{27b}, B. Rottler⁵², D. Rousseau⁶⁵, G. Rovelli^{71a,71b},
 A. Roy¹¹, D. Roy^{33e}, A. Rozanov¹⁰², Y. Rozen¹⁶⁰, X. Ruan^{33e}, T.A. Ruggeri¹, F. Rühr⁵²,
 A. Ruiz-Martinez¹⁷⁴, A. Rummler³⁶, Z. Rurikova⁵², N.A. Rusakovich⁸⁰, H.L. Russell¹⁰⁴, L. Rustige^{38,47},
 J.P. Rutherford⁷, E.M. Rüttinger¹⁴⁹, M. Rybar¹⁴², G. Rybkin⁶⁵, E.B. Rye¹³³, A. Ryzhov¹²³,
 J.A. Sabater Iglesias⁴⁶, P. Sabatini¹⁷⁴, L. Sabetta^{73a,73b}, S. Sacerdoti⁶⁵, H.F-W. Sadrozinski¹⁴⁵,
 R. Sadykov⁸⁰, F. Safai Tehrani^{73a}, B. Safarzadeh Samani¹⁵⁶, M. Safdari¹⁵³, P. Saha¹²¹, S. Saha¹⁰⁴,
 M. Sahinsoy¹¹⁵, A. Sahu¹⁸², M. Saimpert³⁶, M. Saito¹⁶³, T. Saito¹⁶³, H. Sakamoto¹⁶³, D. Salamani⁵⁴,
 G. Salamanna^{75a,75b}, A. Salnikov¹⁵³, J. Salt¹⁷⁴, A. Salvador Salas¹⁴, D. Salvatore^{41b,41a}, F. Salvatore¹⁵⁶,
 A. Salvucci^{63a}, A. Salzburger³⁶, J. Samarati³⁶, D. Sammel⁵², D. Sampsonidis¹⁶², D. Sampsonidou¹⁶²,
 J. Sánchez¹⁷⁴, A. Sanchez Pineda^{67a,36,67c}, H. Sandaker¹³³, C.O. Sander⁴⁶, I.G. Sanderswood⁹⁰,
 M. Sandhoff¹⁸², C. Sandoval^{22b}, D.P.C. Sankey¹⁴³, M. Sannino^{55b,55a}, Y. Sano¹¹⁷, A. Sansoni⁵¹,
 C. Santoni³⁸, H. Santos^{139a,139b}, S.N. Santpur¹⁸, A. Santra¹⁷⁴, K.A. Saoucha¹⁴⁹, A. Sapronov⁸⁰,
 J.G. Saraiva^{139a,139d}, O. Sasaki⁸², K. Sato¹⁶⁹, F. Sauerburger⁵², E. Sauvan⁵, P. Savard^{167,am}, R. Sawada¹⁶³,
 C. Sawyer¹⁴³, L. Sawyer^{96,ag}, I. Sayago Galvan¹⁷⁴, C. Sbarra^{23b}, A. Sbrizzi^{67a,67c}, T. Scanlon⁹⁵,
 J. Schaarschmidt¹⁴⁸, P. Schacht¹¹⁵, D. Schaefer³⁷, L. Schaefer¹³⁶, U. Schäfer¹⁰⁰, A.C. Schaffer⁶⁵,
 D. Schaile¹¹⁴, R.D. Schamberger¹⁵⁵, E. Schanet¹¹⁴, C. Scharf¹⁹, N. Scharmberg¹⁰¹, V.A. Schegelsky¹³⁷,
 D. Scheirich¹⁴², F. Schenck¹⁹, M. Schernau¹⁷¹, C. Schiavi^{55b,55a}, L.K. Schildgen²⁴, Z.M. Schillaci²⁶,
 E.J. Schioppa^{68a,68b}, M. Schioppa^{41b,41a}, K.E. Schleicher⁵², S. Schlenker³⁶, K.R. Schmidt-Sommerfeld¹¹⁵,
 K. Schmieden¹⁰⁰, C. Schmitt¹⁰⁰, S. Schmitt⁴⁶, L. Schoeffel¹⁴⁴, A. Schoening^{61b}, P.G. Scholer⁵²,
 E. Schopf¹³⁴, M. Schott¹⁰⁰, J.F.P. Schouwenberg¹¹⁹, J. Schovancova³⁶, S. Schramm⁵⁴, F. Schroeder¹⁸²,
 A. Schulte¹⁰⁰, H-C. Schultz-Coulon^{61a}, M. Schumacher⁵², B.A. Schumm¹⁴⁵, Ph. Schune¹⁴⁴,
 A. Schwartzman¹⁵³, T.A. Schwarz¹⁰⁶, Ph. Schwemling¹⁴⁴, R. Schwienhorst¹⁰⁷, A. Sciandra¹⁴⁵,
 G. Sciolla²⁶, M. Scornajenghi^{41b,41a}, F. Scuri^{72a}, F. Scutti¹⁰⁵, L.M. Scyboz¹¹⁵, C.D. Sebastiani⁹¹,
 P. Seema¹⁹, S.C. Seidel¹¹⁸, A. Seiden¹⁴⁵, B.D. Seidlitz²⁹, T. Seiss³⁷, C. Seitz⁴⁶, J.M. Seixas^{81b},
 G. Sekhniadze^{70a}, S.J. Sekula⁴², N. Semprini-Cesari^{23b,23a}, S. Sen⁴⁹, C. Serfon²⁹, L. Serin⁶⁵,
 L. Serkin^{67a,67b}, M. Sessa^{60a}, H. Severini¹²⁸, S. Sevova¹⁵³, F. Sforza^{55b,55a}, A. Sfyrla⁵⁴, E. Shabalina⁵³,

J.D. Shahinian¹³⁶, N.W. Shaikh^{45a,45b}, D. Shaked Renous¹⁸⁰, L.Y. Shan^{15a}, M. Shapiro¹⁸, A. Sharma³⁶, A.S. Sharma¹, P.B. Shatalov¹²⁴, K. Shaw¹⁵⁶, S.M. Shaw¹⁰¹, M. Shehade¹⁸⁰, Y. Shen¹²⁸, A.D. Sherman²⁵, P. Sherwood⁹⁵, L. Shi⁹⁵, C.O. Shimmin¹⁸³, Y. Shimogama¹⁷⁹, M. Shimojima¹¹⁶, J.D. Shinner⁹⁴, I.P.J. Shipsey¹³⁴, S. Shirabe¹⁶⁵, M. Shiyakova^{80,z}, J. Shlomi¹⁸⁰, A. Shmeleva¹¹¹, M.J. Shochet³⁷, J. Shojai¹⁰⁵, D.R. Shope¹⁵⁴, S. Shrestha¹²⁷, E.M. Shrif^{33e}, M.J. Shroff¹⁷⁶, E. Shulga¹⁸⁰, P. Sicho¹⁴⁰, A.M. Sickles¹⁷³, E. Sideras Haddad^{33e}, O. Sidiropoulou³⁶, A. Sidoti^{23b,23a}, F. Siegert⁴⁸, Dj. Sijacki¹⁶, M.Jr. Silva¹⁸¹, M.V. Silva Oliveira³⁶, S.B. Silverstein^{45a}, S. Simion⁶⁵, R. Simoniello¹⁰⁰, C.J. Simpson-allsoy²¹, S. Simsek^{12b}, P. Sinervo¹⁶⁷, V. Sinetckii¹¹³, S. Singh¹⁵², M. Sioli^{23b,23a}, I. Siral¹³¹, S. Yu. Sivoklov¹¹³, J. Sjölin^{45a,45b}, A. Skaf⁵³, E. Skorda⁹⁷, P. Skubic¹²⁸, M. Slawinska⁸⁵, K. Sliwa¹⁷⁰, R. Slovak¹⁴², V. Smakhtin¹⁸⁰, B.H. Smart¹⁴³, J. Smiesko^{28b}, N. Smirnov¹¹², S. Yu. Smirnov¹¹², Y. Smirnov¹¹², L.N. Smirnova^{113,r}, O. Smirnova⁹⁷, E.A. Smith³⁷, H.A. Smith¹³⁴, M. Smizanska⁹⁰, K. Smolek¹⁴¹, A. Smykiewicz⁸⁵, A.A. Snesarev¹¹¹, H.L. Snoek¹²⁰, I.M. Snyder¹³¹, S. Snyder²⁹, R. Sobie^{176,ab}, A. Soffer¹⁶¹, A. Sogaard⁵⁰, F. Sohns⁵³, C.A. Solans Sanchez³⁶, E. Yu. Soldatov¹¹², U. Soldevila¹⁷⁴, A.A. Solodkov¹²³, A. Soloshenko⁸⁰, O.V. Solovyanov¹²³, V. Solovyev¹³⁷, P. Sommer¹⁴⁹, H. Son¹⁷⁰, A. Sonay¹⁴, W. Song¹⁴³, W.Y. Song^{168b}, A. Sopczak¹⁴¹, A.L. Soppio⁹⁵, F. Sopkova^{28b}, S. Sottocornola^{71a,71b}, R. Soualah^{67a,67c}, A.M. Soukharev^{122b,122a}, D. South⁴⁶, S. Spagnolo^{68a,68b}, M. Spalla¹¹⁵, M. Spangenberg¹⁷⁸, F. Spanò⁹⁴, D. Sperlich⁵², T.M. Spieker^{61a}, G. Spigo³⁶, M. Spina¹⁵⁶, D.P. Spiteri⁵⁷, M. Spousta¹⁴², A. Stabile^{69a,69b}, B.L. Stamas¹²¹, R. Stamen^{61a}, M. Stamenkovic¹²⁰, A. Stampekiš²¹, E. Stanecka⁸⁵, B. Stanislaus¹³⁴, M.M. Stanitzki⁴⁶, M. Stankaityte¹³⁴, B. Stapf¹²⁰, E.A. Starchenko¹²³, G.H. Stark¹⁴⁵, J. Stark⁵⁸, P. Staroba¹⁴⁰, P. Starovoitov^{61a}, S. Stärz¹⁰⁴, R. Staszewski⁸⁵, G. Stavropoulos⁴⁴, M. Stegler⁴⁶, P. Steinberg²⁹, A.L. Steinhebel¹³¹, B. Stelzer^{152,168a}, H.J. Stelzer¹³⁸, O. Stelzer-Chilton^{168a}, H. Stenzel⁵⁶, T.J. Stevenson¹⁵⁶, G.A. Stewart³⁶, M.C. Stockton³⁶, G. Stoicea^{27b}, M. Stolarski^{139a}, S. Stonjek¹¹⁵, A. Straessner⁴⁸, J. Strandberg¹⁵⁴, S. Strandberg^{45a,45b}, M. Strauss¹²⁸, T. Streblor¹⁰², P. Strizenec^{28b}, R. Ströhmer¹⁷⁷, D.M. Strom¹³¹, R. Stroynowski⁴², A. Strubig^{45a,45b}, S.A. Stucci²⁹, B. Stugu¹⁷, J. Stupak¹²⁸, N.A. Styles⁴⁶, D. Su¹⁵³, W. Su^{60c,148}, X. Su^{60a}, V.V. Sulin¹¹¹, M.J. Sullivan⁹¹, D.M.S. Sultan⁵⁴, S. Sultansoy^{4c}, T. Sumida⁸⁶, S. Sun¹⁰⁶, X. Sun¹⁰¹, C.J.E. Suster¹⁵⁷, M.R. Sutton¹⁵⁶, S. Suzuki⁸², M. Svatos¹⁴⁰, M. Swiatlowski^{168a}, S.P. Swift², T. Swirski¹⁷⁷, A. Sydorenko¹⁰⁰, I. Sykora^{28a}, M. Sykora¹⁴², T. Sykora¹⁴², D. Ta¹⁰⁰, K. Tackmann^{46,x}, J. Taenzer¹⁶¹, A. Taffard¹⁷¹, R. Tafirout^{168a}, E. Tagiev¹²³, R. Takashima⁸⁷, K. Takeda⁸³, T. Takeshita¹⁵⁰, E.P. Takeva⁵⁰, Y. Takubo⁸², M. Talby¹⁰², A.A. Talyshev^{122b,122a}, K.C. Tam^{63b}, N.M. Tamir¹⁶¹, J. Tanaka¹⁶³, R. Tanaka⁶⁵, S. Tapia Araya¹⁷³, S. Tapprogge¹⁰⁰, A. Tarek Abouelfadl Mohamed¹⁰⁷, S. Tarem¹⁶⁰, K. Tariq^{60b}, G. Tarna^{27b,d}, G.F. Tartarelli^{69a}, P. Tas¹⁴², M. Tasevsky¹⁴⁰, E. Tassi^{41b,41a}, A. Tavares Delgado^{139a}, Y. Tayalati^{35e}, A.J. Taylor⁵⁰, G.N. Taylor¹⁰⁵, W. Taylor^{168b}, H. Teagle⁹¹, A.S. Tee⁹⁰, R. Teixeira De Lima¹⁵³, P. Teixeira-Dias⁹⁴, H. Ten Kate³⁶, J.J. Teoh¹²⁰, K. Terashi¹⁶³, J. Terron⁹⁹, S. Terzo¹⁴, M. Testa⁵¹, R.J. Teuscher^{167,ab}, S.J. Thais¹⁸³, N. Themistokleous⁵⁰, T. Theveneaux-Pelzer⁴⁶, F. Thiele⁴⁰, D.W. Thomas⁹⁴, J.O. Thomas⁴², J.P. Thomas²¹, E.A. Thompson⁴⁶, P.D. Thompson²¹, E. Thomson¹³⁶, E.J. Thorpe⁹³, R.E. Ticse Torres⁵³, V.O. Tikhomirov^{111,ai}, Yu.A. Tikhonov^{122b,122a}, S. Timoshenko¹¹², P. Tipton¹⁸³, S. Tisserant¹⁰², K. Todome^{23b,23a}, S. Todorova-Nova¹⁴², S. Todt⁴⁸, J. Tojo⁸⁸, S. Tokár^{28a}, K. Tokushuku⁸², E. Tolley¹²⁷, R. Tombs³², K.G. Tomiwa^{33e}, M. Tomoto^{82,117}, L. Tompkins¹⁵³, P. Tornambe¹⁰³, E. Torrence¹³¹, H. Torres⁴⁸, E. Torró Pastor¹⁷⁴, M. Toscani³⁰, C. Toscirì¹³⁴, J. Toth^{102,aa}, D.R. Tovey¹⁴⁹, A. Traeet¹⁷, C.J. Treado¹²⁵, T. Trefzger¹⁷⁷, F. Tresoldi¹⁵⁶, A. Tricoli²⁹, I.M. Trigger^{168a}, S. Trincaz-Duvoid¹³⁵, D.A. Trischuk¹⁷⁵, W. Trischuk¹⁶⁷, B. Trocme⁵⁸, A. Trofymov⁶⁵, C. Troncon^{69a}, F. Trovato¹⁵⁶, L. Truong^{33c}, M. Trzebinski⁸⁵, A. Trzupek⁸⁵, F. Tsai⁴⁶, J.C.-L. Tseng¹³⁴, P.V. Tsiarshka^{108,af}, A. Tsirigotis^{162,u}, V. Tsiskaridze¹⁵⁵, E.G. Tskhadadze^{159a}, M. Tsopoulou¹⁶², I.I. Tsukerman¹²⁴, V. Tsulaia¹⁸, S. Tsuno⁸², D. Tsybychev¹⁵⁵, Y. Tu^{63b}, A. Tudorache^{27b}, V. Tudorache^{27b}, T.T. Tulbure^{27a}, A.N. Tuna⁵⁹, S. Turchikhin⁸⁰, D. Turgeman¹⁸⁰, I. Turk Cakir^{4b,s}, R.J. Turner²¹, R. Turra^{69a}, P.M. Tuts³⁹, S. Tzamarias¹⁶², E. Tzovara¹⁰⁰, K. Uchida¹⁶³, F. Ukegawa¹⁶⁹,

G. Unal³⁶, M. Unal¹¹, A. Undrus²⁹, G. Unel¹⁷¹, F.C. Ungaro¹⁰⁵, Y. Unno⁸², K. Uno¹⁶³, J. Urban^{28b}, P. Urquijo¹⁰⁵, G. Usai⁸, Z. Uysal^{12d}, V. Vacek¹⁴¹, B. Vachon¹⁰⁴, K.O.H. Vadla¹³³, T. Vafeiadis³⁶, A. Vaidya⁹⁵, C. Valderanis¹¹⁴, E. Valdes Santurio^{45a,45b}, M. Valente^{168a}, S. Valentinetti^{23b,23a}, A. Valero¹⁷⁴, L. Valéry⁴⁶, R.A. Vallance²¹, A. Vallier³⁶, J.A. Valls Ferrer¹⁷⁴, T.R. Van Daalen¹⁴, P. Van Gemmeren⁶, S. Van Stroud⁹⁵, I. Van Vulpen¹²⁰, M. Vanadia^{74a,74b}, W. Vandelli³⁶, M. Vandenbroucke¹⁴⁴, E.R. Vandewall¹²⁹, A. Vaniachine¹⁶⁶, D. Vannicola^{73a,73b}, R. Vari^{73a}, E.W. Varnes⁷, C. Varni^{55b,55a}, T. Varol¹⁵⁸, D. Varouchas⁶⁵, K.E. Varvell¹⁵⁷, M.E. Vasile^{27b}, G.A. Vasquez¹⁷⁶, F. Vazeille³⁸, D. Vazquez Furelos¹⁴, T. Vazquez Schroeder³⁶, J. Veatch⁵³, V. Vecchio¹⁰¹, M.J. Veen¹²⁰, L.M. Veloce¹⁶⁷, F. Veloso^{139a,139c}, S. Veneziano^{73a}, A. Ventura^{68a,68b}, A. Verbytskyi¹¹⁵, V. Vercesi^{71a}, M. Verducci^{72a,72b}, C.M. Vergel Infante⁷⁹, C. Vergis²⁴, W. Verkerke¹²⁰, A.T. Vermeulen¹²⁰, J.C. Vermeulen¹²⁰, C. Vernieri¹⁵³, P.J. Verschuuren⁹⁴, M.C. Vetterli^{152,am}, N. Viaux Maira^{146d}, T. Vickey¹⁴⁹, O.E. Vickey Boeriu¹⁴⁹, G.H.A. Viehhauser¹³⁴, L. Vigani^{61b}, M. Villa^{23b,23a}, M. Villaplana Perez³, E.M. Villhauer⁵⁰, E. Vilucchi⁵¹, M.G. Vincter³⁴, G.S. Virdee²¹, A. Vishwakarma⁵⁰, C. Vittori^{23b,23a}, I. Vivarelli¹⁵⁶, M. Vogel¹⁸², P. Vokac¹⁴¹, S.E. von Buddenbrock^{33e}, E. Von Toerne²⁴, V. Vorobel¹⁴², K. Vorobev¹¹², M. Vos¹⁷⁴, J.H. Vosseveld⁹¹, M. Vozak¹⁰¹, N. Vranjes¹⁶, M. Vranjes Milosavljevic¹⁶, V. Vrba¹⁴¹, M. Vreeswijk¹²⁰, N.K. Vu¹⁰², R. Vuillermet³⁶, I. Vukotic³⁷, S. Wada¹⁶⁹, P. Wagner²⁴, W. Wagner¹⁸², J. Wagner-Kuhr¹¹⁴, S. Wahdan¹⁸², H. Wahlberg⁸⁹, R. Wakasa¹⁶⁹, V.M. Walbrecht¹¹⁵, J. Walder¹⁴³, R. Walker¹¹⁴, S.D. Walker⁹⁴, W. Walkowiak¹⁵¹, V. Wallangen^{45a,45b}, A.M. Wang⁵⁹, A.Z. Wang¹⁸¹, C. Wang^{60a}, C. Wang^{60c}, F. Wang¹⁸¹, H. Wang¹⁸, H. Wang³, J. Wang^{63a}, P. Wang⁴², Q. Wang¹²⁸, R.-J. Wang¹⁰⁰, R. Wang^{60a}, R. Wang⁶, S.M. Wang¹⁵⁸, W.T. Wang^{60a}, W. Wang^{15c}, W.X. Wang^{60a}, Y. Wang^{60a}, Z. Wang¹⁰⁶, C. Wanotayaroj⁴⁶, A. Warburton¹⁰⁴, C.P. Ward³², R.J. Ward²¹, N. Warrack⁵⁷, A.T. Watson²¹, M.F. Watson²¹, G. Watts¹⁴⁸, B.M. Waugh⁹⁵, A.F. Webb¹¹, C. Weber²⁹, M.S. Weber²⁰, S.A. Weber³⁴, S.M. Weber^{61a}, A.R. Weidberg¹³⁴, J. Weingarten⁴⁷, M. Weirich¹⁰⁰, C. Weiser⁵², P.S. Wells³⁶, T. Wenaus²⁹, B. Wendland⁴⁷, T. Wengler³⁶, S. Wenig³⁶, N. Wermes²⁴, M. Wessels^{61a}, T.D. Weston²⁰, K. Whalen¹³¹, A.M. Wharton⁹⁰, A.S. White¹⁰⁶, A. White⁸, M.J. White¹, D. Whiteson¹⁷¹, B.W. Whitmore⁹⁰, W. Wiedenmann¹⁸¹, C. Wiel⁴⁸, M. Wielers¹⁴³, N. Wieseotte¹⁰⁰, C. Wiglesworth⁴⁰, L.A.M. Wiik-Fuchs⁵², H.G. Wilkens³⁶, L.J. Wilkins⁹⁴, H.H. Williams¹³⁶, S. Williams³², S. Willocq¹⁰³, P.J. Windischhofer¹³⁴, I. Wingerter-Seez⁵, E. Winkels¹⁵⁶, F. Winklmeier¹³¹, B.T. Winter⁵², M. Wittgen¹⁵³, M. Wobisch⁹⁶, A. Wolf¹⁰⁰, R. Wölker¹³⁴, J. Wollrath⁵², M.W. Wolter⁸⁵, H. Wolters^{139a,139c}, V.W.S. Wong¹⁷⁵, N.L. Woods¹⁴⁵, S.D. Worm⁴⁶, B.K. Wosiek⁸⁵, K.W. Woźniak⁸⁵, K. Wraight⁵⁷, S.L. Wu¹⁸¹, X. Wu⁵⁴, Y. Wu^{60a}, J. Wuerzinger¹³⁴, T.R. Wyatt¹⁰¹, B.M. Wynne⁵⁰, S. Xella⁴⁰, L. Xia¹⁷⁸, J. Xiang^{63c}, X. Xiao¹⁰⁶, X. Xie^{60a}, I. Xiotidis¹⁵⁶, D. Xu^{15a}, H. Xu^{60a}, H. Xu^{60a}, L. Xu²⁹, T. Xu¹⁴⁴, W. Xu¹⁰⁶, Y. Xu^{15b}, Z. Xu^{60b}, Z. Xu¹⁵³, B. Yabsley¹⁵⁷, S. Yacoub^{33a}, D.P. Yallup⁹⁵, N. Yamaguchi⁸⁸, Y. Yamaguchi¹⁶⁵, A. Yamamoto⁸², M. Yamatani¹⁶³, T. Yamazaki¹⁶³, Y. Yamazaki⁸³, J. Yan^{60c}, Z. Yan²⁵, H.J. Yang^{60c,60d}, H.T. Yang¹⁸, S. Yang^{60a}, T. Yang^{63c}, X. Yang^{60b,58}, Y. Yang¹⁶³, Z. Yang^{60a}, W.-M. Yao¹⁸, Y.C. Yap⁴⁶, E. Yatsenko^{60c}, H. Ye^{15c}, J. Ye⁴², S. Ye²⁹, I. Yeletsikh⁸⁰, M.R. Yexley⁹⁰, E. Yigitbasi²⁵, P. Yin³⁹, K. Yorita¹⁷⁹, K. Yoshihara⁷⁹, C.J.S. Young³⁶, C. Young¹⁵³, J. Yu⁷⁹, R. Yuan^{60b,h}, X. Yue^{61a}, M. Zaazoua^{35e}, B. Zabinski⁸⁵, G. Zacharis¹⁰, E. Zaffaroni⁵⁴, J. Zahreddine¹³⁵, A.M. Zaitsev^{123,ah}, T. Zakareishvili^{159b}, N. Zakharchuk³⁴, S. Zambito³⁶, D. Zanzi³⁶, S.V. Zeißner⁴⁷, C. Zeitnitz¹⁸², G. Zemaityte¹³⁴, J.C. Zeng¹⁷³, O. Zenin¹²³, T. Ženiš^{28a}, D. Zerwas⁶⁵, M. Zgubič¹³⁴, B. Zhang^{15c}, D.F. Zhang^{15b}, G. Zhang^{15b}, J. Zhang⁶, Kaili. Zhang^{15a}, L. Zhang^{15c}, L. Zhang^{60a}, M. Zhang¹⁷³, R. Zhang¹⁸¹, S. Zhang¹⁰⁶, X. Zhang^{60c}, X. Zhang^{60b}, Y. Zhang^{15a,15d}, Z. Zhang^{63a}, Z. Zhang⁶⁵, P. Zhao⁴⁹, Z. Zhao^{60a}, A. Zhemchugov⁸⁰, Z. Zheng¹⁰⁶, D. Zhong¹⁷³, B. Zhou¹⁰⁶, C. Zhou¹⁸¹, H. Zhou⁷, M.S. Zhou^{15a,15d}, M. Zhou¹⁵⁵, N. Zhou^{60c}, Y. Zhou⁷, C.G. Zhu^{60b}, C. Zhu^{15a,15d}, H.L. Zhu^{60a}, H. Zhu^{15a}, J. Zhu¹⁰⁶, Y. Zhu^{60a}, X. Zhuang^{15a}, K. Zhukov¹¹¹, V. Zhulanov^{122b,122a}, D. Ziemska⁶⁶, N.I. Zimine⁸⁰, S. Zimmermann^{52,*}, Z. Zinonos¹¹⁵, M. Ziolkowski¹⁵¹, L. Živković¹⁶, G. Zobernig¹⁸¹, A. Zoccoli^{23b,23a}, K. Zoch⁵³, T.G. Zorbas¹⁴⁹, R. Zou³⁷, L. Zwalinski³⁶.

- ¹Department of Physics, University of Adelaide, Adelaide; Australia.
- ²Physics Department, SUNY Albany, Albany NY; United States of America.
- ³Department of Physics, University of Alberta, Edmonton AB; Canada.
- ⁴(^a)Department of Physics, Ankara University, Ankara; (^b)Istanbul Aydin University, Application and Research Center for Advanced Studies, Istanbul; (^c)Division of Physics, TOBB University of Economics and Technology, Ankara; Turkey.
- ⁵LAPP, Université Grenoble Alpes, Université Savoie Mont Blanc, CNRS/IN2P3, Annecy; France.
- ⁶High Energy Physics Division, Argonne National Laboratory, Argonne IL; United States of America.
- ⁷Department of Physics, University of Arizona, Tucson AZ; United States of America.
- ⁸Department of Physics, University of Texas at Arlington, Arlington TX; United States of America.
- ⁹Physics Department, National and Kapodistrian University of Athens, Athens; Greece.
- ¹⁰Physics Department, National Technical University of Athens, Zografou; Greece.
- ¹¹Department of Physics, University of Texas at Austin, Austin TX; United States of America.
- ¹²(^a)Bahcesehir University, Faculty of Engineering and Natural Sciences, Istanbul; (^b)Istanbul Bilgi University, Faculty of Engineering and Natural Sciences, Istanbul; (^c)Department of Physics, Bogazici University, Istanbul; (^d)Department of Physics Engineering, Gaziantep University, Gaziantep; Turkey.
- ¹³Institute of Physics, Azerbaijan Academy of Sciences, Baku; Azerbaijan.
- ¹⁴Institut de Física d'Altes Energies (IFAE), Barcelona Institute of Science and Technology, Barcelona; Spain.
- ¹⁵(^a)Institute of High Energy Physics, Chinese Academy of Sciences, Beijing; (^b)Physics Department, Tsinghua University, Beijing; (^c)Department of Physics, Nanjing University, Nanjing; (^d)University of Chinese Academy of Science (UCAS), Beijing; China.
- ¹⁶Institute of Physics, University of Belgrade, Belgrade; Serbia.
- ¹⁷Department for Physics and Technology, University of Bergen, Bergen; Norway.
- ¹⁸Physics Division, Lawrence Berkeley National Laboratory and University of California, Berkeley CA; United States of America.
- ¹⁹Institut für Physik, Humboldt Universität zu Berlin, Berlin; Germany.
- ²⁰Albert Einstein Center for Fundamental Physics and Laboratory for High Energy Physics, University of Bern, Bern; Switzerland.
- ²¹School of Physics and Astronomy, University of Birmingham, Birmingham; United Kingdom.
- ²²(^a)Facultad de Ciencias y Centro de Investigaciones, Universidad Antonio Nariño, Bogotá; (^b)Departamento de Física, Universidad Nacional de Colombia, Bogotá, Colombia; Colombia.
- ²³(^a)INFN Bologna and Università di Bologna, Dipartimento di Fisica; (^b)INFN Sezione di Bologna; Italy.
- ²⁴Physikalisches Institut, Universität Bonn, Bonn; Germany.
- ²⁵Department of Physics, Boston University, Boston MA; United States of America.
- ²⁶Department of Physics, Brandeis University, Waltham MA; United States of America.
- ²⁷(^a)Transilvania University of Brasov, Brasov; (^b)Horia Hulubei National Institute of Physics and Nuclear Engineering, Bucharest; (^c)Department of Physics, Alexandru Ioan Cuza University of Iasi, Iasi; (^d)National Institute for Research and Development of Isotopic and Molecular Technologies, Physics Department, Cluj-Napoca; (^e)University Politehnica Bucharest, Bucharest; (^f)West University in Timisoara, Timisoara; Romania.
- ²⁸(^a)Faculty of Mathematics, Physics and Informatics, Comenius University, Bratislava; (^b)Department of Subnuclear Physics, Institute of Experimental Physics of the Slovak Academy of Sciences, Kosice; Slovak Republic.
- ²⁹Physics Department, Brookhaven National Laboratory, Upton NY; United States of America.
- ³⁰Departamento de Física, Universidad de Buenos Aires, Buenos Aires; Argentina.
- ³¹California State University, CA; United States of America.

- ³²Cavendish Laboratory, University of Cambridge, Cambridge; United Kingdom.
- ³³(^a)Department of Physics, University of Cape Town, Cape Town; (^b)iThemba Labs, Western Cape; (^c)Department of Mechanical Engineering Science, University of Johannesburg, Johannesburg; (^d)University of South Africa, Department of Physics, Pretoria; (^e)School of Physics, University of the Witwatersrand, Johannesburg; South Africa.
- ³⁴Department of Physics, Carleton University, Ottawa ON; Canada.
- ³⁵(^a)Faculté des Sciences Ain Chock, Réseau Universitaire de Physique des Hautes Energies - Université Hassan II, Casablanca; (^b)Faculté des Sciences, Université Ibn-Tofail, Kénitra; (^c)Faculté des Sciences Semlalia, Université Cadi Ayyad, LPHEA-Marrakech; (^d)Faculté des Sciences, Université Mohamed Premier and LPTPM, Oujda; (^e)Faculté des sciences, Université Mohammed V, Rabat; Morocco.
- ³⁶CERN, Geneva; Switzerland.
- ³⁷Enrico Fermi Institute, University of Chicago, Chicago IL; United States of America.
- ³⁸LPC, Université Clermont Auvergne, CNRS/IN2P3, Clermont-Ferrand; France.
- ³⁹Nevis Laboratory, Columbia University, Irvington NY; United States of America.
- ⁴⁰Niels Bohr Institute, University of Copenhagen, Copenhagen; Denmark.
- ⁴¹(^a)Dipartimento di Fisica, Università della Calabria, Rende; (^b)INFN Gruppo Collegato di Cosenza, Laboratori Nazionali di Frascati; Italy.
- ⁴²Physics Department, Southern Methodist University, Dallas TX; United States of America.
- ⁴³Physics Department, University of Texas at Dallas, Richardson TX; United States of America.
- ⁴⁴National Centre for Scientific Research "Demokritos", Agia Paraskevi; Greece.
- ⁴⁵(^a)Department of Physics, Stockholm University; (^b)Oskar Klein Centre, Stockholm; Sweden.
- ⁴⁶Deutsches Elektronen-Synchrotron DESY, Hamburg and Zeuthen; Germany.
- ⁴⁷Lehrstuhl für Experimentelle Physik IV, Technische Universität Dortmund, Dortmund; Germany.
- ⁴⁸Institut für Kern- und Teilchenphysik, Technische Universität Dresden, Dresden; Germany.
- ⁴⁹Department of Physics, Duke University, Durham NC; United States of America.
- ⁵⁰SUPA - School of Physics and Astronomy, University of Edinburgh, Edinburgh; United Kingdom.
- ⁵¹INFN e Laboratori Nazionali di Frascati, Frascati; Italy.
- ⁵²Physikalisches Institut, Albert-Ludwigs-Universität Freiburg, Freiburg; Germany.
- ⁵³II. Physikalisches Institut, Georg-August-Universität Göttingen, Göttingen; Germany.
- ⁵⁴Département de Physique Nucléaire et Corpusculaire, Université de Genève, Genève; Switzerland.
- ⁵⁵(^a)Dipartimento di Fisica, Università di Genova, Genova; (^b)INFN Sezione di Genova; Italy.
- ⁵⁶II. Physikalisches Institut, Justus-Liebig-Universität Giessen, Giessen; Germany.
- ⁵⁷SUPA - School of Physics and Astronomy, University of Glasgow, Glasgow; United Kingdom.
- ⁵⁸LPSC, Université Grenoble Alpes, CNRS/IN2P3, Grenoble INP, Grenoble; France.
- ⁵⁹Laboratory for Particle Physics and Cosmology, Harvard University, Cambridge MA; United States of America.
- ⁶⁰(^a)Department of Modern Physics and State Key Laboratory of Particle Detection and Electronics, University of Science and Technology of China, Hefei; (^b)Institute of Frontier and Interdisciplinary Science and Key Laboratory of Particle Physics and Particle Irradiation (MOE), Shandong University, Qingdao; (^c)School of Physics and Astronomy, Shanghai Jiao Tong University, KLPPAC-MoE, SKLPPC, Shanghai; (^d)Tsung-Dao Lee Institute, Shanghai; China.
- ⁶¹(^a)Kirchhoff-Institut für Physik, Ruprecht-Karls-Universität Heidelberg, Heidelberg; (^b)Physikalisches Institut, Ruprecht-Karls-Universität Heidelberg, Heidelberg; Germany.
- ⁶²Faculty of Applied Information Science, Hiroshima Institute of Technology, Hiroshima; Japan.
- ⁶³(^a)Department of Physics, Chinese University of Hong Kong, Shatin, N.T., Hong Kong; (^b)Department of Physics, University of Hong Kong, Hong Kong; (^c)Department of Physics and Institute for Advanced Study, Hong Kong University of Science and Technology, Clear Water Bay, Kowloon, Hong Kong; China.

- ⁶⁴Department of Physics, National Tsing Hua University, Hsinchu; Taiwan.
- ⁶⁵IJCLab, Université Paris-Saclay, CNRS/IN2P3, 91405, Orsay; France.
- ⁶⁶Department of Physics, Indiana University, Bloomington IN; United States of America.
- ⁶⁷(^a)INFN Gruppo Collegato di Udine, Sezione di Trieste, Udine; (^b)ICTP, Trieste; (^c)Dipartimento Politecnico di Ingegneria e Architettura, Università di Udine, Udine; Italy.
- ⁶⁸(^a)INFN Sezione di Lecce; (^b)Dipartimento di Matematica e Fisica, Università del Salento, Lecce; Italy.
- ⁶⁹(^a)INFN Sezione di Milano; (^b)Dipartimento di Fisica, Università di Milano, Milano; Italy.
- ⁷⁰(^a)INFN Sezione di Napoli; (^b)Dipartimento di Fisica, Università di Napoli, Napoli; Italy.
- ⁷¹(^a)INFN Sezione di Pavia; (^b)Dipartimento di Fisica, Università di Pavia, Pavia; Italy.
- ⁷²(^a)INFN Sezione di Pisa; (^b)Dipartimento di Fisica E. Fermi, Università di Pisa, Pisa; Italy.
- ⁷³(^a)INFN Sezione di Roma; (^b)Dipartimento di Fisica, Sapienza Università di Roma, Roma; Italy.
- ⁷⁴(^a)INFN Sezione di Roma Tor Vergata; (^b)Dipartimento di Fisica, Università di Roma Tor Vergata, Roma; Italy.
- ⁷⁵(^a)INFN Sezione di Roma Tre; (^b)Dipartimento di Matematica e Fisica, Università Roma Tre, Roma; Italy.
- ⁷⁶(^a)INFN-TIFPA; (^b)Università degli Studi di Trento, Trento; Italy.
- ⁷⁷Institut für Astro- und Teilchenphysik, Leopold-Franzens-Universität, Innsbruck; Austria.
- ⁷⁸University of Iowa, Iowa City IA; United States of America.
- ⁷⁹Department of Physics and Astronomy, Iowa State University, Ames IA; United States of America.
- ⁸⁰Joint Institute for Nuclear Research, Dubna; Russia.
- ⁸¹(^a)Departamento de Engenharia Elétrica, Universidade Federal de Juiz de Fora (UFJF), Juiz de Fora; (^b)Universidade Federal do Rio De Janeiro COPPE/EE/IF, Rio de Janeiro; (^c)Instituto de Física, Universidade de São Paulo, São Paulo; Brazil.
- ⁸²KEK, High Energy Accelerator Research Organization, Tsukuba; Japan.
- ⁸³Graduate School of Science, Kobe University, Kobe; Japan.
- ⁸⁴(^a)AGH University of Science and Technology, Faculty of Physics and Applied Computer Science, Krakow; (^b)Marian Smoluchowski Institute of Physics, Jagiellonian University, Krakow; Poland.
- ⁸⁵Institute of Nuclear Physics Polish Academy of Sciences, Krakow; Poland.
- ⁸⁶Faculty of Science, Kyoto University, Kyoto; Japan.
- ⁸⁷Kyoto University of Education, Kyoto; Japan.
- ⁸⁸Research Center for Advanced Particle Physics and Department of Physics, Kyushu University, Fukuoka ; Japan.
- ⁸⁹Instituto de Física La Plata, Universidad Nacional de La Plata and CONICET, La Plata; Argentina.
- ⁹⁰Physics Department, Lancaster University, Lancaster; United Kingdom.
- ⁹¹Oliver Lodge Laboratory, University of Liverpool, Liverpool; United Kingdom.
- ⁹²Department of Experimental Particle Physics, Jožef Stefan Institute and Department of Physics, University of Ljubljana, Ljubljana; Slovenia.
- ⁹³School of Physics and Astronomy, Queen Mary University of London, London; United Kingdom.
- ⁹⁴Department of Physics, Royal Holloway University of London, Egham; United Kingdom.
- ⁹⁵Department of Physics and Astronomy, University College London, London; United Kingdom.
- ⁹⁶Louisiana Tech University, Ruston LA; United States of America.
- ⁹⁷Fysiska institutionen, Lunds universitet, Lund; Sweden.
- ⁹⁸Centre de Calcul de l'Institut National de Physique Nucléaire et de Physique des Particules (IN2P3), Villeurbanne; France.
- ⁹⁹Departamento de Física Teórica C-15 and CIAFF, Universidad Autónoma de Madrid, Madrid; Spain.
- ¹⁰⁰Institut für Physik, Universität Mainz, Mainz; Germany.
- ¹⁰¹School of Physics and Astronomy, University of Manchester, Manchester; United Kingdom.

- ¹⁰²CPPM, Aix-Marseille Université, CNRS/IN2P3, Marseille; France.
- ¹⁰³Department of Physics, University of Massachusetts, Amherst MA; United States of America.
- ¹⁰⁴Department of Physics, McGill University, Montreal QC; Canada.
- ¹⁰⁵School of Physics, University of Melbourne, Victoria; Australia.
- ¹⁰⁶Department of Physics, University of Michigan, Ann Arbor MI; United States of America.
- ¹⁰⁷Department of Physics and Astronomy, Michigan State University, East Lansing MI; United States of America.
- ¹⁰⁸B.I. Stepanov Institute of Physics, National Academy of Sciences of Belarus, Minsk; Belarus.
- ¹⁰⁹Research Institute for Nuclear Problems of Byelorussian State University, Minsk; Belarus.
- ¹¹⁰Group of Particle Physics, University of Montreal, Montreal QC; Canada.
- ¹¹¹P.N. Lebedev Physical Institute of the Russian Academy of Sciences, Moscow; Russia.
- ¹¹²National Research Nuclear University MEPhI, Moscow; Russia.
- ¹¹³D.V. Skobel'syn Institute of Nuclear Physics, M.V. Lomonosov Moscow State University, Moscow; Russia.
- ¹¹⁴Fakultät für Physik, Ludwig-Maximilians-Universität München, München; Germany.
- ¹¹⁵Max-Planck-Institut für Physik (Werner-Heisenberg-Institut), München; Germany.
- ¹¹⁶Nagasaki Institute of Applied Science, Nagasaki; Japan.
- ¹¹⁷Graduate School of Science and Kobayashi-Maskawa Institute, Nagoya University, Nagoya; Japan.
- ¹¹⁸Department of Physics and Astronomy, University of New Mexico, Albuquerque NM; United States of America.
- ¹¹⁹Institute for Mathematics, Astrophysics and Particle Physics, Radboud University/Nikhef, Nijmegen; Netherlands.
- ¹²⁰Nikhef National Institute for Subatomic Physics and University of Amsterdam, Amsterdam; Netherlands.
- ¹²¹Department of Physics, Northern Illinois University, DeKalb IL; United States of America.
- ¹²²^(a)Budker Institute of Nuclear Physics and NSU, SB RAS, Novosibirsk; ^(b)Novosibirsk State University Novosibirsk; Russia.
- ¹²³Institute for High Energy Physics of the National Research Centre Kurchatov Institute, Protvino; Russia.
- ¹²⁴Institute for Theoretical and Experimental Physics named by A.I. Alikhanov of National Research Centre "Kurchatov Institute", Moscow; Russia.
- ¹²⁵Department of Physics, New York University, New York NY; United States of America.
- ¹²⁶Ochanomizu University, Otsuka, Bunkyo-ku, Tokyo; Japan.
- ¹²⁷Ohio State University, Columbus OH; United States of America.
- ¹²⁸Homer L. Dodge Department of Physics and Astronomy, University of Oklahoma, Norman OK; United States of America.
- ¹²⁹Department of Physics, Oklahoma State University, Stillwater OK; United States of America.
- ¹³⁰Palacký University, RCPTM, Joint Laboratory of Optics, Olomouc; Czech Republic.
- ¹³¹Institute for Fundamental Science, University of Oregon, Eugene, OR; United States of America.
- ¹³²Graduate School of Science, Osaka University, Osaka; Japan.
- ¹³³Department of Physics, University of Oslo, Oslo; Norway.
- ¹³⁴Department of Physics, Oxford University, Oxford; United Kingdom.
- ¹³⁵LPNHE, Sorbonne Université, Université de Paris, CNRS/IN2P3, Paris; France.
- ¹³⁶Department of Physics, University of Pennsylvania, Philadelphia PA; United States of America.
- ¹³⁷Konstantinov Nuclear Physics Institute of National Research Centre "Kurchatov Institute", PNPI, St. Petersburg; Russia.
- ¹³⁸Department of Physics and Astronomy, University of Pittsburgh, Pittsburgh PA; United States of America.

- ¹³⁹(*a*) Laboratório de Instrumentação e Física Experimental de Partículas - LIP, Lisboa; (*b*) Departamento de Física, Faculdade de Ciências, Universidade de Lisboa, Lisboa; (*c*) Departamento de Física, Universidade de Coimbra, Coimbra; (*d*) Centro de Física Nuclear da Universidade de Lisboa, Lisboa; (*e*) Departamento de Física, Universidade do Minho, Braga; (*f*) Departamento de Física Teórica y del Cosmos, Universidad de Granada, Granada (Spain); (*g*) Dep Física and CEFITEC of Faculdade de Ciências e Tecnologia, Universidade Nova de Lisboa, Caparica; (*h*) Instituto Superior Técnico, Universidade de Lisboa, Lisboa; Portugal.
- ¹⁴⁰Institute of Physics of the Czech Academy of Sciences, Prague; Czech Republic.
- ¹⁴¹Czech Technical University in Prague, Prague; Czech Republic.
- ¹⁴²Charles University, Faculty of Mathematics and Physics, Prague; Czech Republic.
- ¹⁴³Particle Physics Department, Rutherford Appleton Laboratory, Didcot; United Kingdom.
- ¹⁴⁴IRFU, CEA, Université Paris-Saclay, Gif-sur-Yvette; France.
- ¹⁴⁵Santa Cruz Institute for Particle Physics, University of California Santa Cruz, Santa Cruz CA; United States of America.
- ¹⁴⁶(*a*) Departamento de Física, Pontificia Universidad Católica de Chile, Santiago; (*b*) Universidad Andres Bello, Department of Physics, Santiago; (*c*) Instituto de Alta Investigación, Universidad de Tarapacá; (*d*) Departamento de Física, Universidad Técnica Federico Santa María, Valparaíso; Chile.
- ¹⁴⁷Universidade Federal de São João del Rei (UFSJ), São João del Rei; Brazil.
- ¹⁴⁸Department of Physics, University of Washington, Seattle WA; United States of America.
- ¹⁴⁹Department of Physics and Astronomy, University of Sheffield, Sheffield; United Kingdom.
- ¹⁵⁰Department of Physics, Shinshu University, Nagano; Japan.
- ¹⁵¹Department Physik, Universität Siegen, Siegen; Germany.
- ¹⁵²Department of Physics, Simon Fraser University, Burnaby BC; Canada.
- ¹⁵³SLAC National Accelerator Laboratory, Stanford CA; United States of America.
- ¹⁵⁴Physics Department, Royal Institute of Technology, Stockholm; Sweden.
- ¹⁵⁵Departments of Physics and Astronomy, Stony Brook University, Stony Brook NY; United States of America.
- ¹⁵⁶Department of Physics and Astronomy, University of Sussex, Brighton; United Kingdom.
- ¹⁵⁷School of Physics, University of Sydney, Sydney; Australia.
- ¹⁵⁸Institute of Physics, Academia Sinica, Taipei; Taiwan.
- ¹⁵⁹(*a*) E. Andronikashvili Institute of Physics, Iv. Javakhishvili Tbilisi State University, Tbilisi; (*b*) High Energy Physics Institute, Tbilisi State University, Tbilisi; Georgia.
- ¹⁶⁰Department of Physics, Technion, Israel Institute of Technology, Haifa; Israel.
- ¹⁶¹Raymond and Beverly Sackler School of Physics and Astronomy, Tel Aviv University, Tel Aviv; Israel.
- ¹⁶²Department of Physics, Aristotle University of Thessaloniki, Thessaloniki; Greece.
- ¹⁶³International Center for Elementary Particle Physics and Department of Physics, University of Tokyo, Tokyo; Japan.
- ¹⁶⁴Graduate School of Science and Technology, Tokyo Metropolitan University, Tokyo; Japan.
- ¹⁶⁵Department of Physics, Tokyo Institute of Technology, Tokyo; Japan.
- ¹⁶⁶Tomsk State University, Tomsk; Russia.
- ¹⁶⁷Department of Physics, University of Toronto, Toronto ON; Canada.
- ¹⁶⁸(*a*) TRIUMF, Vancouver BC; (*b*) Department of Physics and Astronomy, York University, Toronto ON; Canada.
- ¹⁶⁹Division of Physics and Tomonaga Center for the History of the Universe, Faculty of Pure and Applied Sciences, University of Tsukuba, Tsukuba; Japan.
- ¹⁷⁰Department of Physics and Astronomy, Tufts University, Medford MA; United States of America.
- ¹⁷¹Department of Physics and Astronomy, University of California Irvine, Irvine CA; United States of

America.

¹⁷²Department of Physics and Astronomy, University of Uppsala, Uppsala; Sweden.

¹⁷³Department of Physics, University of Illinois, Urbana IL; United States of America.

¹⁷⁴Instituto de Física Corpuscular (IFIC), Centro Mixto Universidad de Valencia - CSIC, Valencia; Spain.

¹⁷⁵Department of Physics, University of British Columbia, Vancouver BC; Canada.

¹⁷⁶Department of Physics and Astronomy, University of Victoria, Victoria BC; Canada.

¹⁷⁷Fakultät für Physik und Astronomie, Julius-Maximilians-Universität Würzburg, Würzburg; Germany.

¹⁷⁸Department of Physics, University of Warwick, Coventry; United Kingdom.

¹⁷⁹Waseda University, Tokyo; Japan.

¹⁸⁰Department of Particle Physics and Astrophysics, Weizmann Institute of Science, Rehovot; Israel.

¹⁸¹Department of Physics, University of Wisconsin, Madison WI; United States of America.

¹⁸²Fakultät für Mathematik und Naturwissenschaften, Fachgruppe Physik, Bergische Universität Wuppertal, Wuppertal; Germany.

¹⁸³Department of Physics, Yale University, New Haven CT; United States of America.

^a Also at Borough of Manhattan Community College, City University of New York, New York NY; United States of America.

^b Also at Centro Studi e Ricerche Enrico Fermi; Italy.

^c Also at CERN, Geneva; Switzerland.

^d Also at CPPM, Aix-Marseille Université, CNRS/IN2P3, Marseille; France.

^e Also at Département de Physique Nucléaire et Corpusculaire, Université de Genève, Genève; Switzerland.

^f Also at Departament de Física de la Universitat Autònoma de Barcelona, Barcelona; Spain.

^g Also at Department of Financial and Management Engineering, University of the Aegean, Chios; Greece.

^h Also at Department of Physics and Astronomy, Michigan State University, East Lansing MI; United States of America.

ⁱ Also at Department of Physics and Astronomy, University of Louisville, Louisville, KY; United States of America.

^j Also at Department of Physics, Ben Gurion University of the Negev, Beer Sheva; Israel.

^k Also at Department of Physics, California State University, East Bay; United States of America.

^l Also at Department of Physics, California State University, Fresno; United States of America.

^m Also at Department of Physics, California State University, Sacramento; United States of America.

ⁿ Also at Department of Physics, King's College London, London; United Kingdom.

^o Also at Department of Physics, St. Petersburg State Polytechnical University, St. Petersburg; Russia.

^p Also at Department of Physics, University of Fribourg, Fribourg; Switzerland.

^q Also at Dipartimento di Matematica, Informatica e Fisica, Università di Udine, Udine; Italy.

^r Also at Faculty of Physics, M.V. Lomonosov Moscow State University, Moscow; Russia.

^s Also at Giresun University, Faculty of Engineering, Giresun; Turkey.

^t Also at Graduate School of Science, Osaka University, Osaka; Japan.

^u Also at Hellenic Open University, Patras; Greece.

^v Also at IJCLab, Université Paris-Saclay, CNRS/IN2P3, 91405, Orsay; France.

^w Also at Institutio Catalana de Recerca i Estudis Avancats, ICREA, Barcelona; Spain.

^x Also at Institut für Experimentalphysik, Universität Hamburg, Hamburg; Germany.

^y Also at Institute for Mathematics, Astrophysics and Particle Physics, Radboud University/Nikhef, Nijmegen; Netherlands.

^z Also at Institute for Nuclear Research and Nuclear Energy (INRNE) of the Bulgarian Academy of Sciences, Sofia; Bulgaria.

^{aa} Also at Institute for Particle and Nuclear Physics, Wigner Research Centre for Physics, Budapest;

Hungary.

ab Also at Institute of Particle Physics (IPP); Canada.

ac Also at Institute of Physics, Azerbaijan Academy of Sciences, Baku; Azerbaijan.

ad Also at Instituto de Fisica Teorica, IFT-UAM/CSIC, Madrid; Spain.

ae Also at Istanbul University, Dept. of Physics, Istanbul; Turkey.

af Also at Joint Institute for Nuclear Research, Dubna; Russia.

ag Also at Louisiana Tech University, Ruston LA; United States of America.

ah Also at Moscow Institute of Physics and Technology State University, Dolgoprudny; Russia.

ai Also at National Research Nuclear University MEPhI, Moscow; Russia.

aj Also at Physics Department, An-Najah National University, Nablus; Palestine.

ak Also at Physikalisches Institut, Albert-Ludwigs-Universität Freiburg, Freiburg; Germany.

al Also at The City College of New York, New York NY; United States of America.

am Also at TRIUMF, Vancouver BC; Canada.

an Also at Università di Napoli Parthenope, Napoli; Italy.

ao Also at University of Chinese Academy of Sciences (UCAS), Beijing; China.

* Deceased